Peter A.
Markowich

Applied Partial Differential Equations

A VISUAL APPROACH

Springer

Applied Partial Differential Equations: A Visual Approach

Peter A. Markowich

Applied Partial Differential Equations:

A VISUAL APPROACH

Springer

Peter A. Markowich
Faculty of Mathematics
University Vienna
Nordbergstraße 15
1090 Vienna
Austria
peter.markowich@univie.ac.at

Library of Congress Control Number: 2006936979

ISBN 978-3-540-34645-6 Springer Berlin Heidelberg New York

Springer is part of Springer Science+Business Media
springer.com

Production and typesetting: LE-TEX Jelonek, Schmidt & Vöckler GbR, Leipzig
Cover design: Erich Kirchner, Heidelberg, based on a photograph by P. A. Markowich

Printed on acid-free paper 46/3100/YL 5 4 3 2 1 0

Foreword

To Frédéric (Frédo) Poupaud, who inspired my mind and soul.

> … They are going to look for the highest dune so they can see all the Sahara. They walk a long time. Outka says: 'I see a high dune', and they go to it and climb up to the top. Then Mimouna says: 'I see a dune over there. It's much higher and we can see all the way to In Salah from it.' So they go to it and it is much higher. But when they go to the top, Aicha says: 'Look! There's the highest dune of all. We can see to Tamanrasset.' …
>
> (Paul Bowles, The Sheltering Sky, 1911)

The project for this book started in the beginning of the year 2005, when I looked through some of my photographs taken in various parts of the world over the last ten years or so. In fact, I have been interested and active in photography for some decades and my pleasure in it has even increased exponentially since the rise of digital imaging[1]. It then happened that I started to look at some of my images in mathematical terms, more precisely, I started to see partial differential equations 'behind' certain images. For example, a waterfall is modeled by the Saint-Venant approximation of the Euler or Navier–Stokes equations, flows of and in sand dunes obey the laws of the granular material inelastic Boltzmann equation, patterns in animal skins are described by an instability phenomenon in reaction-diffusion equations … All this has been clear to me for a long time, but all of a sudden the idea came up to use photography as a vehicle to transport and convey 'my' mathematics.

So the generic connection between my two favorite subjects, applied partial differential equations and photography was found …

Actually, this is precisely what this book is all about. Topics in applied partial differential equations are described mathematically in non-specialistic terms to make the book accessible to a large audience – hopefully also getting young researchers interested in the subject – and these topics are illustrated by (as I like to think) beautiful photographs, taken by myself in the last few years (there are two exemptions, which were taken by Andrea Baczynski). All the

[1] see my image galleries at *www.pbase.com/markowich*

images were acquired using digital cameras, among them a Nikon D100, Nikon D2x, Nikon D200, Kodak 14nx, Hasselblad H1 with a PhaseOne P25/45 digital backs. I always choose the RAW format for digital image acqusition, process the images first in a RAW converter and then do the necessary post-processing in Photoshop CS2.

The photographs are here for enjoyment but also – and more importantly in a scientific context – they shall convey a message: applied mathematics, particularly partial differential equation modeling, is useful for a wide range of problems and applications originating from the nature which surrounds us, from socio-economics and from technological applications.

So much about the photographs, but what can be said about the math? Actually, the choice of the topics Chapter 1 to Chapter 11 was mainly decided by my own research background and expertise, 'completeness' was never intended nor can it be achieved. The depth and style of the mathematical presentation is supposed to be such that everybody with a solid knowledge of multi-dimensional calculus can understand the text. In particular, students and researchers interested in modeling with partial differential equations are a clear target group of this book. But also, analytically or numerically oriented researchers in partial differential equations who are interested in new applications will hopefully get something out. Then, of course, the material of this book is accessible to engineers, physicists and other scientists with a basic mathematical education.

I have taken mathematical inspiration from many people. In particular I want to mention my dear friend Frédéric Poupaud, who passed away in the year 2004. Then my former students and friends Anton Arnold, Ansgar Jüngel, Ingo Gasser, Norbert Mauser and Christof Sparber, my colleagues and friends Christian Schmeiser, Christian Ringhofer, Andreas Unterreiter, Franco Brezzi, Giuseppe Toscani, Luis Caffarelli, Norayr Matevosyan, Irene Gamba, Pierre Degond, Naoufel Ben Abdallah, Henrik Shagholian, Benoit Perthame, Yann Brenier, Claude Bardos, David Levermore, Patrick Gerard, Paola Pietra, Martin Burger, Lorenzo Pareschi, Shi Jin, Weizhu Bao, Kazuo Aoki, Ester Gabetta, Claudia Lederman, Jorge Zubelli, Antonio Leitao, Heinz Engl, Jose Carrillo, Juan-Luis Vazquez and Cedric Villani. In particular I thank Giuseppe Toscani and Dietmar Ölz for coauthoring Chapters of this book with me.

My special gratitude goes to my friend and Administrator of my research grants, Renate Feikes, for friendship and many organisational miracles, to Andrea Baczynski, for love and photographic advice and to my daughter Anna for sitting (suffering …) through some of my talks at various conferences all over the world.

I acknowledge funding of my research over the past five years from the Austrian Research Fund FWF through my Wittgenstein Award 2000 (financed by the Austrian Ministry for Education, Science and Culture), from the EC

through various research networks (among them HYKE), from the Austrian Academy of Sciences through the Johann Radon Institute for Computational and Applied Mathematics and from the Austrian research funding agency FFG through a project on mathematical image processing.

Last but not least I thank Hans Gmasz for helping me out with his expert LaTeX skills.

Vienna, June 2006

Table of Contents

Introduction

Differential calculus[1], as introduced by Sir Isaac Newton[2] and Gottfried Wilhelm Leibniz[3] in the late 17th century, opened up a wealth of new possibilities for mathematical modeling in the natural and – later on – in the life sciences and in technology. Partial Differential Equations (PDEs), entirely based on the concepts of differential and integral calculus, relate one or more state variables to their variations (differentials) with respect to certain independent variables like time, space, velocity etc.

Just to name a few examples, PDEs were used by James Clerk Maxwell[4] to model electromagnetic fields interacting with electrical charges and currents, by Ludwig Boltzmann[5] to describe the non-equilibrium dynamics of rarified gases, by Albert Einstein[6] to phrase the laws of gravitation in the general theory of relativity and by Erwin Schrödinger[7] and Werner Heisenberg[8] to formulate quantum mechanics in mathematical-analytical terms.

The purpose of this book is to illustrate the fact that PDEs govern, or put in more modest terms, model many aspects of the nature surrounding us, of the technology we use on a daily basis and of our socio-economic interactions: PDEs have a significant importance for the scientific and technological progress of our society. Two entirely different descriptive levels are used in this book: firstly, in the subsequent eleven Chapters different scientific and technological problems are presented, modeled and analyzed by PDE methodology and secondly, photographic images are shown to illustrate these problems and some of their specific features. Every Chapter contains comments on the photographs which relate them directly to the presented mathematical models. Almost all images have a significant direct impact on and connection to PDE modeling issues, a few exceptions to this rule have 'only' an allegoric meaning. The attentive reader will easily find out which images belong to the latter class.

It is important to understand that the main purpose of the photographs is NOT to depict particular solutions of the partial differential equations under considerations – although some photographs do precisely that, but only as a by-product. Much more importantly, the photographs show concrete modeling

1 *http://en.wikipedia.org/wiki/Calculus*
2 *http://en.wikipedia.org/wiki/Sir_Isaac_Newton*
3 *http://en.wikipedia.org/wiki/Gottfried_Leibniz*
4 *http://de.wikipedia.org/wiki/James_Clerk_Maxwell*
5 *http://de.wikipedia.org/wiki/Ludwig_Boltzmann*
6 *http://de.wikipedia.org/wiki/Albert_Einstein*
7 *http://de.wikipedia.org/wiki/Erwin_Schroedinger*
8 *http://de.wikipedia.org/wiki/Werner_Heisenberg*

issues, which can be translated into the language of partial differential equations and further investigated by mathematical analysis and numerical computations. The photographs should focus the reader's attention to real-life/natural problems, appeal to his esthetic senses and connect directly to the modeling by partial differential equations. The actual representation of their solutions usually is done through numerical computations and graphic output algorithms, but this is NOT the purpose of this book.

Clearly, the choice of the PDE topics in Chapter 1 to Chapter 11 is personally biased by the author's mathematical taste, his mathematical experience and research interests. Some of the chosen topics have been in the center of his scientific interests and production for many years or even decades (Chapters 1, 4, 5 and 9), some are important sidelines of his research (Chapters 2, 6 and 10) and the others are in the realm of his passive scientific interests. Completeness of a presentation of PDEs in applications is not an issue of this book and many important topics are not covered here (an example is the recent surge in PDE applications in mathematical finance theory).

The texts are accessible to a broad range of mathematically interested people, in particular readers with a basic knowledge of differential and integral calculus in more than one dimension will be able to follow the exposition without difficulty. For example the author believes that advanced undergraduate students of mathematics, physics or engineering will enjoy the reading and profit from this book. Also, it could provide motivations and case studies for graduate courses in applied partial differential equations, with many loose ends which have to be tied up by further (literature) research. In some instances references are made to high powered mathematical techniques, which are supposed to be of interest to the mathematically more advanced readers, who have a direct research interest in applications and analysis of partial differential equations. Those readers might learn about some applications which had not crossed their minds before …

Each Chapter is self-contained to a very large extent, with its own bibliography. So readers can follow their personal preferences, choose their own sequence for reading the Chapters or even skip Chapters of lesser interest to them without loosing the general context.

There is, however, a certain scientifically arguable motivation of the chosen sequence of topics, albeit to some extent again dictated by the author's research background. The first Chapter is on kinetic phase space models, which give rise to many position space based macroscopic PDE systems, like the Navier–Stokes and Euler systems describing fluid and gas motion presented in Chapter 2, the granular flow equations of Chapter 3, the chemotaxis equations of Chapter 4 and the semiconductor models of Chapter 5. Chapter 6 deals with free boundaries, Chapter 7 with reaction-diffusion equations (see also the Turing instability discussed in Chapter 4), Chapter 8 focuses on the Monge–Kantorovich mass transportation theories which strongly connect to the areas of kinetic theory, fully nonlinear elliptic partial differential equations, diffusive theories etc. Linear and nonlinear wave propagation is the topic of Chapter 9, with a strong interplay

with kinetic transport theory and Chapter 10 'closes the loop' dealing with modern PDEs and variational tools of image analysis and processing. We remark that some of the techniques discussed in Chapter 10 were used to elaborate the images shown in this book. Finally, Chapter 11 – being somewhat isolated from a thematic point of view but not from the mathematical background – deals with socio-economic modeling, also based on kinetic equations.

Finally, a comment on mathematical depth (or lack of it …) in the presentation of the topics is in order. There is only a thin line between mathematical superficiality and excess of mathematical detail for a project like this. The author has done his best to stay on this line, keeping in mind that the basic idea in writing this book has been to TOUCH on certain topics in applied PDEs and – in the best of all cases – to arouse the reader's interest to go deeper in certain directions of modern PDE research. For this, historic facts are presented, references to the scientific literature are included in all Chapters (also these are strongly biased by the author's scientific background and taste, no completeness can be expected …), important open problems are pointed out and also references to related internet sites are given. The author is fully aware of the fact that webpages are not set up for eternity, so it may very well be that some links will not be in operation anymore when the reader tries them out at some later point of time, although they were checked out thoroughly at the time of writing this book. However, it seemed too much of an omission to forsake internet-based information in the context of this book.

1. Kinetic Equations: From Newton to Boltzmann

Consider a mass particle, which moves under the action of a force. Let the positive constant m be the particle mass and $F = F(x,t)$ the force field. Here x in $\mathbb{R}^d$ is the position variable ($d = 3$ in physical space but there is at this point no mathematical reason why m cannot be an arbitrary positive integer) and $t > 0$ the time. The force field is a d-dimensional vector field on $\mathbb{R}^d$, possibly time dependent. By $v \in \mathbb{R}^d$ we denote the velocity variable. Then the motion of the particle is characterized by the Newtonian phase space (i.e. $\mathbb{R}^d_x \times \mathbb{R}^d_v$) trajectories, which satisfy the system of ordinary differential equations (ODEs):

$$\dot{x} = v \tag{1.1}$$

$$\dot{v} = \frac{1}{m} F(x,t)\ . \tag{1.2}$$

Note that the first equation simply states that the particle's velocity is the time derivative of its position and the second equation is just Newton's[1] celebrated second law, stating

$$\text{force} = \text{mass} \cdot \text{acceleration}\ .$$

If the field F is sufficiently smooth, then by standard ODE theory we conclude that, given an initial state

$$\big(x(t=0), v(t=0)\big) = (x_0, v_0) \in \mathbb{R}^{2d}$$

there exists a locally defined, unique and smooth trajectory $(x(t; x_0, v_0), v(t; x_0, v_0))$. Thus, given the force and the initial position and velocity, the motion of the mass particle is – in the framework of classical Newtonian mechanics – completely determined. However, in many applications, there are additional complications …

Assume at first that the intial state (x_0, v_0) is not known a priorily, instead let $f_0 = f_0(x,v)$ be a given probability distribution of the initial state, i.e. f_0 is non-negative, its integral over the whole phase space is 1 and, for any measurable subset A of the phase space,

$$\int_A f_0(x,v)dxdv =: P_0(A)$$

[1] We refer to the webpage *http://scienceworld.wolfram.com/biography/Newton.html* for a biography of Isaac Newton (1642–1727).

Fig. 1.1. Airplane departing from Rio de Janeiro's City Airport

is the probability of finding the particle at time $t = 0$ in the set A. Then, instead of calculating the evolution of the phase space trajectories we can try to compute the location probability density $f = f(x, v, t)$, evolving out of f_0. For this we impose the condition that f remains constant along the Newtonian trajectories:

$$\frac{d}{dt} f\left(x(t; x_0, v_0)\,, v(t; x_0, v_0), t\right) = 0\,.$$

Carrying out the differentiation with respect to time, taking into account the Newtonian equations (1.1, 1.2) and renaming coordinates gives the so called Liouville equation:

$$f_t + v\,.\,\mathrm{grad}_x\, f + \frac{1}{m} F\,.\,\mathrm{grad}_v\, f = 0\,, \quad x \in \mathbb{R}^d\,, v \in \mathbb{R}^d;, t > 0\,, \tag{1.3}$$

subject to the initial condition

$$f(t = 0) = f_0\,. \tag{1.4}$$

Note that the Liouville equation is a linear hyperbolic PDE, whose charcteristics are precisely the Newtonian trajectories. Thus, its solution can be written as

$$f(x, v, t) = f_0\left(T_{-t}(x, v)\right)\,,$$

where T_t denotes the Newtonian flow map, which maps a point in phase space into the state of the Newtonian trajectory at time t. Here we assumed that the Newtonian map is defined globally for $t > 0$.

Another complication arises from the fact that in the most important physical cases there is not only one isolated particle to observe but instead a swarm consisting of a large number of particles, which interact with each other. Two types of interactions are distinguished, namely long range and short range interactions. Typical long range interactions are either given by the repulsive Coulomb force of electrodynamics, occurring in charged particle transport, or the attractive gravitational force, e.g. occurring in the modeling of galaxy motion. Short range interactions can be classified as particle collisions, they will be discussed in detail later.

In the small coupling thermodynamical limit (i.e. small force, number of particles tends to infinity) long range forces typically lead to nonlocal nonlinearities in the effective Liouville equation, when the total chaos assumption (Hartree ansatz) is made (see [11]). In the Coulomb/gravitational case we obtain (after appropriate scaling) the so called Vlasov–Poisson system[2] (see [7]):

$$f_t + v \,.\, \mathrm{grad}_x f - \mathrm{grad}\, V \,.\, \mathrm{grad}_v f = 0 \tag{1.5}$$

$$\pm \Delta V = n \tag{1.6}$$

$$n = \int_{\mathbb{R}^d} f dv \,. \tag{1.7}$$

Here f is the effective particle number density on $2d$-dimensional phase space, dependent on time t of course, V is the mean field Coulomb/gravitational potential (the + sign in front of the Laplacian in the Poisson equation (1.6) corresponds to the gravitational case and the − sign to the Coulomb case), and n denotes the position space number density.

The existence and uniqueness of smooth solutions of the Vlasov–Poisson in the 6-dimensional phase space case was a longstanding open problem, finally answered positively in [14] and shortly afterwards in [10].

Short range interactions (so called particle collisions) typically lead to additional terms in Liouville-type kinetic equations, which are nonlocal in the velocity variable. In the absence of an external potential and neglecting long range interactions, the number (or mass) phase space density of a particle swarm undergoing collisional events, satisfies a kinetic equation posed in the $2d$ dimensional phase space (after the Boltzmann–Grad limit):

$$f_t + v \,.\, \mathrm{grad}_x f = Q(f,f)\,, \tag{1.8}$$

where $Q(f,f)$ is the nonlocal collision operator (typically an integral operator). The equation (1.8) models a dynamic balance between the free streaming particle motion, represented by the left hand side of the equation, and the collisions.

[2] *http://relativity.livingreviews.org/open?pubNo=lrr-2002-7&page=articlesu2.html*

The classical example for a collisional model of the form (1.8) is encountered in the kinetic theory of rarified gases.

Actually, most of the gas flows around us are rather accurately modeled by macroscopic flow equations (the viscous Navier–Stokes or the inviscid Euler system, see Chapter 2). However, it is nevertheless of paramount importance to understand the underlying flow dynamics from a microscopic 'molecular' point of view. A main reason for this is that we need to know the physical limits of validity of macroscopic flow equations, which are based on microscopic dynamics.

Typical gaseous flow examples can be seen in the Images 1.1–1.6, showing an airplane in its take-off phase (Image 1.1) and various (meteorological) clouds (Images 1.2–1.6), among them images with a front of clouds being convected by a strong wind towards a high mountain (Images 1.3, 1.4). Note that fluid dynamic modeling of airplane flow and cloud dynamics may still give sufficiently accurate results for many practical purposes (see the comments to the images below). For some more exotic cases of rarified gas flow macroscopic equations are completely insufficient and a microscopic model has to be employed directly.

Fig. 1.2. Altocumulus lenticularis duplicatus over the planes of Patagonia

To understand the modeling hierarchy consider a space shuttle orbiting the earth outside its atmospheric layer, i.e. in a vacuum. Obviously, the shuttle moves there in ballistic motion free of interactions. Then, when the shuttle starts its re-entry phase, interactions of the shuttle hull with the molecules of the upper atmosphere will start to take place. Since the upper atmosphere is highly rarified, only few interactions will occur within a given time unit. After a short time, when the shuttle enters more deeply into the earth's atmospheric layer, the effect of these gas molecule-shuttle hull collisions will dynamically balance the free-streaming shuttle motion. Deeper down in the atmosphere, close to the surface of the earth, the air becomes even less rarified such that there will be many collisions of air particles with the shuttle hull (and many air molecule-air molecule collisions) within a given unit of time such that they start to dominate the shuttle motion. This re-entry process shows a typical transition from ballistic motion (infinite mean free path between consecutive collisions) to ballistic-collision equilibrated motion (order 1 mean free path) to collision dominated motion (small mean free path). The former regime has a very simple mathematical description (namely free streaming phase space flow, i.e. the Liouville equation without external force), the latter is precisely the fluid regime covered by macroscopic flow equations and the middle regime requires a microscopic molecular-based model, as presented below.

Let $f = f(x, v, t)$ be the expected mass density in (position x, velocity v) phase space of the gas at time t, i.e. the expected mass per unit volume, at time t, in the six-dimensional phase space. Assume that the gas consists of perfectly spherical identical molecules of diameter D. Now consider two gas molecules, immediately after a collision event between themselves, with states (x, v) and, resp., $(x - Dn, w)$, where n is the unit vector along the directions connecting the centers of the spheres. Then, immediately prior to this collision, the phase space states of these two molecules were (x, v^*) and, resp., $(x - Dn, w^*)$, where the pre-collisional velocities v^* and w^* satisfy momentum conservation

$$m(v + w) = m(v^* + w^*)$$

and energy conservation

$$m(v^2 + w^2) = m\big((v^*)^2 + (w^*)^2\big)$$

in the collision process. Here m denotes the mass of the gas molecules. The pre-collisional velocities read:

$$v^* = v + n\,.(w - v)n\,, \quad w^* = w + n\,.(v - w)n\,.$$

Then the celebrated Boltzmann equation, named after the Viennese Physicist Ludwig Boltzmann [3] (1844–1906) describing the temporal evolution of the phase

[3] *http://www-groups.dcs.st-and.ac.uk/~history/Mathematicians/Boltzmann.html*

space mass density f of a single particle rarified gas with identical, perfectly spherical, elastically colliding molecules reads:

$$\frac{\partial}{\partial t} f(x,v,t) + v \,.\, \mathrm{grad}_x f(x,v,t) + \frac{F}{m} \,.\, \mathrm{grad}_v f(x,v,t)$$
$$= \int_{\mathbb{R}^3} \int_{S^2} B(v,w,n) \left[f(x,v^*,t) f(x,w^*,t) - f(x,v,t) f(x,w,t) \right] dndw := Q(f,f) \,.$$

Here S^2 is the unit sphere in $\mathbb{R}^3$ and $B = B(v,w,n)$ stands for the collision kernel representing the microscopic properties of the molecular collisions. Typically B only depends on the relative post-collisional velocity $V = w - v$ and on the angle between the vectors n and V.

As mentioned above, the integral operator $Q(f,f)$ on the right hand side is usually referred to as collision integral. It represents the statistics of all possible collision events leading to the post-collisional velocity v (first integrand term, called gain term after the integrations) and of all possible outgoing collisions (second integrand term, called loss term after the integrations). Note that the bilinear nature of the collision integral is due to the fact that only binary molecular collisions are taken into account by the Boltzmann equation. Collisions of three and more molecules are neglected, which implies that the considered gas has to be sufficiently rarified.

External interactions of the gas, e.g. with the hull of the re-entrant space shuttle mentioned above, have to be modeled by appropriate boundary conditions.

For a wealth of mathematical detail, including a derivation from multi-particle physics and important mathematical properties of the Boltzmann equation we refer to the books [4] and [16].

A fascinating reading about the life of Ludwig Boltzmann, to whom the equation is attributed, at least in the case of hard sphere molecules with $B(v,w,n) = \text{const.}\ |V.n|$, after his celebrated paper from 1872 [3], the role of Maxwell[4] in the derivation of the Boltzmann equation and about the cultural-scientific background of their times, is provided by [5].

For mathematical purposes it is convenient to rewrite the Boltzmann equation in terms of dimensionless quantites. Then a parameter ε, the so called Knudsen number (= normalized particle mean free path), appears:

$$\varepsilon \left(f_t + v \,.\, \mathrm{grad}_x f + \frac{F}{m} \,.\, \mathrm{grad}_v f \right) = Q(f,f) \,.$$

(for the sake of simplicity we use the same notations for the dimensionless quantities). Note that the case 'ε large' corresponds to ballistic transport, 'ε of order 1' represents a dynamic balance between free transport and collisional

[4] *http://www-groups.dcs.st-and.ac.uk/~history/Mathematicians/Maxwell.html*

effects and 'ε small' is the case of collision-dominated transport (cf. the space shuttle example cited above!). The operator Q has 5 so-called collision invariants, i.e. when it is multiplied by the 5-vector $(1, v, |v|^2)$ and integrated over velocity space, then (at least formally) zero is obtained. This corresponds to the classical physical requirements of mass, momentum und energy conservation in gas flows, which are thus verified on a formal level. Also the Boltzmann equation preserves positivity, i.e. solutions f with nonnegative initial data $f(t = 0)$ will remain nonnegative during the time evolution (as long as they exist), as required for probability densities.

It is a trivial exercise to show that the post-collisional velocities become the pre-collisional ones when another collision process is applied to them, i.e. the map from (v, w) to (v^*, w^*) is an involution. This implies that each individual collision process is reversible, i.e. when the post-collisional velocities are reversed and put through a collision then the negative original pre-collisional velocities are obtained. Boltzmann realized that this micro-reversibility does not imply reversibility of the gas flow. On the contrary the Boltzmann equation is non-reversible (although based on reversible binary micro-collisions!). In particular, the Boltzmann equation dissipates the convex functional H given by

$$H(f) := \int_{\mathbb{R}^6} f \log f dv dx \,.$$

This means that along a sufficiently smooth nonnegative solution f of the Boltzmann equation the inequality

$$\frac{d}{dt} H\big(f(t)\big) =: S(f(t)) \leq 0$$

holds, with equality iff f is a local Maxwellian function:

$$f(x, v, t) = \frac{\rho(x, t)}{\big(2\pi T(x, t)\big)^{3/2}} \exp\left(-\frac{|u(x, t) - v|^2}{2T(x, t)}\right),$$

where ρ, u, T are the position density, mean velocity and, resp., temperature associated to f.

The quantity $H(f)$ is the (negative) physical entropy of the phase space density f and $S(f)$ is its dissipation generated by the time evolution of the Boltzmann equation. This explains also – again on a formal level – the tendency of solutions of the Boltzmann equation to converge to (global) Maxwellians in the large time limit and the connection to the macroscopic Euler and Navier–Stokes equations obtained (formally!) by the limit procedure '$\varepsilon \to 0$' and by assuming that f is a local Maxwellian.

The Boltzmann equation has been a great challenge for mathematicians (a long list starts with David Hilbert[5]) but some important analytical results are

[5] *http://www-groups.dcs.st-and.ac.uk/~history/Mathematicians/Hilbert.html*

Fig. 1.3. Cumulus fractus approaching the volcano Cotopaxi in Ecuador

Fig. 1.4. Cumulus fractus approaching the volcano Cotopaxi in Ecuador

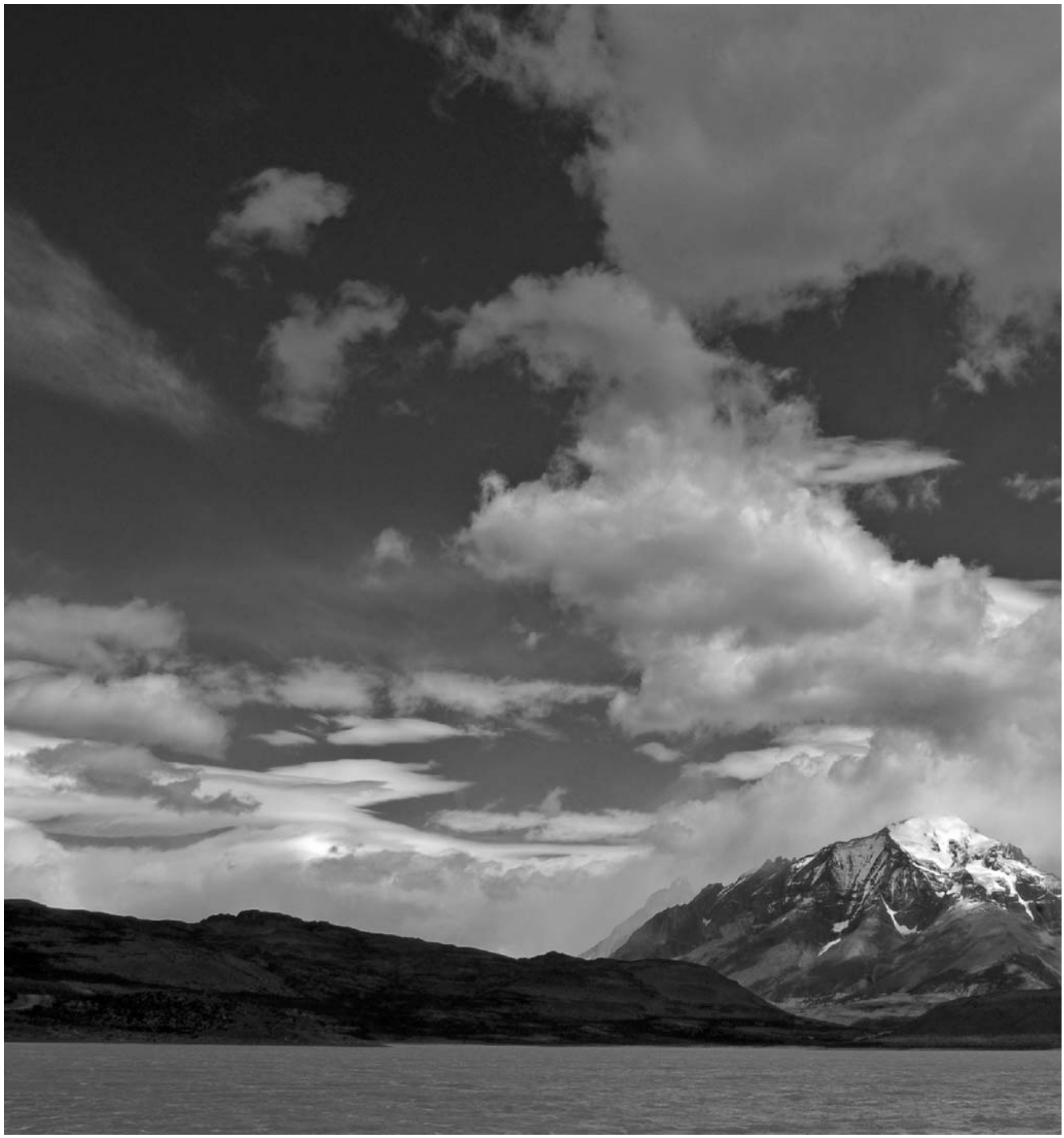

Fig. 1.5. Various cumulus clouds over Torres del Paine in Chilean Patagonia

still missing. For example, the existence of solutions, globally defined for positive time, for all nonnegative arbitrarily large initial data with finite mass, energy, moment of inertia and entropy has been proven only in 1989 in an important paper of Ron DiPerna and Pierre-Louis Lions[6] [9].

These solutions are obtained by a so-called renormalisation procedure of the Boltzmann equation dealing effectively with the quadratic nature of the collision integral. They are rather weak, so that neither their uniqueness nor their conservation of energy is ascertained! The lack of smoothness of the renormalized solutions of the Boltzmann equation is also a major obstacle in the quest of the mathematically rigorous justification of its small Knudsen number limits, although in recent years a lot of progress has been made in this area, see [1] and consecutive papers by the same authors[7].

Clearly, the gas dynamics Boltzmann equation is still in the core of modern kinetic theory. However, other applications of Boltzmann-type equations

Fig. 1.6. Stratocumulus stratiformis translucidus (background) and cumulus (foreground)

[6] *http://www-groups.dcs.st-and.ac.uk/∼history/Mathematicians/Lions.html*

[7] check *http://www.dma.ens.fr/∼golse/Publications/pubs.html* for a list of references

have arisen recently, namely in solid state physics (see Chapter 5), Bosonic and Fermionic transport, granular flows (see Chapter 3), traffic modeling, chemotactic cell motion (see Chapter 4), just to name a few.

Comment on the Image 1.1 Aircraft and in particular airfoil design and optimisation is a classic task for computational fluid dynamics (CFL). Typically, the three-dimensional incompressible Navier–Stokes equations are used for accurate results while incompressible Euler computations (which disregard boundary layer effects) or even irrotational flow simulations (zero vorticity) give in many cases usable quantitative results. Compressibility effects start to play a role for transonic flows with sufficiently high Mach number. The theoretical basis for these macroscopic gas dynamics systems is the microscopic Boltzmann equation, but the involved numerical effort, due to the high dimension of the phase space (three velocity directions plus three spatial directions, and time!), does usually not justify its application in industrial aircraft design. Recently however, lattice Boltzmann equation simulations (for more details see below) have been employed for airfoil simulations and turbulence modeling in different applications, with striking success [6].

Comments on the Images 1.2–1.6 The modeling of the formation and motion of atmospheric clouds is often done by macroscopic fluid equations (Navier–Stokes or Euler) incorporating the interaction of air with cloud particles like water droplets, ice crystals or non-volatile aerosols, again on a macroscopic basis [8]. The main difficulty lies in the phase transitions from water vapor to water droplets and then, in certain cases, to ice particles (multi-phase flow). Boltzmann-type kinetic models [13], [2] and an associated moment system for particle dynamics in clouds were introduced in [13]. A somewhat related kinetic approach for cloud, wind, smoke, aerosol and pheromone kinetics employs lattice Boltzmann equation (LBM) simulation. In the language of kinetic equations, LBM equations are discrete-velocity Boltzmann equations, posed on a discrete grid in position space. Actually, they can be regarded as a numerical discretisation of the Boltzmann equation, with an appropriate collision term, and LBM solutions are known to converge (in a certain scaling limit and when the grids are refined) in a suitable sense to solutions of the Navier–Stokes equations. Alternatively, LBM models can be seen as cellular automata, where the collision process under consideration defines the redistribution of density values after each time step. They have proven great flexibility in applications of complex flows, involving complicated geometries, incorporation of chemical reactions, phase transitions etc.[8].

Interesting applications can be found in [15], [17], [6], [12].

Another interesting application of kinetic theory occurs in cloud microphysics. Typically, clouds contain water drops, which increase their masses due

[8] For more information we refer to *http://www.science.uva.nl/research/scs/projects/lbm_web/index.html*

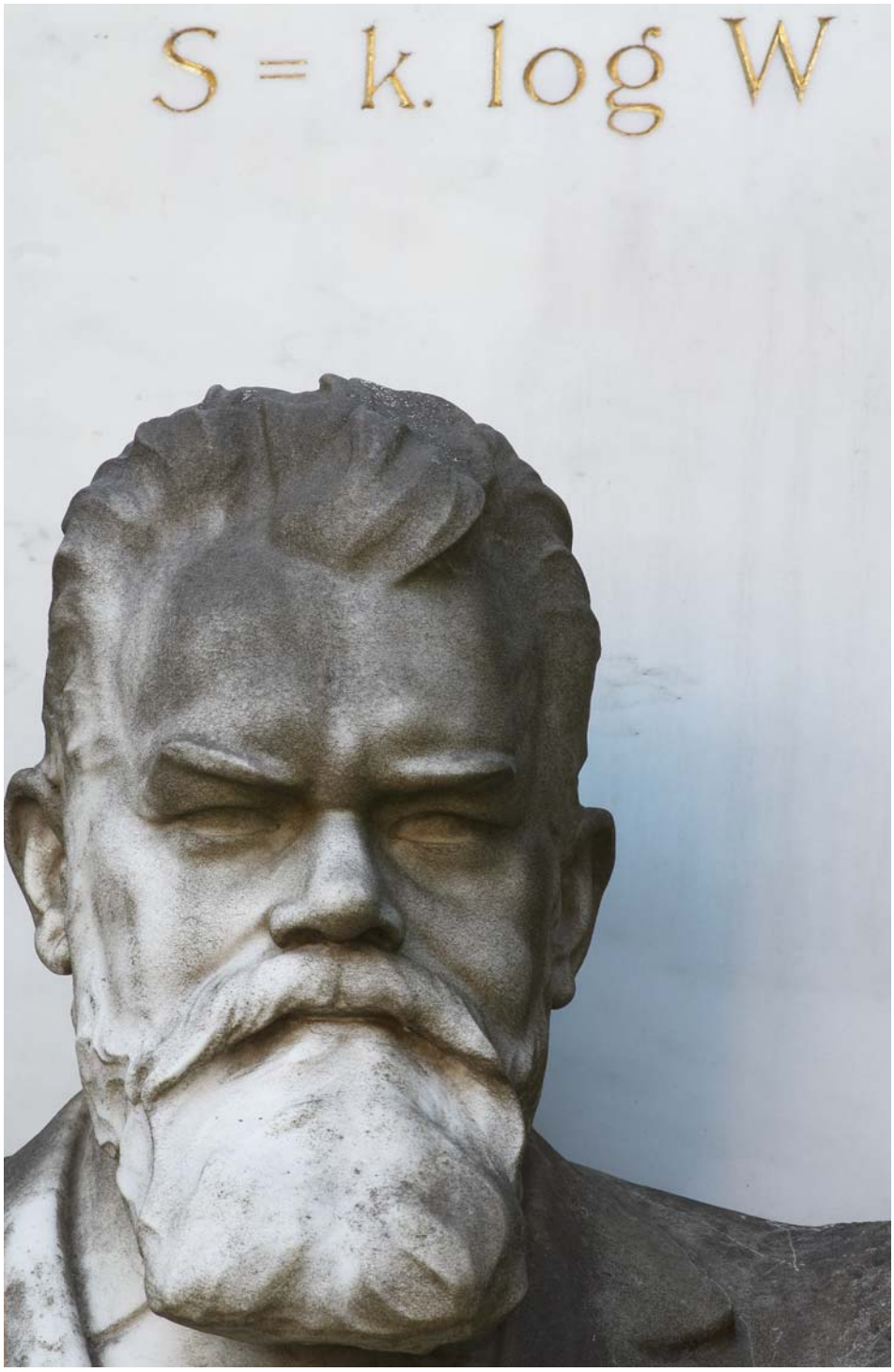
S = k. log W

Fig. 1.7. Bust of Ludwig Boltzmann

to collisions leading to coalescence of the colliding drops. The time evolution of the number density f of water drops in a cloud, as function of the drop mass $m > 0$ is known to be described by the so-called stochastic coalescence equation, which has the form of a space-homogeneous (kinetic) Boltzmann-type equation, where the drop mass m plays the role of the independent variable. The equation reads:

$$\partial_t f(m,t) = \frac{1}{2}\int_0^m K(m-m',m')f(m-m',t)f(m',t)\,dm' - \int_0^\infty K(m,m')f(m',t)f(m,t)\,dm'.$$

The quadratic operator on the right hand side models coalescing collisions of drops. The function $K(m, m')$ denotes the non-negative cross-section. For details on the physics we refer to [18], mathematical results can be found in [19].

Acknowledgement The author is indebted to Benedikt Bica from the Institute for Meteorology and Geophysics of the University of Vienna for providing the cloud classification of the Images 1.2 to 1.6.

Comment on Image 1.7 The bust of Ludwig Boltzmann at his grave at the Central Cemetery of Vienna, Austria. The entropy formula is engraved. We acknowledge the courtesy of Andrea Baczynski[9], who took this photograph.

References

[1] C. Bardos, F. Golse and D. Levermore, *Fluid Dynamic Limits of Kinetic Theory I: Formal Asymptotics Leading to Incompressible Hydrodynamics*; J. Stat. Phys. 63, pp. 323–344, 1991
[2] E.X. Berry, *A Mathematical Framework for Cloud Models*, Journal of the Atmospheric Sciences, Vol. 26, No. 1, pp. 109–111, 1969
[3] L. Boltzmann, *Weitere Studien über das Wärmegleichgewicht unter Gasmolekülen*, Sitzungsberichte der Akademie der Wissenschaften, Wien, Ber. 66, pp. 275–370, 1872
[4] C. Cercignani, *The Boltzmann Equation and its Applications*, Springer Verlag, 1988

[9] *www.pbase.com/lacandonna*

[5] C. Cercignani, *Ludwig Boltzmann: The Man Who Trusted Atoms*, Oxford University Press, 1998
[6] H. Chen et al., *Extended Boltzmann Kinetic Equation for Turbulent Flows*, Science 1, Vol. 301, No. 5633, pp. 633–636, 2003
[7] R. Glassey, *The Cauchy Problem in Kinetic Theory*, SIAM, Philadelphia, 1996
[8] M.J. Harris, *Real-Time Cloud Simulation and Rendering*, Ph.D. Thesis, University of North Carolina at Chapel Hill, Department of Computer Science, 2003[10]
[9] P.L. Lions and R. Di Perna, *On the Cauchy Problem for Boltzmann Equations*, Annals of Mathematics, 130, 321–366, 1989
[10] P.L. Lions and B. Perthame, *Propagation of moments and regularity for the 3-dimensional Vlasov–Poisson system*, Invent. Math., 105, 415–430, 1991
[11] P.A. Markowich, C. Ringhofer and C. Schmeiser, *Semiconductor Equations*, Springer Verlag Wien – New York, 1990
[12] R. Myazaki et al., *Simulation of Cumuliform Clouds Based on Computational Fluid Dynamics*, Eurographics, 2002[11]
[13] R. Paoli and K. Shariff, *Particle Size Distribution in Atmospheric Clouds*, Center for Turbulence Research, Stanford University, Annual Research Briefs, 2003[12]
[14] K. Pfaffelmoser, *Global classical solutions of the Vlasov–Poisson system in three dimensions for general initial data*, J. Differ. Equations, 95, 281–303, 1992
[15] F. Qiu et al., *Dispersion Simulation and Visualisation for Urban Security*, IEEE Visualization 2004, Austin Texas, 2004[13]
[16] Y. Sone, *Kinetic Theory and Fluid Dynamics*, Birkhäuser, 2002
[17] X. Wei et al., *Blowing in the Wind*, Eurographics/SIGGRAPH Symposium on Computer Animation, D. Breen, M. Lin (Editors), 2003
[18] R.A. Houze, Jr., *Cloud Dynamics*, International Geophysics Series, Vol. 53, Academic Press, 1993
[19] N. Fournier and S. Mischler, *On a Boltzmann equation for elastic, inelastic and coalescing collisions*, to appear in J. Math. Pures Appl., 2006[14]

[10] Can be downloaded from: *http://www.markmark.net/dissertation/harrisDissertation.pdf*
[11] Can be downloaded from: *http://nis-ei.eng.hokudai.ac.jp/∼doba/papers/EGshort02_cloud.pdf*
[12] Can be downloaded from: *http://ctr.stanford.edu/ResBriefs03/paoli.pdf*
[13] Can be downloaded from: *http://www.cs.sunysb.edu/∼vislab/projects/amorphous/WXMWebsite/Urban.pdf*
[14] Can be downloaded from: *http://www.ceremade.dauphine.fr/ mischler/articles/31BEIC.pdf*

2. The Navier–Stokes and Euler Equations – Fluid and Gas Dynamics

Fluid and gas dynamics have a decisive impact on our daily lives. There are the fine droplets of water which sprinkle down in our morning shower, the waves which we face swimming or surfing in the ocean, the river which adapts to the topography by forming a waterfall, the turbulent air currents which often disturb our transatlantic flight in a jet plane, the tsunami[1] which can wreck an entire region of our world, the athmospheric flows creating tornados[2] and hurricanes[3], the live-giving flow of blood in our arteries and veins[4]… All these flows have a great complexity from the geometrical, (bio)physical and (bio)mechanical viewpoints and their mathematical modeling is a highly challenging task.

Clearly, the dynamics of fluids and gases is governed by the interaction of their atoms/molecules, which theoretically can be modeled microscopically, i.e. by individual particle dynamics, relying on a grand Hamiltonian function depending on $3N$ space coordinates and $3N$ momentum coordinates, where N is the number of particles in the fluid/gas. Note that the Newtonian ensemble trajectories live in $6N$ dimensional phase space! For most practical purposes this is prohibitive and it is essential to carry out the thermodynamic Boltzmann–Grad limit, which – under certain hypothesis on the particle interactions – gives the Boltzmann equation of gas dynamics (see Chapter 1 on kinetic equations) for the evolution of the effective mass density function in 6-dimensional phase space.

Under the assumption of a small particle mean free path (i.e. in the collision dominated regime) a further approximation is possible, leading to time-dependent macroscopic equations in position space $\mathbb{R}^3$, referred to as Navier–Stokes and Euler systems. These systems of nonlinear partial differential equations are absolutely central in the modeling of fluid and gas flows.

For more (precise) information on this modeling hierarchy we refer to [3].

The Navier–Stokes system[5] was written down in the 19th century. It is named after the French engineer and physicist Claude–Luis Navier[6] and the Irish mathematician and physicist George Gabriel Stokes[7].

---

1 *http://www.tsunami.org/*
2 *http://www.spc.noaa.gov/faq/tornado/*
3 *http://www.nhc.noaa.gov/*
4 *http://iacs.epfl.ch/cmcs/NewResearch/vascular.php3*
5 *http://www.navier–stokes.net/*
6 *http://www-groups.dcs.st-and.ac.uk/∼history/Mathematicians/Navier.html*
7 *http://www-groups.dcs.st-and.ac.uk/∼history/Mathematicians/Stokes.html*

Fig. 2.1. Iguassu Falls, Border of Brazil-Argentina

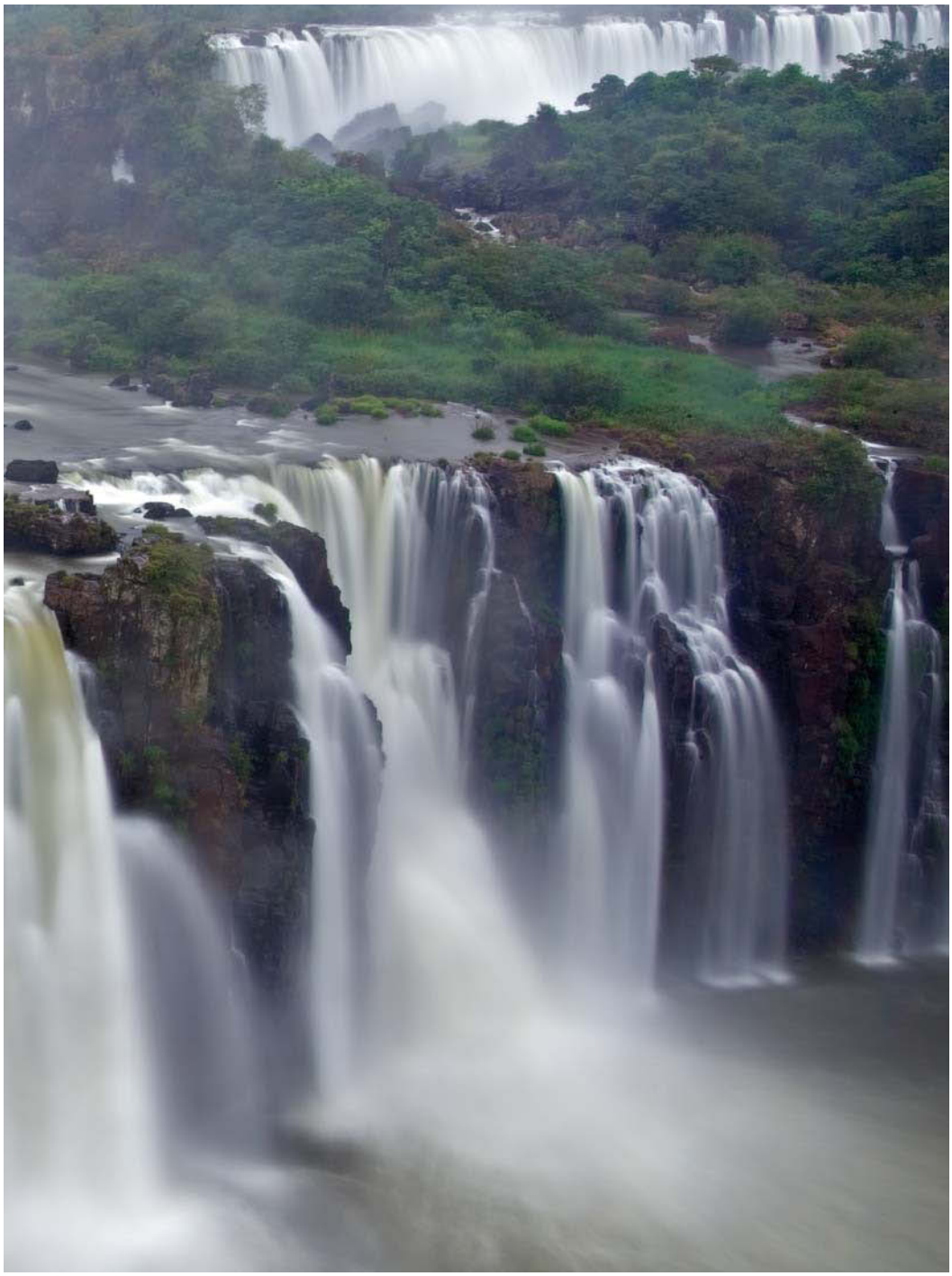

Fig. 2.2. Iguassu Falls, Border of Brazil-Argentina

Under the assumption of incompressibility of the fluid the Navier–Stokes equations, determining the fluid velocity u and the fluid pressure p, read:

$$\frac{\partial u}{\partial t} + (u \cdot \operatorname{grad})u + \operatorname{grad} p = \nu \Delta u + f$$
$$\operatorname{div} u = 0$$

Here x denotes the space variable in $\mathbb{R}^2$ or $\mathbb{R}^3$ depending on whether 2 or 3 dimensional flows are to be modeled and $t > 0$ is the time variable. The velocity field $u = u(x, t)$ (vector field on $\mathbb{R}^2$ or, resp., $\mathbb{R}^3$) is in $\mathbb{R}^2$ or $\mathbb{R}^3$, resp., and the pressure $p = p(x, t)$ is a scalar function. $f = f(x, t)$ is the (given) external force field (again two and, resp. three-dimensional) acting on the fluid and $\nu > 0$ the kinematic viscosity parameter. The functions u and p are the solutions of the PDE system, the fluid density is assumed to be constant (say, 1) here as consistent with the incompressibility assumption. The nonlinear Navier–Stokes system has to be supplemented by an initial condition for the velocity field and by boundary conditions if spatially confined fluid flows are considered (or by decay conditions on whole space). A typical boundary condition is the so-called no-slip condition which reads

$$u = 0$$

on the boundary of the fluid domain.

The constraint $\operatorname{div} u = 0$ enforces the incompressibility of the fluid and serves to determine the pressure p from the evolution equation for the fluid velocity u.

If $\nu = 0$ then the so called incompressible Euler[8] equations, valid for very small viscosity flows (ideal fluids), are obtained. Note that the viscous Navier–Stokes equations form a parabolic system while the Euler equations (inviscid case) are hyperbolic. The Navier–Stokes and Euler equations are based on Newton's celebrated second law: force equals mass times acceleration. They are consistent with the basic physical requirements of mass, momentum and energy conservation.

The incompressible Navier–Stokes and Euler equations allow an interesting simple interpretation, when they are written in terms of the fluid vorticity, defined by

$$\omega := \operatorname{curl} u \, .$$

Clearly, the advantage of applying the curl operator to the velocity equation is the elimination of the pressure. In the two-dimensional case (when vorticity can be regarded as a scalar since it points into the x_3 direction when u_3 is zero) we obtain

$$\frac{D\omega}{Dt} = \nu \Delta \omega + \operatorname{curl} f \, ,$$

[8] *http://gap-system.org/~history/Mathematicians/Euler.html*

where $\frac{Dg}{Dt}$ denotes the material derivative of the scalar function g:

$$\frac{Dg}{Dt} = g_t + u.\,\mathrm{grad}\, g\ .$$

Thus, for two-dimensional flows, the vorticity gets convected by the velocity field, is diffused with diffusion coefficient ν and externally produced/destroyed by the curl of the external force. For three dimensional flows an additional term appears in the vorticity formulation of the Navier–Stokes equations, which corresponds to vorticity distortion.

The Navier–Stokes and Euler equations had tremendous impact on applied mathematics in the 20th century, e.g. they have given rise to Prandtl's[9] boundary layer theory which is at the origin of modern singular perturbation theory. Nevertheless the analytical understanding of the Navier–Stokes equations is still somewhat limited: In three space dimensions, with smooth, decaying (in the far field) initial datum and force field, a global-in-time weak solution is known to exist (Leray solution[10]), however it is not known whether this weak solution is unique and the existence/uniqueness of global-in-time smooth solutions is also unknown for three-dimensional flows with arbitrarily large smooth initial data and forcing fields, decaying in the far field. In fact, this is precisely the content of a Clay Institute Millennium Problem[11] with an award of USD 1 000 000!! A very deep theorem (see [2]) proves that possible singularity sets of weak solutions of the three-dimensional Navier–Stokes equations are 'small' (e.g. they cannot contain a space-time curve) but it has not been shown that they are empty …

We remark that the theory of two dimensional incompressible flows is much simpler, in fact smooth global $2-d$ solutions exist for arbitrarily large smooth data in the viscid and inviscid case (see [6]).

Why is it so important to know whether time-global smooth solutions of the incompressible Navier–Stokes system exist for all smooth data? If smoothness breaks down in finite time then – close to break-down time – the velocity field u of the fluid becomes unbounded. Obviously, we conceive flows of viscous real fluids as smooth with a locally finite velocity field, so breakdown of smoothness in finite time would be highly counterintuitive. Here our natural conception of the world surrounding us is at stake!

The theory of mathematical hydrology is a direct important consequence of the Navier–Stokes or, resp., Euler equations. The flow of rivers in general – and in particular in waterfalls like the famous ones of the Rio Iguassu on the Argentinian-Brazilian border, of the Oranje river in the South African Augrabies National Park and others shown in the Figs. 2.1–2.6, are often modeled by the so called Saint–Venant system, named after the French civil engineer

[9] *http://www.fluidmech.net/msc/prandtl.htm*
[10] *http://www-groups.dcs.st-and.ac.uk/~history/Mathematicians/Leray.html*
[11] *http://www.claymath.org/millennium/Navier–Stokes_Equations/*

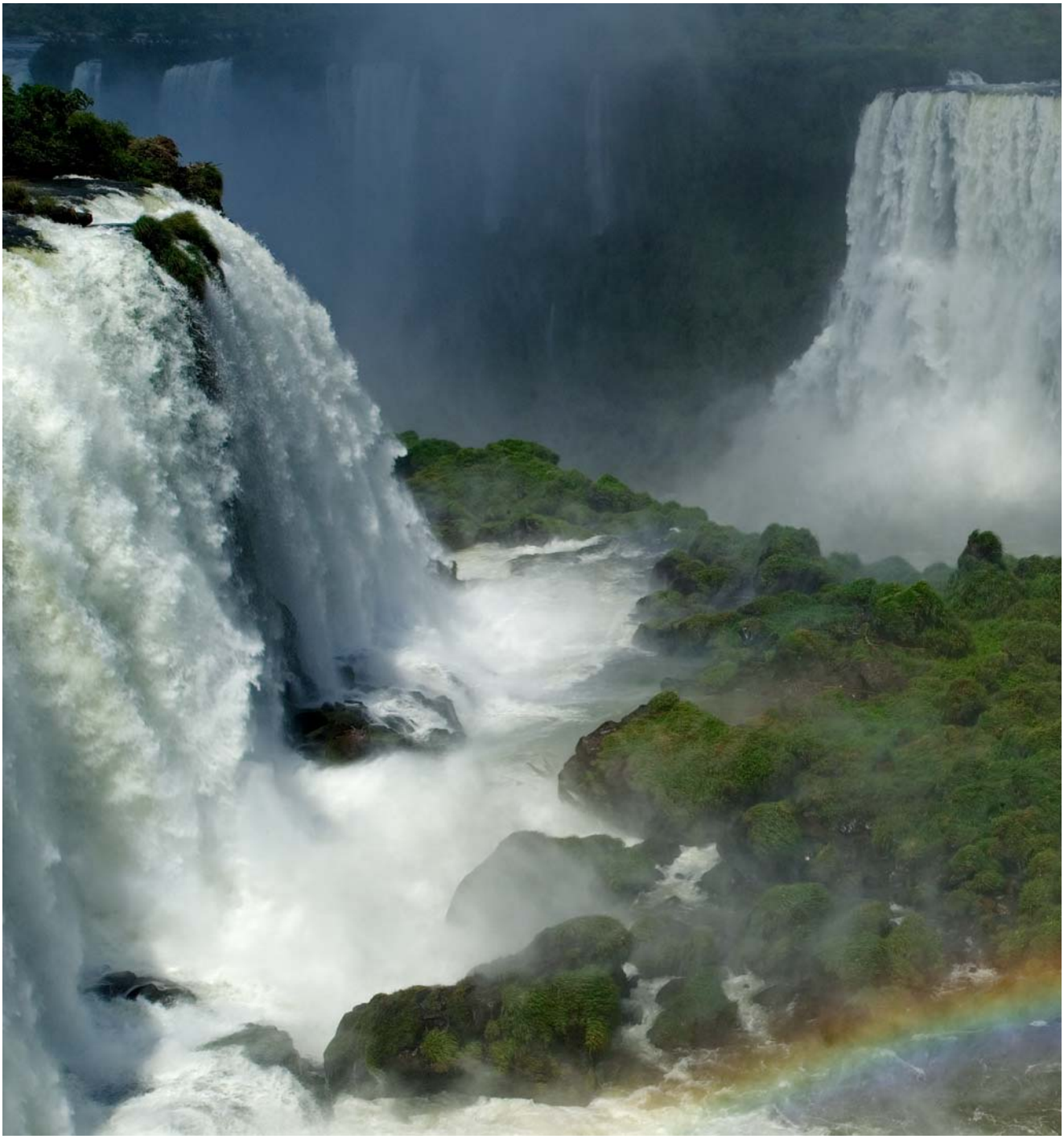

Fig. 2.3. Iguassu Falls, Border of Brazil-Argentina

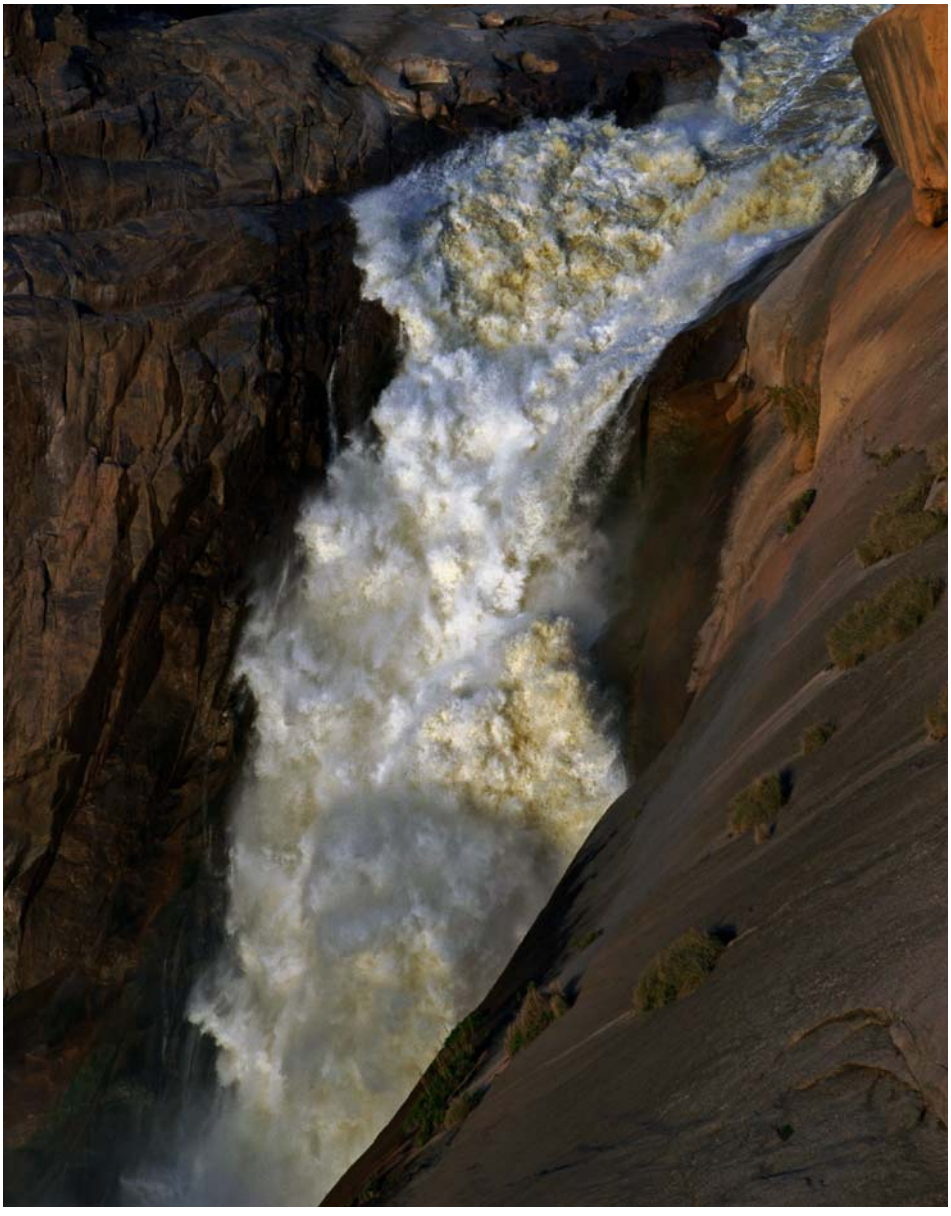

Fig. 2.4. Augrabies Falls, South Africa

Adhémar Jean Claude Barré de Saint–Venant[12]. The main issue is to incorporate the free boundary representing the height-over-bottom $h = h(x,t)$ of the water (measured vertically from the bottom of the river). Let $Z = Z(x)$ be the height of the bottom of the river measured vertically from a constant 0-level below the bottom (thus describing the river bottom topography), which in the most simple setting is assumed to have a small variation. Note that here the space variable x in $\mathbb{R}^1$ or $\mathbb{R}^2$ denotes the horizontal direction(s) und $u = u(x,t)$ the horizontal velocity component(s), the vertical velocity component is assumed to vanish. The dependence on the vertical coordinate enters only through the free boundary h. Then, under certain assumptions, most notably incompressibility, vanishing viscosity, small variation of the river bottom topography and small water height h, the Saint–Venant system reads:

$$\frac{\partial h}{\partial t} + \operatorname{div}(hu) = 0$$

$$\frac{\partial (hu)}{\partial t} + \operatorname{div}(h\,u \otimes u) + \operatorname{grad}\left(\frac{g}{2}h^2\right) + gh \operatorname{grad} Z = 0$$

Here g denotes the gravity constant. Note that $h + Z$ is the local level of the water surface, measured vertically again from the constant 0-level below the bottom of the river. For analytical and numerical work on (even more general) Saint–Venant systems we refer to the paper [4]. Spectacular simulations of the breaking of a dam and of river flooding using Saint–Venant systems can be found in Benoit Perthame's webpage[13].

Many gas flows cannot generically be considered to be incompressible, particularly at sufficiently large velocities. Then the incompressibility constraint $\operatorname{div} u = 0$ on the velocity field has to be dropped and the compressible Euler or Navier–Stokes systems, depending on whether the viscosity is small or not, have to be used to model the flow.

Here we state these systems under the simplifying assumption of an isentropic flow, i.e. the pressure p is a given function of the (nonconstant!) gas density: $p = p(\varrho)$, where p is, say, an increasing differentiable function of ϱ. Under this constitutive assumption the compressible Navier–Stokes equations read:

$$\varrho_t + \operatorname{div}(\varrho u) = 0$$

$$(\varrho u)_t + \operatorname{div}(\varrho u \otimes u) + \operatorname{grad} p(\varrho) = \nu \Delta u + (\lambda + \nu) \operatorname{grad}(\operatorname{div} u) + \varrho f \ .$$

Here λ is the so called shear viscosity and $\nu + \lambda$ is non-negative.

For a comprehensive review of modern results on the compressible Navier–Stokes equations we refer to the text [5].

For the compressible Euler equations, obtained by setting $\lambda = 0$ and $\nu = 0$, globally smooth solutions do not exist in general. Consider the one-dimensional

[12] *http://www-groups.dcs.st-and.ac.uk/~history/Mathematicians/Saint–Venant.html*
[13] *http://www.dma.ens.fr/users/perthame/*

case, the so called p-system, without external force:

$$\varrho_t + (\varrho u)_x = 0$$
$$(\varrho u)_t + \left(\varrho u^2 + p(\varrho)\right)_x = 0$$

This is a nonlinear hyperbolic system, degenerate at the vacuum state $\varrho = 0$. For an extensive study of the Riemann problem we refer to [7] and for the pioneering proof of global weak solutions, using entropy waves and compensated compactness, to [8].

Finally, we remark that the incompressible inviscid Saint–Venant system of hydrology has the mathematical structure of an isotropic compressible Euler system with quadratic pressure law in 1 or, resp., 2 dimensions, where the spatial ground fluctuations play the role of an external force field.

Comments on the Figs. 2.1–2.4 An important assumption in the derivation of the Saint–Venant system from the Euler or, resp., Navier–Stokes equations – apart from the shallow water condition – is a smallness assumption on the variation of the bottom topography, i.e. grad Z has to be small. Clearly, this restricts the applicability of the model, in particular its use for waterfall modelling. Recently, an extension of the Saint–Venant system was presented in [1], which eliminates all assumptions on the bottom topography. There the curvature of the river bottom is taken into account explicitely in the derivation from the hydrostatic Euler system (assuming a small fluid velocity in orthogonal direction to the fluid bottom). We remark that extensions of the Saint–Venant models to granular flows (like debris avalanches) exist in the literature, see also [1].

Comments on the Figs. 2.5–2.6 Turbulent flows[14] are charcacterized by seemingly chaotic, random changes of velocities, with vortices appearing on a variety of scales, occurring at sufficiently large Reynolds number[15]. Non-turbulent flows are called laminar, represented by streamline flow, where different layers of the fluid are not disturbed by scale interaction. Simulations of turbulent flows are highly complicated and expensive since small and large scales in the solutions of the Navier–Stokes equations have to be resolved contemporarily. Various simplifying attempts ('turbulence modeling') exist, typically based on time-averaging the Navier–Stokes equations and using (more or less) empirical closure conditions for the correlations of velocity fluctuations. The flows depicted in the Figs. 2.5 and 2.6 are highly turbulent, with apparent micro-scales.

We remark that the turbulent parts of the flows depicted in the Figs. 2.1–2.6 are two-phase flows, due to the air bubbles entrained close to the free water-air surface interacting with the turbulent water flow.

Fig. 2.5. Turbulent Flow, Cascada de Agua Azul, Chiapas, Mexico

[14] *http://en.wikipedia.org/wiki/Turbulence*
[15] *http://www.efunda.com/formulae/fluids/calc_reynolds.cfm*

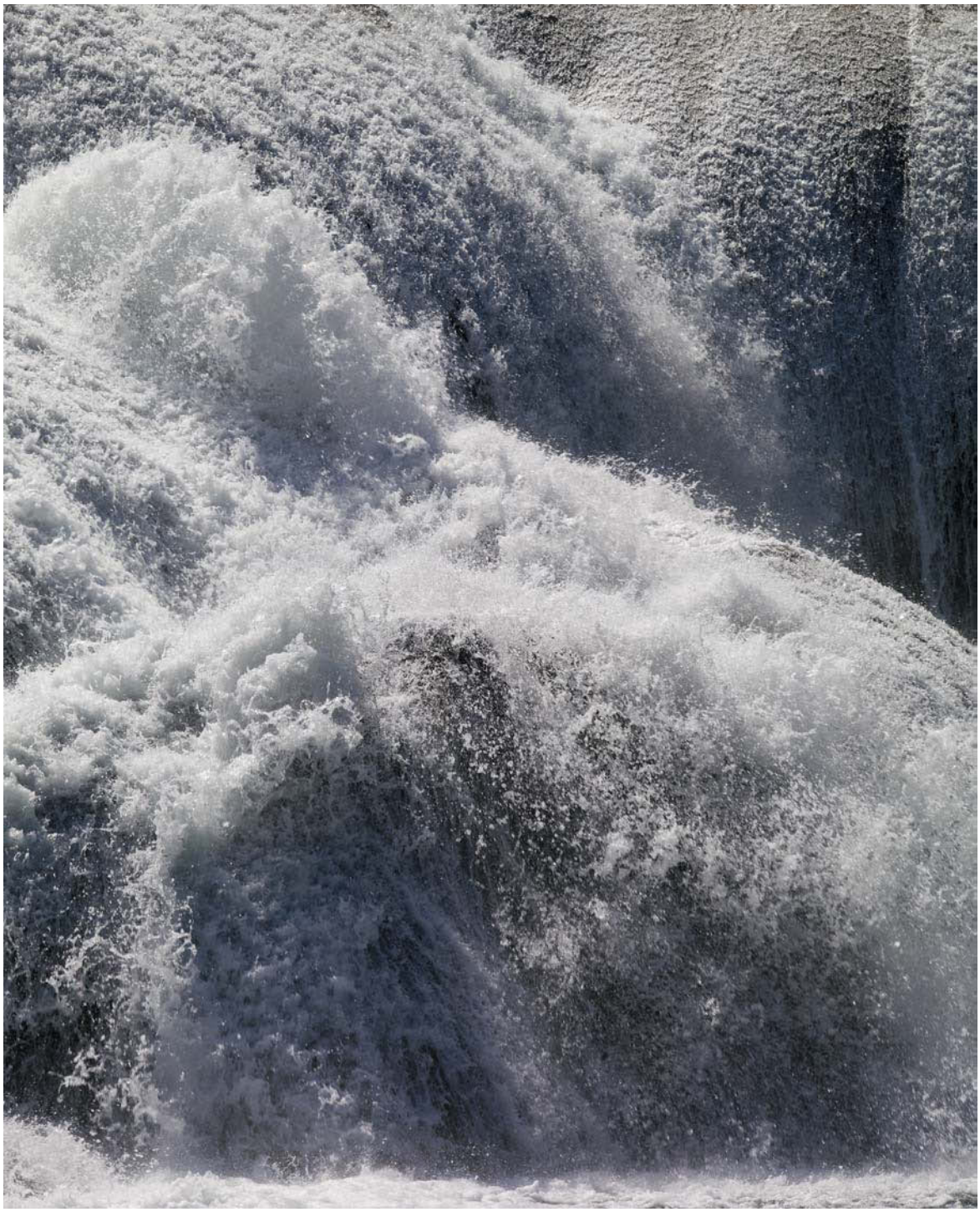

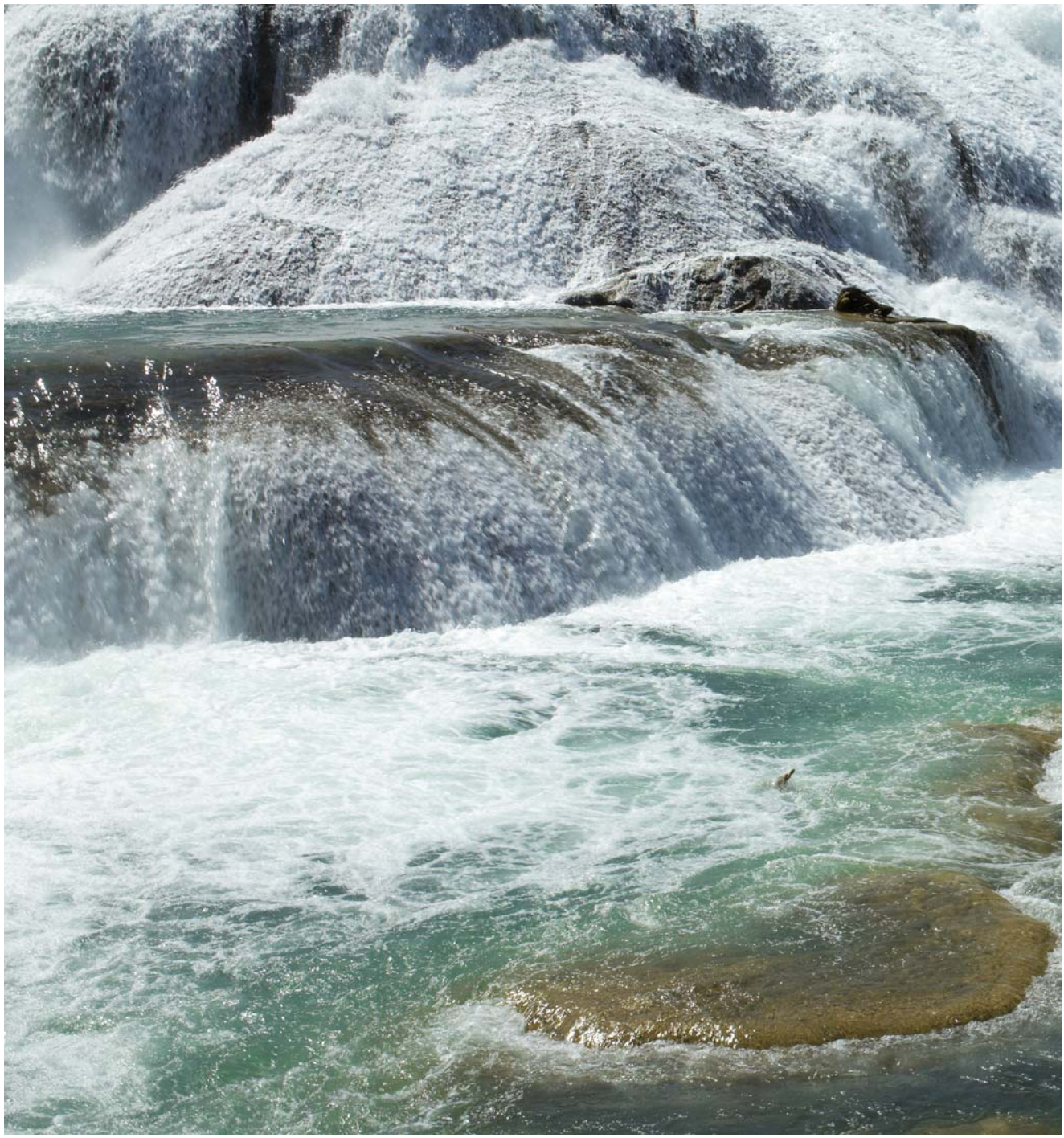

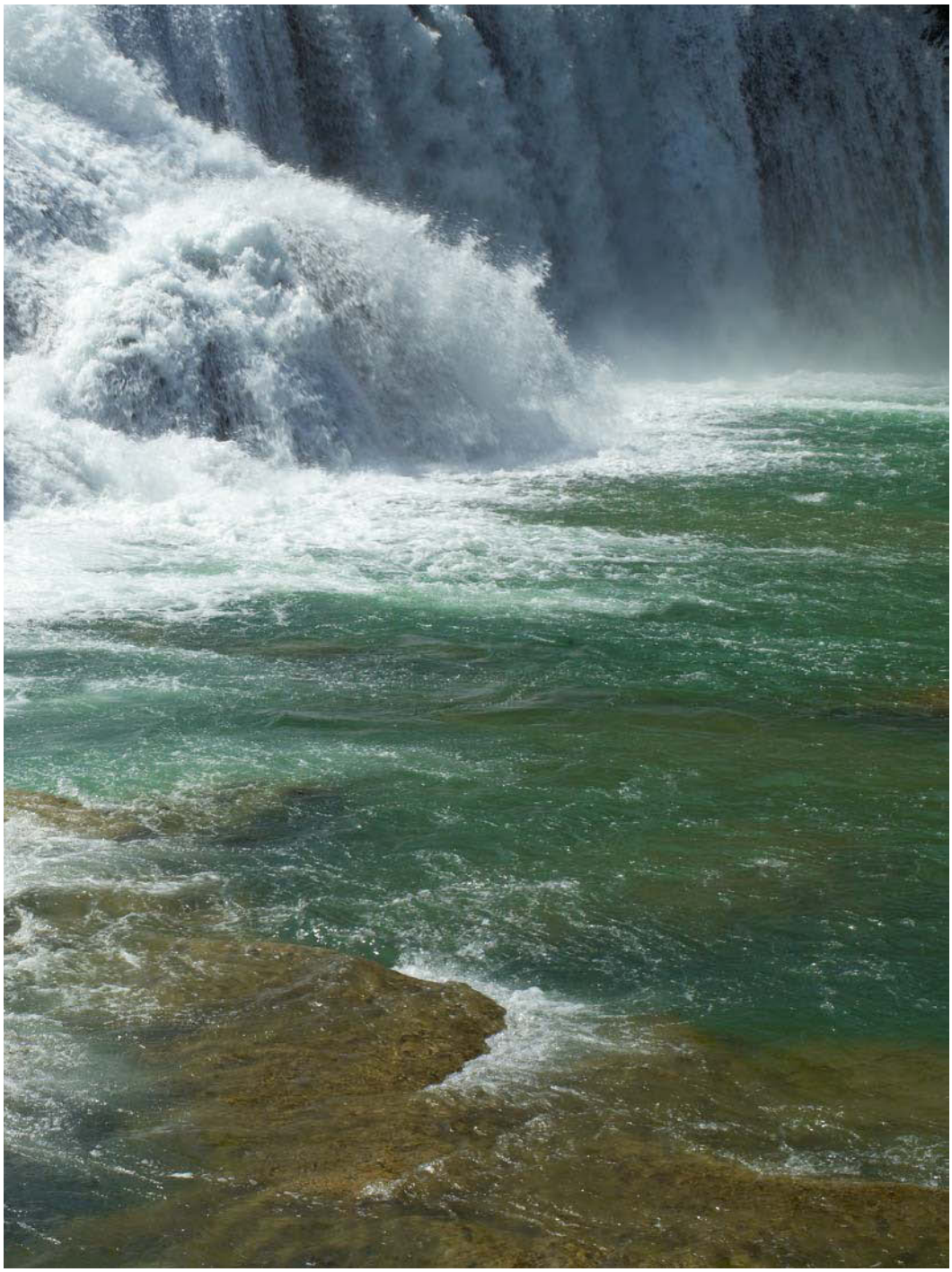

Fig. 2.6. Turbulent (upper part) and laminar (lower part) flow in Cascada de Agua Azul, Chiapas, Mexico, with highly apparent transition region

References

[1] F. Bouchut, A. Mangeney-Castelnau, B. Perthame and J.-P. Vilotte, *A new model of Saint Venant and Savage–Hutter type for gravity driven shallow water flows*, C. R. Acad. Sci. Paris, Ser. I 336, pp. 531–536, 2003

[2] L. Caffarelli, R. Kohn, and L. Nirenberg, *Partial regularity of suitable weak solutions of the Navier–Stokes equations*, Comm. Pure & Appl. Math. 35, pp. 771–831, 1982

[3] C. Cercignani, *The Boltzmann equation and its Application*, Springer-Verlag, 1988

[4] J.-F. Gerbeau and B. Pertame, *Derivation of viscous Saint–Venant system for laminar shallow water; numerical validation*. INRIA RR-4084

[5] P-L. Lions, *Mathematical Topics in Fluid Dynamics, Vol. 2, Compressible Models*, Oxford Science Publication, 1998

[6] O. Ladyzhenskaya, *The Mathematical Theory of Viscous Incompressible Flows (2nd edition)*, Gordon and Breach, 1969

[7] J. Smoller, *Shock Waves and Reaction-Diffusion Equations, (second edition)*, Springer-Verlag, Vol. 258, Grundlehren Series, 1994

[8] R. DiPerna, *Convergence of the Viscosity Method for Isentropic Gas Dynamics*, Comm. Math. Phys., Vol. 91, Nr. 1, 1983

3. Granular Material Flows

Peter A. Markowich and Giuseppe Toscani[1]

We cite from the webpage of the granular flows research group of the California Institute of Technology[2]:

> A granular material flow is a form of two-phase flow consisting of particulates and an interstitial fluid. When sheared the particulates may either flow in a manner similar to a fluid, or resist the shearing like a solid. The dual nature of these types of flows makes them very difficult to analyze.

Granular materials are all around us – examples include food products such as rice, corn, and breakfast cereal flakes, building materials such as sand, gravel and soil, chemicals such as plastics, and pharmaceutical pills.

Another important example of granular flow is the motion of sand dunes[3]. James Jenkins[4] of Cornell University says:

> Moving sand dunes are an example of granular flow – a poorly understood branch of physics,

and

> …the goal is to characterize sheet flows and avalanches using partial differential equations that model the movement of sand grains as if they were particles in a fluid. These equations should contain within them the way avalanches scale with viscosity, velocity of turbulent wind, grain diameter, and gravity…

A distinguishing feature between flows of granular materials and other solid-fluid mixtures is that in granular flows the direct interaction of particles leads to energy dissipation which plays an important role in the flow mechanics. For example, take a pebble and drop it onto the sand on a beach. The pebble will immediately stick in the sand without bouncing back (as would occur in an elastic contact). The reason for this is that a significant fraction of the energy dissipation and momentum transfer in granular flows occurs when particles are in contact with each other or with a boundary. Also, when the pebble is removed from the sand, then only a part of the hole will be filled by sand again-but not the entire hole, typically a dent will remain. The thermal fluctuations are not strong enough to take the granular sand arrangement back into a global energy minimizing state, instead it settles into (one of many possible) local equilibria.

---

1 *http://www-dimat.unipv.it/toscani/*

2 *http://www.its.caltech.edu/~granflow/*

3 see, e.g.,*http://science.nasa.gov/headlines/y2002/06dec_dunes.htm*

4 *http://www.tam.cornell.edu/Jim.html*

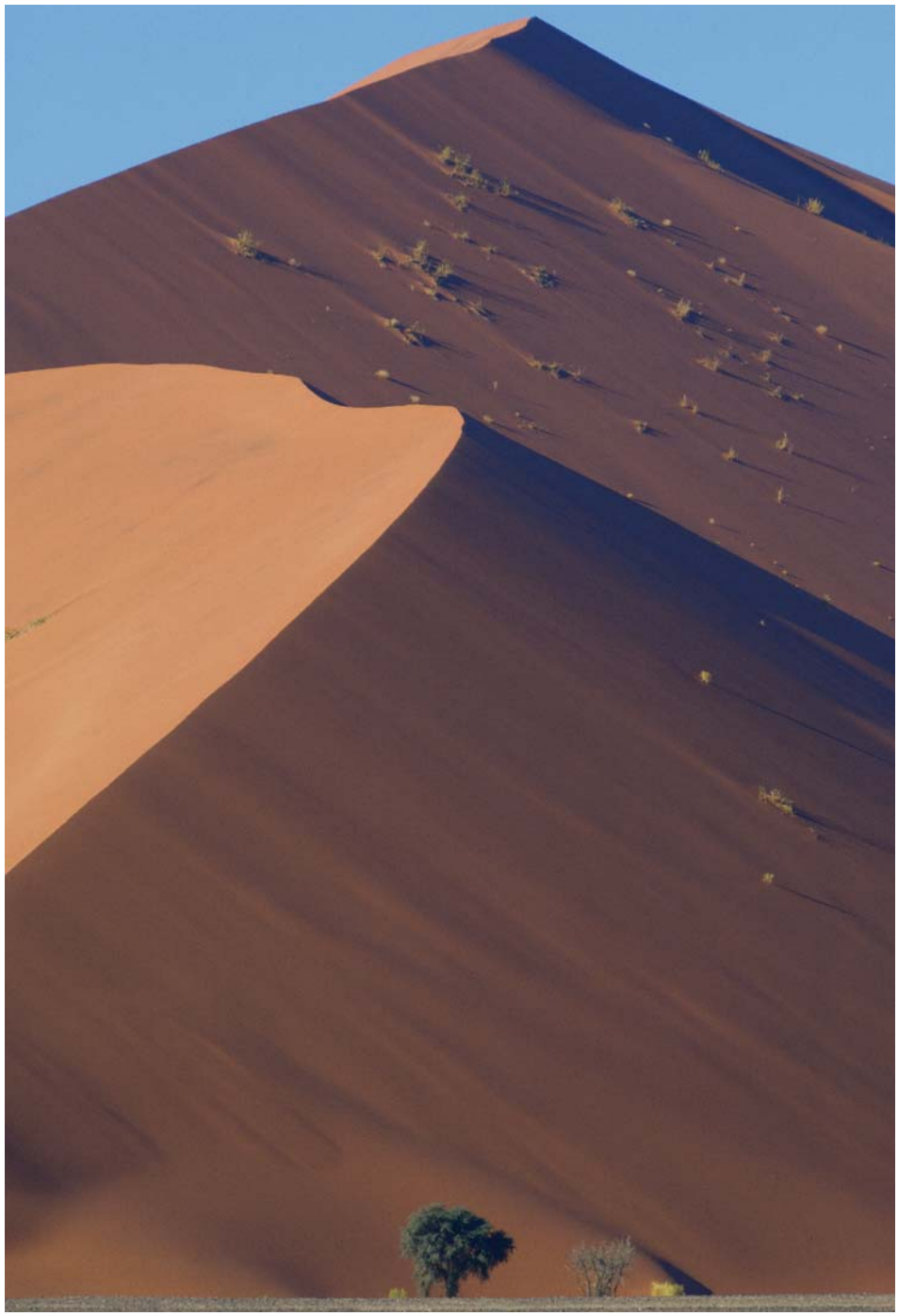

Fig. 3.1. Dune 45 in Sossus Vlei, Namibia

Here are a few more examples of granular flows: grains such as corn or wheat flowing from a silo; landslides of boulders and debris; rock and ice collisions in planetary rings; transport and handling of coal or certain chemicals in industrial plants; powder metallurgy; powder spray coating and lava flow in volcanic eruptions.

A good understanding of the physics of granular flows is of paramount importance in order to design efficient industrial processing and handling systems. The significance of this is apparent when one considers the following data:

- In the chemical industry approximately one-half of the products and at least three-quarters of the raw materials are in granular form.
- Landslides cause more than one billion dollars of property damage and at least 25 fatalities in the United States annually (FEMA).
- In Mexico 5 million tons of corn are handled each year, 30% of which is lost due to poor handling systems.

Even small increases in efficiency can make a significant economic impact.

So far, there still is a poor understanding of how to model granular materials mathematically. Most of the knowledge is empirical and no general approach for analyzing these flows exists. So what can the mathematical modeling be based upon? Clearly, granular material flows are a special topic in the physics of dissipative systems, consisting of dilute systems of inelastically colliding particles. As common for open systems, granular materials reveal a rich variety of self-organized structures such as large scale clusters, vortex fields, characteristic shock waves and others, which are still far from being completely understood.

Most basically, granular flow modeling is often done with molecular dynamics techniques, treating the interactions of individual grains in the material. This technique requires a significant computational overhead and has been to a large extent replaced by continuum models (see [1]). In recent years, granular flows were studied in many aspects from a kinetic point of view, by means of techniques borrowed from the kinetic theory of rarefied gases. The main difference of granular models and the classical kinetic theory of ideal gases (see Chapter 1) lies in the loss of conservation of the second moment of the solution (the energy), which leads to new mathematical questions in kinetic flow equations and the derived hydrodynamics (limit of validity, closure, role of the cooling state).

In a granular gas, the microscopic dynamics of grains heavily depend on the so called restitution coefficient e which relates the normal components of the particle velocities before and after a collision. If we assume that the grains are identical perfect spheres (in $\mathbb{R}^3$) of diameter $D > 0$, (x, v) and $(x - Dn, w)$ are their states before a collision, where $n \in S^2$ is the unit vector along the center of both spheres, and x the position vector of the center of the first sphere, the post collisional velocities (v^*, w^*) then are such that

$$(v^* - w^*) \cdot n = -e\left((v - w) \cdot n\right) . \tag{3.1}$$

Fig. 3.2. Dunes in Sossus Vlei, Namibia

From (3.1), and assuming the conservation of momentum, one finds the change of velocity for the colliding particles as

$$v^* = v - \frac{1}{2}(1+e)\left((v-w)\cdot n\right) n\,, \quad w^* = w + \frac{1}{2}(1+e)\left((v-w)\cdot n\right) n\,. \tag{3.2}$$

For elastic collisions (e.g. atoms in an ideal gas) one has $e = 1$, while for inelastic collisions e decreases with increasing degree of inelasticity.

Following the standard procedures of kinetic theory, the evolution of the distribution function can be described by the Boltzmann–Enskog equation for inelastic hard-spheres,

$$\frac{\partial f}{\partial t} + v\cdot \mathrm{grad}_x\, f = G(\varrho)\bar{Q}\,(f,f)(x,v,t)\,, \tag{3.3}$$

where $\bar{Q}$ is the so-called granular collision operator, which describes the change in the density function due to creation and annihilation of particles in binary collisions:

$$\bar{Q}(f,f)(v) = 4\sigma^2 \int_{\mathbb{R}^3} \int_{S_+} q \cdot n \left\{ \chi f(v^{**}) f(w^{**}) - f(v) f(w) \right\} dw\, dn\,. \qquad (3.4)$$

In (3.3)

$$\rho(x,t) = \int_{\mathbb{R}^3} f(x,v,t)\, dv$$

is the position space grain density at time t, and the function $G(\rho)$ is the statistical correlation function between particles, which accounts for the increasing collision frequency due to the excluded volume effects.

In (3.4), $q = v_1 - v_2$, and S_+ is the hemisphere corresponding to $q \cdot n > 0$. The velocities (v^{**}, w^{**}) are the pre collisional velocities of the so-called inverse collision, which results from (v, w) as post collisional velocities. The factor χ in the gain term stems from the Jacobian of the transformation $dv^{**}dw^{**}$ into $dvdw$ and from the lengths of the collisional cylinders $e|q^{**} \cdot n||q \cdot n|$. For a constant restitution coefficient, $\chi = e^{-2}$.

Fig. 3.3. Barchan Dune in Sossus Vlei, Namibia

Due to dissipation, a granular gas cools down. One of the main problems is to describe this cooling in the hydrodynamic setting, by scaling limits from the granular Enskog–Boltzmann equation.

For the following, we define the scaled mean free path of the granular material in a density-dependent way, by the reciprocal of

$$G(\varrho) = \frac{1}{\varepsilon} g(\varrho) \,,$$

where ε is a small positive parameter (microscopic/macroscopic ratio).

Under the assumption of sufficiently weak inelasticity the Enskog–Boltzmann equation can be approximated in leading order by

$$\frac{\partial f}{\partial t} + v \cdot \operatorname{grad}_x f = G(\varrho) Q(f,f)(x,v,t) + G(\varrho)\beta I(f,f)(x,v,t) \,, \tag{3.5}$$

where Q is the classical elastic Boltzmann collision operator, and I is a dissipative nonlinear friction operator which is based on inelastic collisions between particles. The parameter β determines the strength of the inelasticityof the particle

collisions and is often assumed to be related to the restitution coefficient e by the equation

$$\beta = \frac{1-e}{2} .$$

Note that the operator Q has mass, momentum and energy as collision invariants while the collision invariants of the friction operator are only mass and momentum, not energy. From this expansion of the total collision operator, one can derive the fluid dynamical equations assuming that β is of the same order of magnitude as ε.

To this aim, assuming that Q is the classical elastic ideal gas Boltzmann collision operator, we obtain

$$\int_{\mathbb{R}^3} \psi(v) \left(\frac{\partial f}{\partial t} + v \cdot \operatorname{grad}_x f - g(\varrho) \frac{\beta}{\varepsilon} I(f,f)(x,v,t) \right) dv = 0 \tag{3.6}$$

since

$$\frac{1}{\varepsilon} g(\varrho) \int_{\mathbb{R}^3} \psi(v) Q(f,f)(x,v,t)\, dv = 0 ,$$

provided ψ is a collision invariant of Q, i.e. $\psi = 1, v, \frac{1}{2}|v|^2$. It is well-known that the system (3.6) for the moments of f , which is in general not closed, can be closed in the usual way by assuming f to be the local Maxwellian distribution function M:

$$M(x,v,t) = \varrho(x,t)/(2\pi T(x,t))^{3/2} \exp\left(-\frac{|v-u(x,t)|^2}{2T(x,t)} \right) ,$$

where the parameter functions (unknowns) are the density $\varrho(x,t)$, mean velocity $u(x,t)$ and temperature $T(x,t)$.

Since the dissipative operator I is such that $\psi = 1, v$ are collision invariants, substituting $f = M$ into (3.6), leads to the following macroscopic Euler-type PDE system

$$\begin{aligned} \frac{\partial \varrho}{\partial t} + \operatorname{div}(\varrho u) &= 0 \\ \frac{\partial u}{\partial t} + (u \cdot \operatorname{grad}) u + \frac{1}{\varrho} \operatorname{grad} p &= 0 \\ \frac{\partial T}{\partial t} + (u \cdot \operatorname{grad}) T + \frac{2}{3} T \operatorname{div} u &= -\frac{\beta}{\varepsilon} C g(\varrho) \varrho T^{3/2} \end{aligned} \tag{3.7}$$

where the pressure is given by the constitutive equation $p = \varrho T$, and C is an explicitly evaluable constant. As mentioned above, this approximation is valid when both $\varepsilon \ll 1, \beta = \frac{1-e}{2} \ll 1$ in such a way that $\frac{\beta}{\varepsilon} = \lambda = \text{const}$.

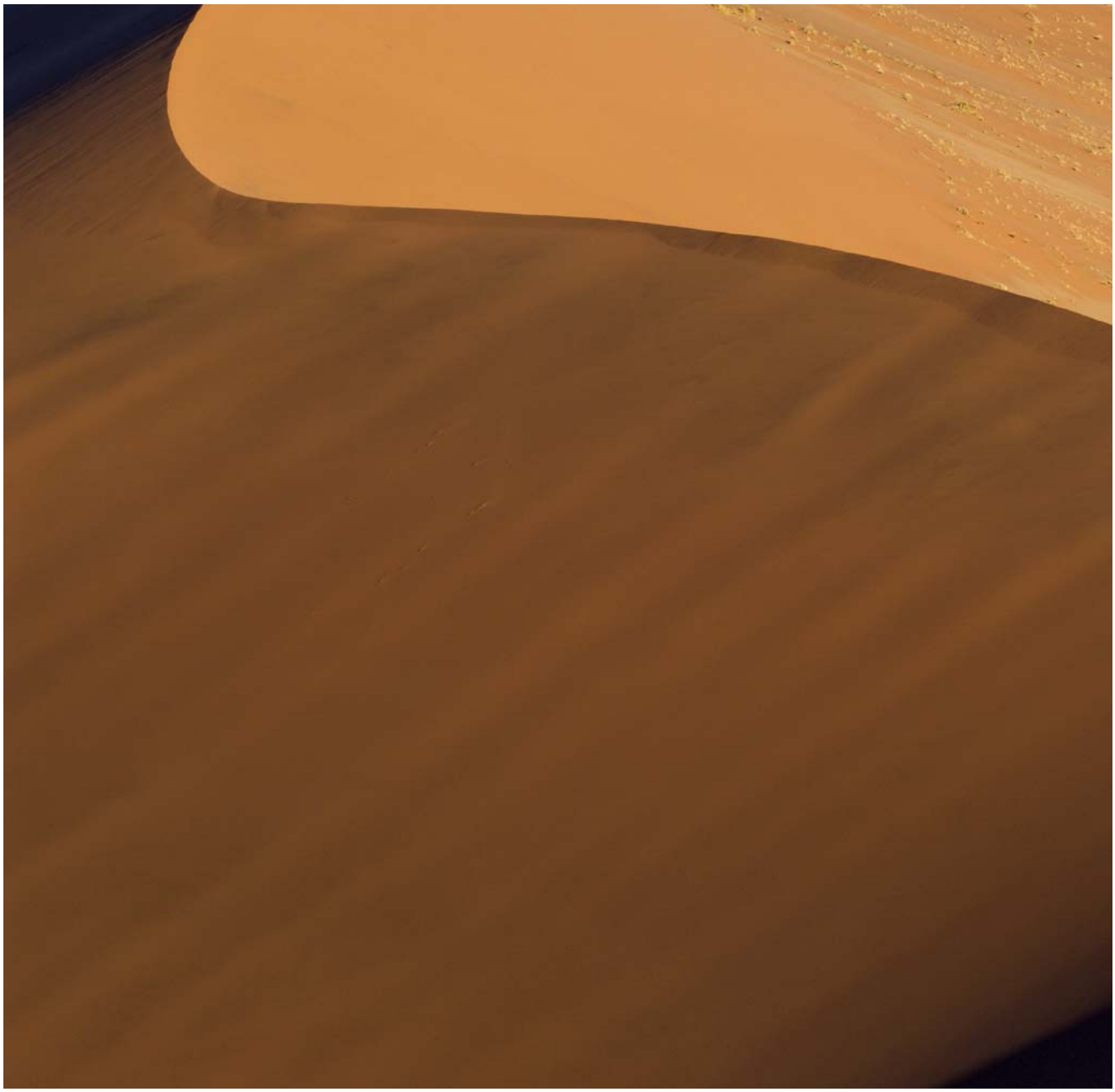

Fig. 3.4. Ridge of a Dune in Sossus Vlei, Namibia

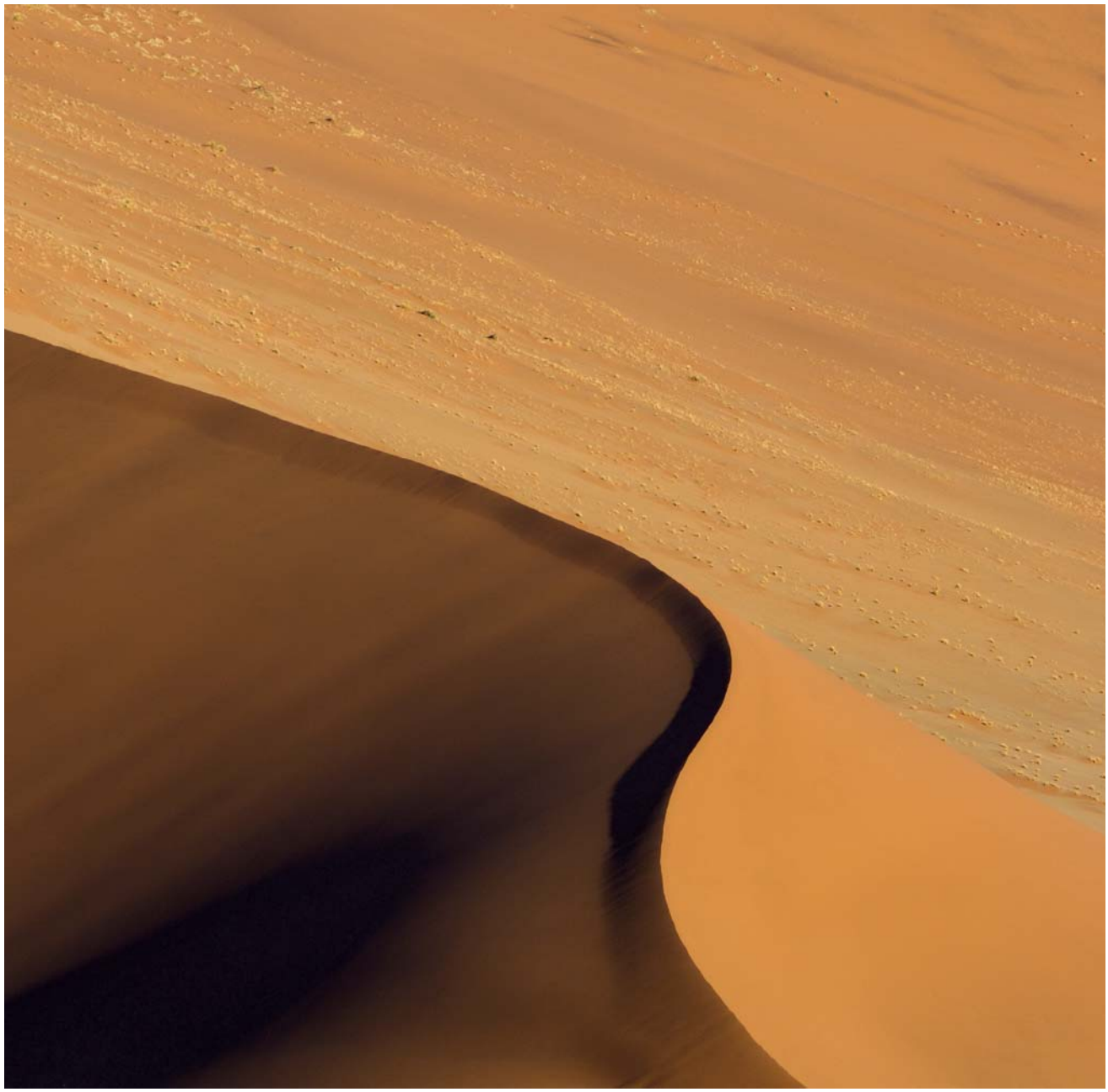

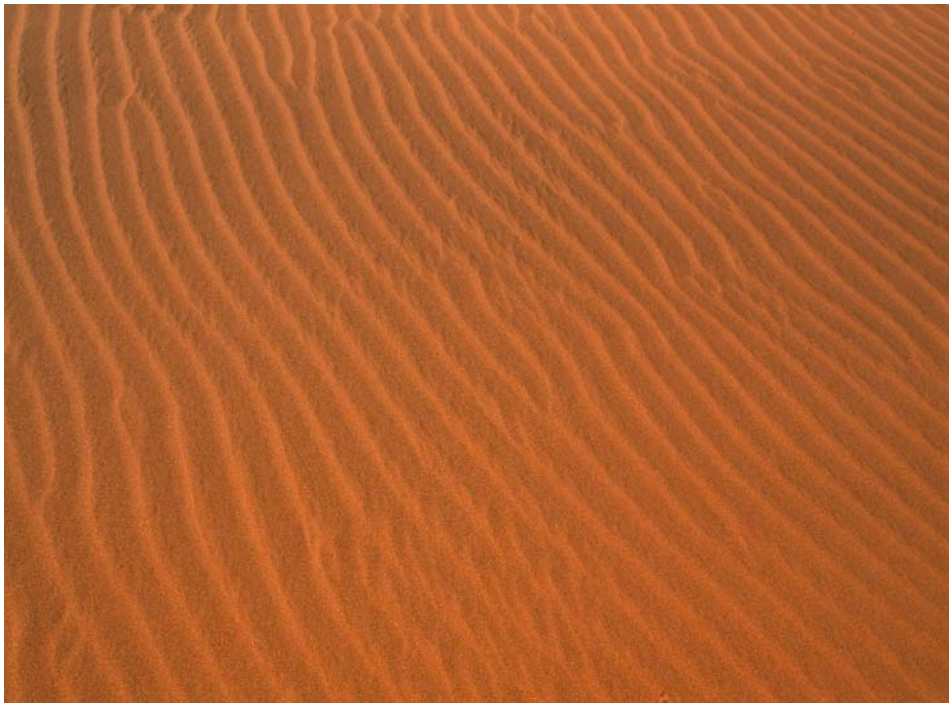

Fig. 3.5. Wind ripples in Sossus Vlei, Namibia

The obtained flow equations have the form of a compressible Euler system with a temperature relaxation term. More precisely, the temperature $T(x,t)$ relaxes according to the so-called Haff's law. This implies that – in the case of vanishing bulk velocity and time-independent position density – the temperature relaxes to 0 with the algebraic rate t^{-2}.

For details and for a collection of references on granular flows we refer to [5] and [6].

Comments on the Images 3.1– 3.10 The formation of sand dunes involves various complicated geophysical mechanisms: sediment transport, avalanches, wind field driven aeolian transport of course taking into account that sand is a typical granular material, with transport being dominated by localised inelastic collisions between sand grains and by saltation (jumping movement of grains over the surface), driven by turbulent wind flow. Clearly, these two types of sand grain movement require different mathematical modeling: the former is described by short range interactions modeled by the granular material Boltzmann-type equation as stated in Chapter 3, the latter by convection representing the wind field in conjunction with inelastic collisions when grains hit the sand surface after saltation. Also, we remark that the microscopic properties (shape, size etc.) of sand grains may vary substantially! We refer to the Ph.D. thesis [4] for various

fluid type modeling approaches, with interesting simulations of barchan dune evolution. Also we refer to the webpage of Dr. H. Momiji[5] for more information on dune dynamics and its mathematical modeling. For fascinating images of sand dunes on Mars see: *http://mars.jpl.nasa.gov/gallery/sanddunes/*.

[5] *http://www.geog.ucl.ac.uk/~hmomiji/*

Fig. 3.6. Sunset in a dune field, Sossus Vlei, Namibia

Fig. 3.7. A sand dune, Atacama desert, Chile

Fig. 3.8. Dunes, Death Valley, California

Fig. 3.9. Footprints in a sand dune, Death Valley, California. Just one stable configuration, out of many possible ones…

Fig. 3.10. Pattern of wind ripples, Death Valley California

Fig. 3.11. A granular (pattern) equilibrium state in a Zen garden in Kyoto, Japan

Fig. 3.12. A stable pile of small pebbles in a Zen garden in Kyoto, Japan. For the modeling of the growth, collapse and stability of piles of granular materials, in the context of the Monge–Kantorovich mass transportation theory, using p-Laplace equations we refer to the survey of L. C. Evans [2] and, for more mathematical detail, to [3]

References

[1] I.S. Aranson, L. S. Tsimring, and D. Volfson, *Partially fluidized shear granular flows: Continuum theory and molecular dynamics simulations*, PHYSICAL REVIEW 68, 021301, 2003

[2] L.C. Evans, *Partial Differential Equations and Monge–Kantorovich Mass Transfer*, in: Current Developments in Mathematics 1997, ed. by S.T. Yau[6]

[3] L.C. Evans, M. Feldman and R. Gariepy, *Fast/slow Diffusion and collapsing Sandpiles*, J. Differential Equations 137, pp. 166–209, 1997

[4] G. Sauermann, *Modeling of Wind Blown Sand and Desert Dunes*, Ph.D. Thesis, Universität Stuttgart, Institut für Computeranwendungen, Logos Verlag Berlin, 2001

[5] G. Toscani, *Hydrodynamics from the dissipative Boltzmann equation*, in Mathematical models of granular matter, Lecture Notes in Mathematics, Springer, G. Capriz, P. Giovine and P.M. Mariano Edts, (in press) (2006)[7]

[6] C. Villani, *Mathematics of Granular Materials*, to appear in J. Stat. Phys.[8], 2006

[6] can be downloaded from *www.math.berkeley.edu/∼evans*

[7] can be downloaded from *http://www-dimat.unipv.it/toscani/*

[8] can be downloaded from *http://www.umpa.ens-lyon.fr/ cvillani/Cedrif/B06.Granular.pdf*

4. Chemotactic Cell Motion and Biological Pattern Formation

Peter A. Markowich and Dietmar Ölz[1]

One of the most important principles governing the movement of biological cells is represented by chemotaxis, which refers to cell motion in direction of the gradient of a chemical substance. In some cases the chemical is externally produced, in others the cells themselves generate the chemical in order to facilitate cell aggregation. In certain biological processes more than one chemical is actually responsible for the chemotactic cell motion. Typical examples of chemotaxis occur in embryology, in immunology, tumor biology, aggregation of bacteria or amoeba etc.

The most basic and most famous mathematical model for chemotaxis was originally derived in 1953 by C.S. Patlak [7] and then in 1970 by E. Keller and L.A. Segel [4]. Meanwhile, this so called Keller–Segel model has become one of the most well analyzed systems of partial differential equations in mathematical biology, giving many insights into cell biology as well as into the analysis of nonlinear partial differential equations.

The main unknowns of the Keller–Segel system are the nonnegative cell density $r = r(x,t)$ and the chemical concentration $S = S(x,t)$, where x denotes the one, two or three dimensional space variable and $t > 0$ the time variable. Then, based on the hypothesis that cell motion is driven by diffusion on one hand and by the gradient of the chemical as driving force on the other hand, the cell density satisfies the (parabolic) partial differential equation of convection-diffusion or Fokker/Planck type:

$$r_t = \operatorname{div}(D_0 \operatorname{grad} r - cr \operatorname{grad} S) \tag{4.1}$$

where D_0 is the positive cell diffusivity and c the positive chemotactic sensitivity. In many realistic modeling situations, D_0 and c have to be allowed to depend on the cell density r and on the chemical concentration S. We remark that diffusion corresponds to undirected random (Brownian) motion of the cells, while the convection by the chemo-attractant stems from the reorientation phase of the cell motion, in direction of the gradient of the chemical concentration. These two phases in the cell motion have been observed very well for the slime mold Dictyostelium discoideum.

The temporal variation of the chemical is also determined by diffusion on one hand and, on the other hand, by its production (by external sources or by the cells themselves) and its degradation (e.g. due to chemical reactions). This

[1] *http://homepage.univie.ac.at/dietmar.oelz/*

leads to the reaction-diffusion equation:

$$S_t = \operatorname{div}(D_1 \operatorname{grad} S) + g(r, S) \,. \tag{4.2}$$

Here D_1 stands for the (positive) diffusivity of the chemical and g for its production/degradation rate, i.e. $g > 0$ describes production of the chemical and $g < 0$ its degradation. The Keller–Segel model is thus comprised of the coupled parabolic system (4.1) and (4.2), supplemented by appropriate conditions for r and S on the boundary of the modeling domain B (e.g. the Petri dish boundaries) and by initial conditions for r and S. The classical Keller–Segel model refers to equations (4.1) and (4.2), with constant and positive diffusivities and chemotactic sensitivity and with the linear production/degradation model:

$$g(r, S) := dr - eS \,, \tag{4.3}$$

where d and e are positive constants. This classical Keller-Segel model, with appropriately fitted parameters, is often sufficient to describe real chemotactic processes with good qualitative and reasonable quantitative agreement.

In many cases, however, it is of great importance to include specific features of individual cells, to deal with stochasticity [8] or to employ microscopic

Fig. 4.1. Giraffe fur pattern

phase-space models replacing the macroscopic Fokker–Planck equation (4.1), similarly to the framework of the Boltzmann equation of gas dynamics (the macroscopic Euler or Navier–Stokes equations correspond to the Fokker–Planck equation (4.1) in this comparison!). A presentation of the corresponding model hierarchy, the connections of the different PDE models in the hierarchy and a collection of references on the mathematical analysis of kinetic and macroscopic chemotaxis models can be found in [3]. The scaling limit of a phase space chemotaxis model leading to the Keller–Segel model was rigorously analysed in [1].

For what follows we consider the classical Keller–Segel model consisting of (4.1), (4.2) and (4.3) with the additional assumption $e = 0$ (no degradation of the chemical and d and D_1 very large, such that the parabolic reaction diffusion equation (4.2) can be approximated by the linear elliptic equation

$$-\Delta S = r \tag{4.4}$$

(after appropriate rescaling). We assume that (4.1) and (4.4) are posed on $\mathbb{R}^n$, $n = 1, 2$ or 3 and look for solutions such that r decays to 0 as $|x|$ tends to infinity. This nonlinear, nonlocally coupled elliptic-parabolic system of partial

Fig. 4.2. Kudu coat

Fig. 4.3. Zebra coat pattern

differential equations exhibits a fascinating feature, under certain conditions on the initial datum

$$r(x, t = 0) = r_0 \ , \tag{4.5}$$

namely finite time blow-up of solutions. More precisely, two cases have to be distinguished for $n = 2$ (two space dimensions!), where we denote the total initial cell mass by:

$$M_0 := \int\limits_{\mathbb{R}^2} r_0(x) \ dx \ .$$

These cases are:

Case A: $M_0 < 8\pi D_0/c$. Then a global weak solution of (4.1), (4.4), (4.5) exists.
Case B: $M_0 > 8\pi D_0/c$. Then solutions r of (4.1), (4.4), (4.5) blow up in finite time, global in time solutions do not exist.

Usually, Case A is referred to as subcritical case (mass is small enough such that finite time blow up can be avoided) and Case B (mass is too big, finite time blow up occurs) as supercritical. There is no finite time blow up for the one dimensional classical Keller–Segel model while three dimensional solutions generically concentrate in finite time. We remark that the mechanism, which inhibits the global existence of solutions in the supercritical case, is concentration of the cell density, i.e. $r(x, t)$ tends locally to a Dirac-δ distribution when t approaches a finite blow-up time T. Beyond blow up time the solutions cannot be extended without somewhat redefining the problem. The reason for the non-existence of time-global solutions is that the production of the chemical by the cells generates an attractive force field, just as for PDE models of gravitational particles. This is totally different from the situation where the cells (presumably) destroy the chemical (which corresponds to changing the sign of the chemotactic sensitivity c in (4.1)), analogously to the repulsive Coulomb force acting on the charged particles in semiconductors, modeled by the semiconductor drift-diffusion system. To better understand the mechanism of an attractive resp. repulsive force, choose a number $q > 1$, multiply the Fokker–Planck equation (4.1) by qr^{q-1} and integrate over $\mathbb{R}^n$. Then, after integration by parts and using (4.4) we obtain, assuming that c is constant:

$$\frac{d}{dt} \int r(x, t)^q \ dx = - \int q(q-1)D_0 |\nabla r|^2 r^{q-2} \ dx + (q-1)c \int r^{q+1} \ dx \ .$$

Thus, the right hand side is nonpositive if c is nonpositive (repulsive case) and consequently the L^q-norm of the position density r is uniformly bounded for $t > 0$. Clearly, this excludes a concentration in the density r. Note that this argument fails in the case of an attractive force $c > 0$!

The phenomenon of finite time blow up of solutions of the classical Keller–Segel model has been extensively discussed in the bio-mathematical literature. Clearly, the local pre-blow up behaviour corresponds to biologically reasonable cell accumulation due to the chemotactic attraction and has been observed in experiments, e.g. with the slime mold Dictyostelium discoideum. However, concentration of the cell density in a single point is clearly biologically unreasonable and has to be considered a defect of the model. We remark that this defect can be repaired rather easily, for example by taking a chemotactic sensitivity $c = c(r)$, which decays to zero as r tends to infinity. This is referred to as "quorum sensing".

We now turn our attention to the modeling of pattern formation in the context of embryology. Embryology is the area of biology, which is concerned with the formation and development of a embryos from fertilisation until birth. Morphogenesis as a part of embryology deals with the development of patterns and forms. One of the major problems in biology is how genetic information is physically translated into the desired patters and forms. We typically observe that cells move around within the embryo and finally differentiate according to their position. But why does this happen?

Positional information is a phenomenological concept of pattern formation and differentiation introduced by Wolpert [10]. He suggested that cells are pre-programmed to react to a chemical ("morphogen") concentration and differentiate accordingly. The first step however is the creation of the morphogen concentration spatial (pre)pattern. The further morphogenesis is then a slave process. Often, chemotaxis is considered to be a mechanism for density pre-pattern formation. More precisely, cell differentiation occurs in regions of high cell density [6], possibly generated by chemotactic attraction. A mathematical study of spatial patterns and their stability in one-dimensional Keller–Segel models with small cell diffusivity can be found in [2].

In the sequel we shall discuss (cp. [5]) a model for morphogenesis, based on reaction-diffusion equations, as introduced by A.M. Turing[2] in the year 1952 [9]. The unknowns are the concentrations of two chemical species, $u > 0$ and $v > 0$. We assume that the modeling domain B is a subset of $\mathbb{R}^n$ with the dimension n either 1, 2 or 3 and that within the set B the two concentrations satisfy the reaction-diffusion system

$$\begin{aligned} u_t &= \Delta u + \gamma f(u, v) \\ v_t &= d\Delta v + \gamma g(u, v) \,. \end{aligned} \tag{4.6}$$

Hence both chemicals are subject to diffusion, but with different diffusion coefficients. Here, already after non-dimensionalisation, the diffusion coefficient of the chemical u is set to one, whereas the diffusivity of v is represented by the constant d. This constant represents the ratio of the diffusion coefficients before non-dimensionalisation. Furthermore both chemicals are subject to production and decay respectively. From non-dimensionalisation we obtain that the extent

[2] *http://www.turing.org.uk/turing/*

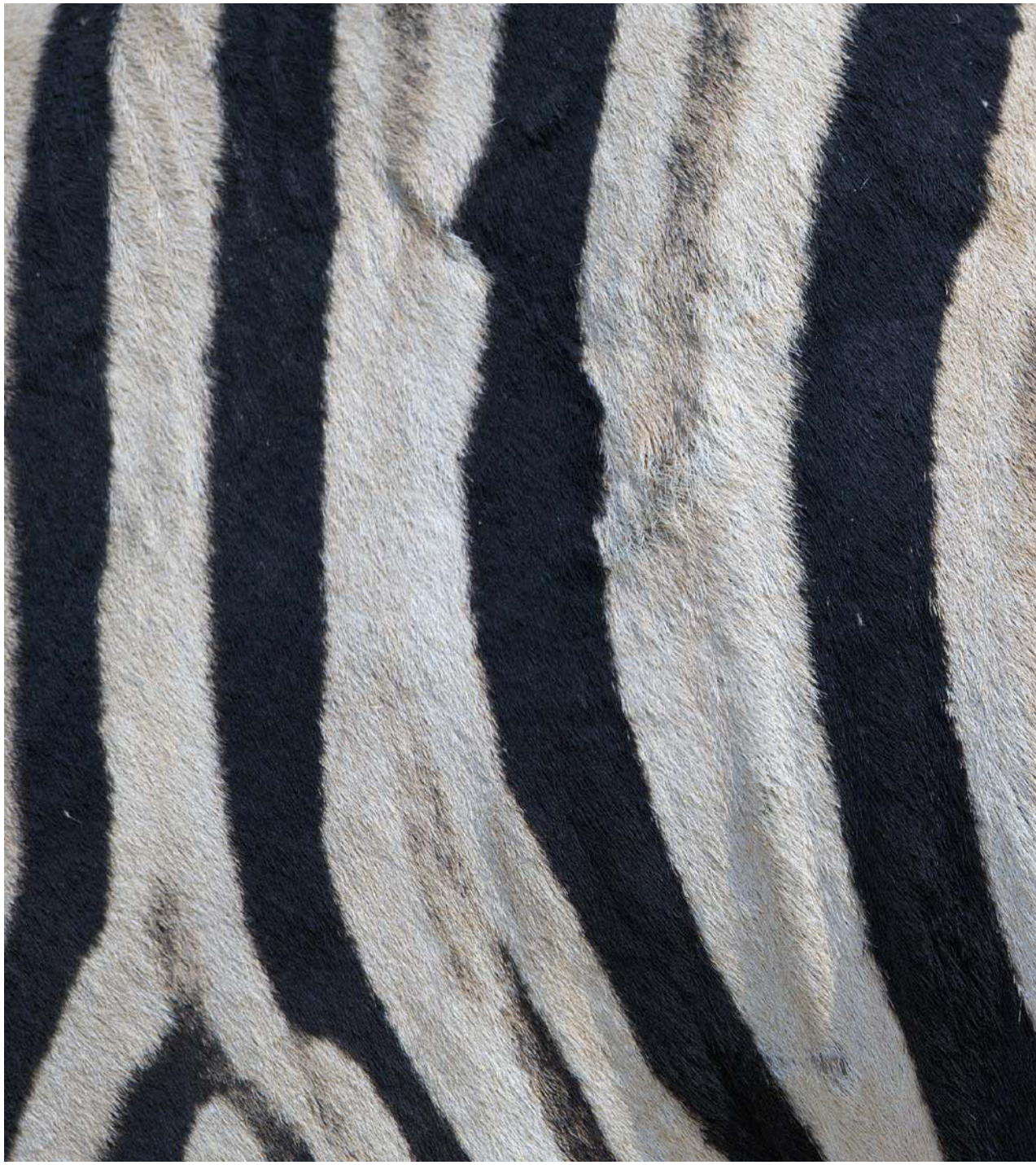

Fig. 4.4. Zebra coat pattern

of production/decay is a multiple of a constant γ which depends on the 'size' of the modeling domain B. To complete the model, we assume that we know the concentrations of the chemicals at time $t = 0$

$$u(., t = 0) = u_I \quad \text{and} \quad v(., t = 0) = v_I \tag{4.7}$$

and that, starting from the initial point in time, the two chemicals can neither flow out of the domain B, nor is any of the two chemicals added. In mathematical terms we express this by the homogeneous Neumann boundary conditions

$$\nu \cdot \operatorname{grad} u = \nu \cdot \operatorname{grad} v = 0 \quad \text{on} \quad \partial B\,, \tag{4.8}$$

where ∂B is the boundary of the domain B and ν is the unit outward normal vector to this boundary. Note that the formulation of production/decay using the two functions $f(u, v)$ and $g(u, v)$ allows that both chemicals may influence their own production/decay as well as production/decay of the other one. Nevertheless from now on we shall interpret the chemical with concentration u as the activator, i.e. it is likely to increase morphogen production, whereas we shall interpret the chemical associated to the concentration v as the deactivator. Hence the presence of the latter chemical is likely to reduce production or even stimulates consumption of the morphogen.

The central idea of *Turing instability* is to construct systems of chemicals with the following property: The concentrations of the chemicals are linearly stable if they are homogeneous. Clearly, variations of concentrations necessarily lead to diffusive effects. If the diffusion coefficients are different (i.e. $d \neq 1$), then diffusion shall lead to instability ("diffusion driven instability") in the sense that initial variations in concentrations get amplified.

This was a novel concept since in the mathematical field of partial differential equations (PDEs) diffusion is usually considered to be a stabilising process, just like variations in temperature in general get equilibrated and inhomogeneous concentrations are expected to smooth out.

The mechanism which in the present case leads to instability works as follows: Imagine regions where, for whatever reason, there is a high concentration of activators and where, as a consequence of activation, lots of inhibitors are produced. The Turing mechanism is based on the fact that the inhibitor substance diffuses faster than the activator chemical. So in these regions the deactivators will diffuse away quickly and will not be able to reduce the concentration of activators.

Most notably in situations, where the size of the modeling domain is finite and where chemicals can neither leave nor enter the domain, the inhibitors

Fig. 4.5. Zebra coat pattern

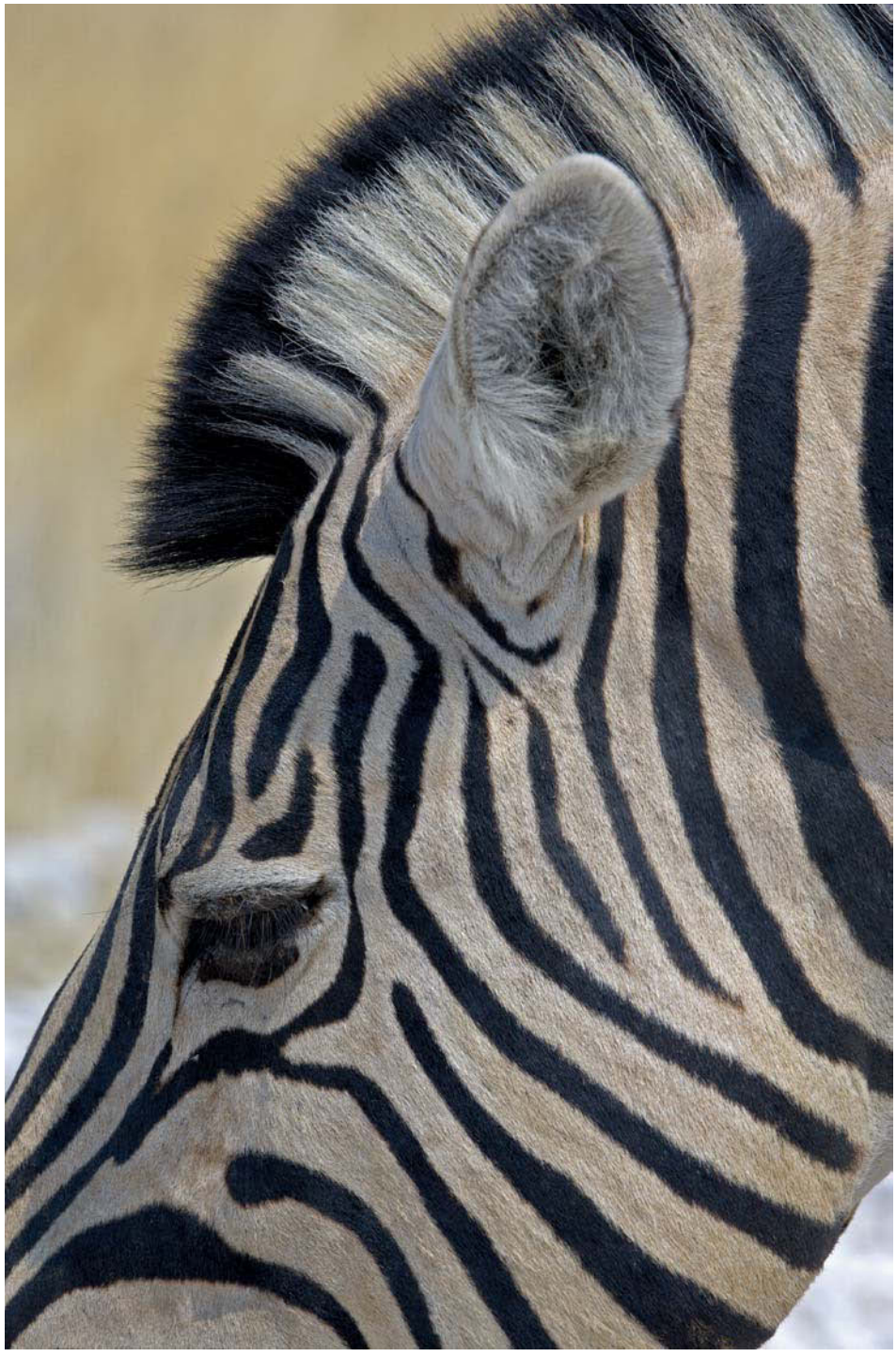

Fig. 4.6. Crocodile Skin

will finally gather at remote positions with only little activator reactant. There they will successfully inhibit the rise of the activator concentration. In total this explains that starting from a small perturbation of a homogeneous situation a pattern of activators and deactivators can finally emerge and stabilise.

We only remark here that the situation is different if the modeling domain is not bounded. Then inhibitors are likely to diffuse farther and farther away from activators, finally to infinity.

We shall analyse now the system (4.6), (4.8), (4.7) in the special case, where the modeling domain is a bounded (one-dimensional) interval,

$$B = [0, L] \quad \text{with length} \quad L > 0\,. \tag{4.9}$$

Most notably we shall determine the so called *Turing space*, i.e. the set of parameter values (the functions f and g and the constants d and γ) for which *Turing instability* can be observed.

We assume that (u_0, v_0) is a homogeneous steady state. Hence u_0 and v_0 are two constants and looking at (4.6) we observe that for this combination of the

Fig. 4.7. Australian saltwater crocodile, skin pattern

two concentrations we have zero production and zero decay,

$$f(u_0, v_0) = g(u_0, v_0) = 0 \,. \tag{4.10}$$

In the sequel we shall analyse the equations (4.6) near this steady state. If we only look at spatially homogeneous, but time-dependent solutions of (4.6) and if we simplify this problem even more by linearisation at the steady state, then we conclude that it is (*linearly*) *stable* at (u_0, v_0) if

$$f_u + g_v < 0 \quad \text{and} \quad f_u g_v - f_v g_u > 0 \,. \tag{4.11}$$

Note that the partial derivatives of f and g here and in the sequel are evaluated at (u_0, v_0). Typically, in the theory of ordinary differential equations linear stability implies local (nonlinear) stability meaning that solutions of the nonlinear problem (4.6), which are constant in space and which are sufficiently close to the steady state (u_0, v_0), will not depart from the steady state as time increases.

The prerequisite of Turing instability is *instability in the presence of spatial inhomogeneity* of the concentrations. To understand this we look at eigenfunctions of the Laplacian such that $w_{xx} = -k^2 w$ and such that the boundary conditions $w_x(0) = w_x(L) = 0$ are satisfied. The functions $w = w_k(x)$ are then multiples of $\cos(n\pi x/L)$, where $n \in \mathbb{Z}$ and $k := n\pi/L$. The value k is called the wave number.

Fig. 4.8. Galapagos giant turtle

We know that linear diffusive systems as (4.6) with zero reaction nonlinearities act (componentwise) on eigenvectors of the Laplacian by damping them with a certain exponential rate $\lambda < 0$. Such solutions are then given by a product $\exp(\lambda t)w_k(x)$. Thus after linearizing (4.6) at (u_0, v_0) we expect that perturbations of the steady state $(u - u_0, v - v_0)$ can be written as $\sum_k \boldsymbol{c}_k \exp(\lambda(k^2)t)w_k(x)$, where the components of $\boldsymbol{c}_k$ are the Fourier coefficients of $u_I - u_0$ and $v_I - v_0$ respectively.

If $\Re\lambda(k^2) < 0$ then the eigenmode with wave number k is damped, but if for some wave number $k \neq 0$ we have $\Re\lambda(k^2) > 0$, then the respective component of the solution blows up as $t \to \infty$ and we call the the system (4.6) (linearly) unstable at (u_0, v_0).

In fact, we even can compute explicitly the largest values $\lambda(k^2)$, which is called *dispersion relation*. Doing so it turns out that we only have instability if

$$a > 0 \quad \text{and} \quad a^2 - 4db > 0$$

where $a := df_u + g_v$ and $b := f_u g_v - f_v g_u$. Most notably the first inequality implies that the diffusion coefficient satisfies $d > 1$. Furthermore it turns out that $\lambda(k^2)$ has positive real part only for those wave numbers k which satisfy

$$\gamma \frac{a - \sqrt{a^2 - 4db}}{2d} < k^2 < \gamma \frac{a + \sqrt{a^2 - 4db}}{2d},$$

The above k-interval is called the *unstable range*. The associated wavelengths will increase in amplitude during the evolution of the system, whereas other wavelengths are damped. Bear in mind that in biological applications γ is a multiple of L^2!

Exemplary choices for the reaction terms, which exhibit Turing instability, are

$$f(u,v) = a - bu + \frac{u^2}{v} \quad \text{and} \quad g(u,v) = u^2 - v \qquad [15]\,,$$

and

$$f(u,v) = a - u - h(u,v) \quad \text{and} \quad g(u,v) = \alpha(b-v) - h(u,v)\,,$$
$$\text{with} \quad h(u,v) := \frac{\varrho uv}{1 + u + Ku^2}\,, \qquad [16]\,,$$

where a, b, α, ϱ and K are positive parameters which have to be chosen appropriately to satisfy the above conditions.

In animal tissue, these unstable modes are interpreted to characterise the patterns, which are amplified during the development of the embryo and which therefore develop spatial inhomogeneity in departing from the homogeneous stationary state. Since k may only adopt discrete values, there is only a finite number of amplified wavelengths.

Unbounded domains B correspond to relevant models in situations where the size of the embryo is much larger than the pattern to be formed and where therefore the boundaries cannot play a major role in isolating specific wavelengths. The analysis is somewhat simpler in this case. In general there is no finite band of amplified modes but one specific wave-number which is associated to the largest eigenvalue. Its pattern will finally emerge.

If the domain B is growing as a function in time, let us say during the growth of the embryo, then the value γ increases and at certain bifurcation points, either dominant modes turn into damped ones, i.e. they fall out of the unstable range, or higher wave-numbers turn from stable to unstable. This process is called *mode selection* and is a possible explanation for the complex evolution of patterns during morphogenesis.

Comments on the Images 4.1–4.8 Various modeling approaches for pattern formation in animal coats, with simulation results, can be found in the Ph.D. thesis [11]. Also Turing's reaction-diffusion model is presented there. For a wealth of information on Turing models for morphogenesis we refer to the webpage[3].

For a cellular automata model, based on Turing's reaction-diffusion model, describing the morphogenesis of zebra coat patterns, we refer to [12].

For images of an artistic interpretation of patterns on human bodies we refer to the webpage[4].

[3] *http://www.math.wm.edu/∼shij/*

[4] *http://www.pbase.com/gpfoto/bianco_nero*

A study on the formation of crocodile skin, discussing the origin of the pigmentation pattern, can be found in [13].

Is has been conjectured in the biological literature that the formation of tortoise shells is based on a chemotactic process, responsible for the lateral growth of the ribs, which then undergo ossification. We refer to [14].

The Images 4.1–4.5 were shot in South Africa and Namibia, 4.6 in the Mexican province Chiapas, 4.7 in northern Queensland (Australia) and 4.8 on the Galapagos Islands (Ecuador).

References

[1] B. Perthame, F. Chalub, P.A. Markowich and C. Schmeiser, *Kinetic models for chemotaxis and their drift-diffusion limits*, Monatsh. Math., 142(1-2), pp. 123–141, 2004

[2] Y. Dolak and C. Schmeiser, *The Keller–Segel model with logistic sensitivity function and small diffusivity*, to appear in SIAM J. Appl. Math., 2005

[3] P.A. Markowich, D. Oelz, C. Schmeiser, F. Chalub, Y. Dolak-Struss and A. Soreff, *Model hierarchies for cell aggregation by chemotaxis*, to appear in M3AS, 2006

[4] E. Keller and L.A. Segel, *Initiation of slime mold aggregation viewed as an instability*, J. Theoret. Biol., 26, pp. 399–415, 1970

[5] J.D. Murray, *Mathematical Biology*, Volume 19 of *Biomathematics*, second edition, Springer, 1993

[6] K.J. Painter, *Chemotaxis as a mechanism for Morphogenesis*, PhD thesis, University of Oxford, 1997

[7] C.S. Patlak, *Random walk with persistence and external bias*, Bull. Math. Biophys., 15, pp. 311–338, 1953

[8] A. Stevens, *The derivation of chemotaxis equations as limit dynamics of moderately interacting stochastic many-particle systems*, SIAM of Appl. Math, 61(1), pp. 183–212, 2000

[9] A.M. Turing, *The chemical basis of morphogenesis*, Philosophical Transactions of the Royal Society (B), 237, pp. 37–72, 1952

[10] L. Wolpert, *Positional information and the spatial pattern of cellular differentiation*, J. theor. Biol., 25, pp. 1–47, 1969

[11] M. Walter, *Integration of Complex Shapes and natural Patterns*, Ph. D. thesis, Department of Computer Science, University of British Columbia, Canada, 1998

[12] C.P. Gravan and R. Lahoz-Beltra, *Evolving Morphogenetic Fields in the Zebra Skin Pattern Based on Turing's Morphogen Hypothesis*, Int. J. Appl. Math. Comput. Sci., Vol. 14, No. 3, pp. 351–361, 2004

[13] L. Alibardi, *Immunocytochemistry and Keratinization in the Epidermis of Crocodilians*, Zoological Studies 42 (2), pp. 346–356, 2003

[14] J. Cebra-Thomas et al., *How the Turtle Forms its Shell: A Paracrine Hypothesis of Carapace Formation*, Journal of Experimental Zoology (Mod Dev Evol), 304B, pp. 558–569, 2005
[15] A. Gierer and H. Meinhardt, *A theory of biological pattern formation*, Kybernetik 12, pp. 30–39, 1972
[16] D. Thomas, *Artificial enzyme membranes, transport, memory, and oscillatory phenomena*, in: D. Thomas and J.-P. Kernevez (eds.): Analysis and Control of Immobilized Enzyme Systems, Berlin Heidelberg New York: Springer, pp. 115–150, 1975

5. Semiconductor Modeling

In pedestrian solid state physics terms semiconductors (e.g. silicon, germanium, gallium arsenide …) are materials whose electrical conductivity properties lie between those of a conductor (i.e. a metal) and those of an insulator (e.g. glass). This is precisely what allows to control the electrical properties of the material by systematic and appropriate modification from the outside. This modification is usually done by implanting impurity atoms into the semiconductor, which – once inserted into the semiconductor crystal lattice – become ionised by either donating a conduction band electron (creating an additional free negative charge) or absorbing a valence band electron (creating an additional free positive charge, a so called hole). The implantation process is called doping of the semiconductor. Typically, a semiconductor has a conduction band density of 10^{11} free electrons per cm^3, by doping this number can be raised to 10^{20}!!! The doping process, typically carried out through diffusion processes in high tech clean rooms of the chip production companies and laboratories, controls the electrical properties of semiconductor devices. More precisely, the position densities of the dopants, for electron donors and for electron acceptors, determine the electrical functioning of the produced device.

For the subsequent mathematical discussion we denote by $C = C(x)$ the signed dopant position density, i.e. the difference of the donor and acceptor densities. Here x denotes the position variable as element of the (three-dimensional) domain D representing the semiconductor device.

The main use of industrially produced semiconductor devices is in VLSI (= Very Large Scale Integration) structures, where millions of devices are fabricated on a single semiconductor chip with a specific usage, i.e. a processor or a RAM modul of a modern computer or a CCD or CMOS imaging sensor in a digital camera. The Images 5.1 to 5.6 show a motherboard with two processor slots, an ATA controller chip, a Celeron Processor[1], a RAM modul array and chips on a graphics card.

The most important semiconductor device, making up at least 95% of the overall semiconductor device production, is the transistor, more specifically the MOS (Metal-Oxide-Semiconductor) transistor, which acts as a switch, allowing current to flow between its source and drain contacts when the voltage between the gate and the base contact is turned on. It represents a 'bit' having the state 1 when current flows and 0 when no current flows. It is the main 'logical' device in VLSI chipsets.

[1] *http://www.intel.com/products/processor/celeron/index.htm*

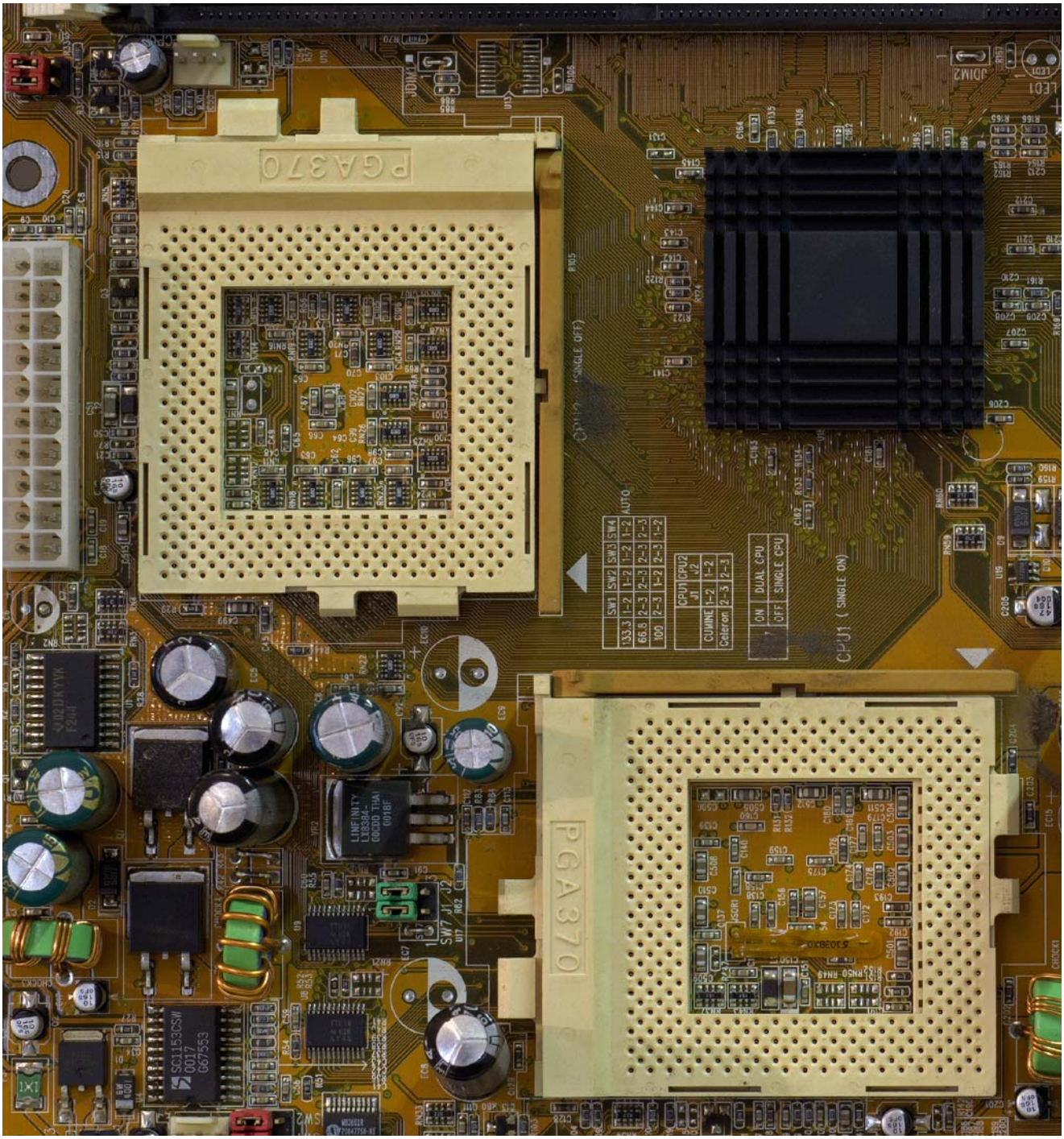

Fig. 5.1. Dual Processor Motherboard (main circuit board controller)

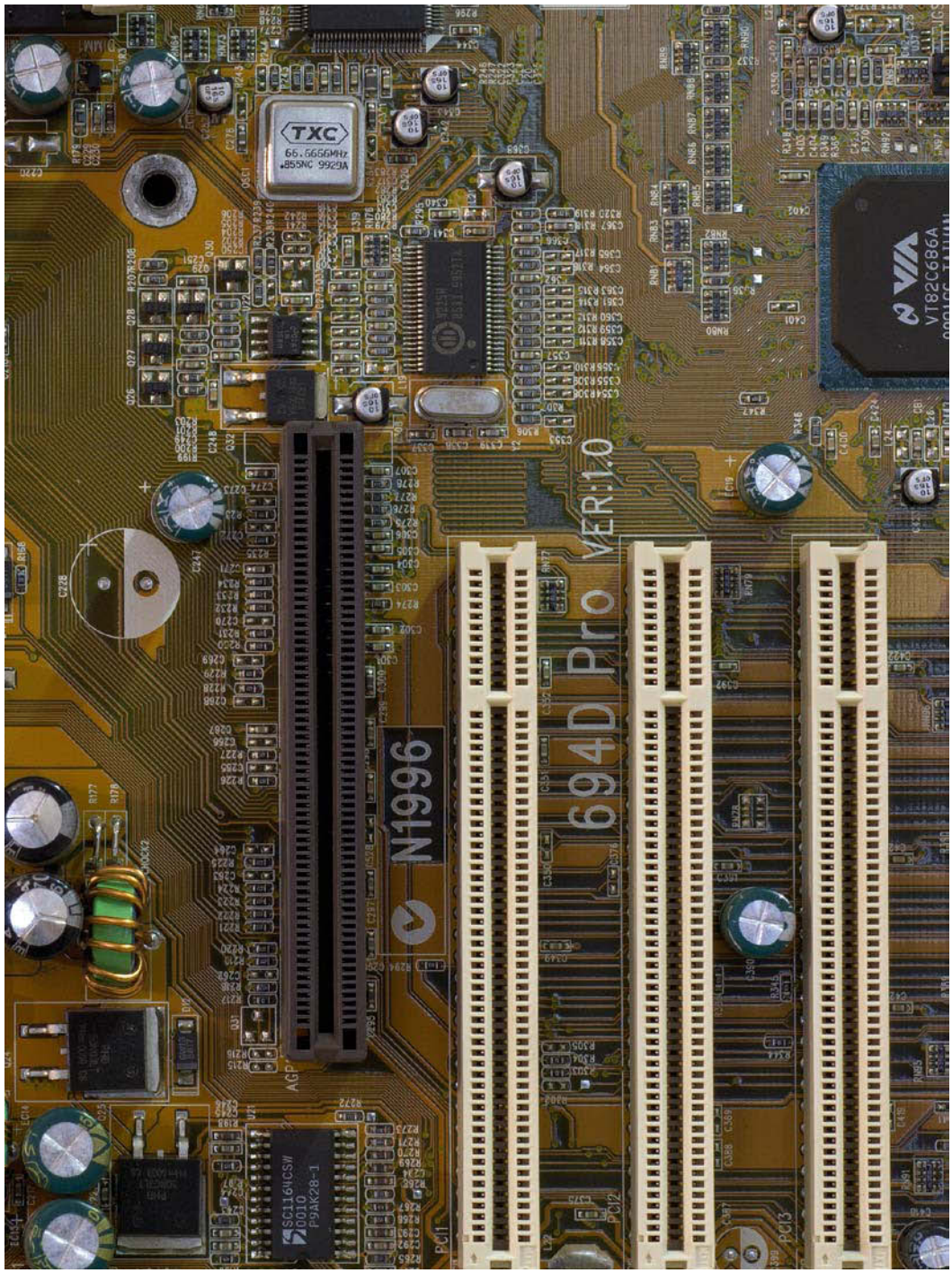
TXC
66.6666MHz
VIA
VT82C686A
694D Pro VER:1.0
N1996
AGP
PCI1
PCI2
PCI3

Silicon transistors were invented in the USA, more precisely at Bell Labs in the year 1947, by J. Bardeen[2], W. A Shockley[3] and W. Brattain[4]. The first transistor had a dimension of about one centimetre, today's MOS transistors feature a gate length of less than 100 nanometres! Consequently, the integrated circuit was invented in the year 1958, by J. Kilby[5] at Texas Instruments, putting together a few devices on one chip. Today's world would be entirely different without semiconductor devices …

The mathematical modeling and simulation of semiconductor structures acts on different levels:

1. Modeling of the doping process (= fabrication of the device/chip) by nonlinear diffusion equations. The main goal is to better understand and control the doping process. We refer to the book [6].
2. Modeling of the electrical functioning of individual semiconductor devices. Here the doping profile is taken as input function and the current flow in the device is modeled exploiting insights into the solid state physics of semiconductors. A wealth of information on this subject can be found in the books of the Springer Series on Computational Microelectronics[6], edited by Siegfried Selberherr[7]. In particular we refer to [4] and [5].
3. VLSI circuit modeling. The functioning of a whole chip is modeled by using the individual device model result as input. Typically very large systems of ordinary differential equations are obtained which have to be solved numerically in a fast way. We refer to [2].

In the sequel we shall focus on the second level, that means on mathematical semiconductor modeling. Clearly, the basis for this is quantum particle physics and, in a semiclassical framework, solid state physics. There is a semiconductor modeling hierarchy, based on different scales and accuracy levels of the description. Roughly speaking, it looks like this:

Quantum Mechanical Modeling relies on the Schrödinger equation and various equivalent formulations (Heisenberg formalism, Wigner transport equation, quantum hydrodynamics). There are (somewhat exotic) semiconductor devices whose performance is entirely based on quantistic phenomena, e.g. resonant tunnelling diodes. In many other devices, however, spurious quantistic effects occur. In both cases, classical mechanics or even a semiclassical framework do not suffice.

Semiclassical Modeling relies on the Boltzmann equation of solid state physics. This is a phase-space based integro-differential equation, describing the

[2] *http://nobelprize.org/physics/laureates/1956/bardeen-bio.html*
[3] *http://nobelprize.org/physics/laureates/1956/shockley-bio.html*
[4] *http://nobelprize.org/physics/laureates/1956/brattain-bio.html*
[5] *http://nobelprize.org/physics/laureates/2000/kilby-autobio.html*
[6] *http://www.springer.com/sgw/cda/frontpage/0,11855,1-40109-69-1187595-0,00.html*
[7] *http://info.tuwien.ac.at/histu/pers/12152.html*

dynamic balance of ballistic particle motion and particle collisions (predominantly collisions of electrons/holes with the crystal lattice of the semiconductor, quantized as phonons). Obviously, there is a structural similarity to the gas dynamics Boltzmann equation of Chapter 1, the main difference lying in the form of the collision operator, which in the solid state physics case is predominantly inelastic and allows only Fermi-Dirac distribution as Fermion equilibria.

Macroscopic Modeling is based on various scaling limits of solutions of the semiclassical Boltzmann equation. There are so called hydrodynamic semiconductor models, similar to the compressible Euler/Navier–Stokes system of fluid dynamics, energy transport equations and drift-diffusion systems.

For a review of these models, their interrelation and mathematical properties we refer to [5] and to the references therein.

Here we want to give some details on the oldest and still most important semiconductor device model, namely on the drift-diffusion-Poisson (DDP) system.

Phenomenologically speaking, the main factors for current flow in semiconductors are diffusion of conduction electrons and holes as well as convection of charged particles by the electric field in the device. Now let $n = n(x,t)$ denote the density of (negatively charged) conduction electrons in the doped semiconductor at position x and time t, $p = p(x,t)$ the density of (positively charged) holes, $V = V(x,t)$ the electrical potential and J_n (J_p) the electron (hole) current density vector fields. Clearly, the functions n and p are nonnegative. Then, after appropriate non-dimensionalisation and scaling, the electron and hole current densities in the DD model read:

$$\begin{aligned} J_n &= D_n \operatorname{grad} n - \mu_n\, n \operatorname{grad} V \\ J_p &= -(D_p \operatorname{grad} p + \mu_p\, p \operatorname{grad} V)\ . \end{aligned}$$

Here D_n and D_p denote the (positive) electron and, resp., hole diffusion coefficients and μ_n and μ_p the (positive) electron and hole mobilities. Note that the first terms in the current densities are the diffusion currents and the second terms the drift currents, generated by the electrical field $E = -\operatorname{grad} V$. The total current density is

$$J = J_n + J_p\ .$$

Continuity equations for both carrier types are assumed to hold:

$$\begin{aligned} n_t &= \operatorname{div} J_n + R \\ p_t &= -\operatorname{div} J_p + R\ , \end{aligned}$$

where R denotes the so called recombination-generation rate, which accounts for instantaneous generation/annihilation of electron-hole carrier pairs and acts as a reaction term in the continuity equations. In most applications it is modeled as a function of the position densities n and p.

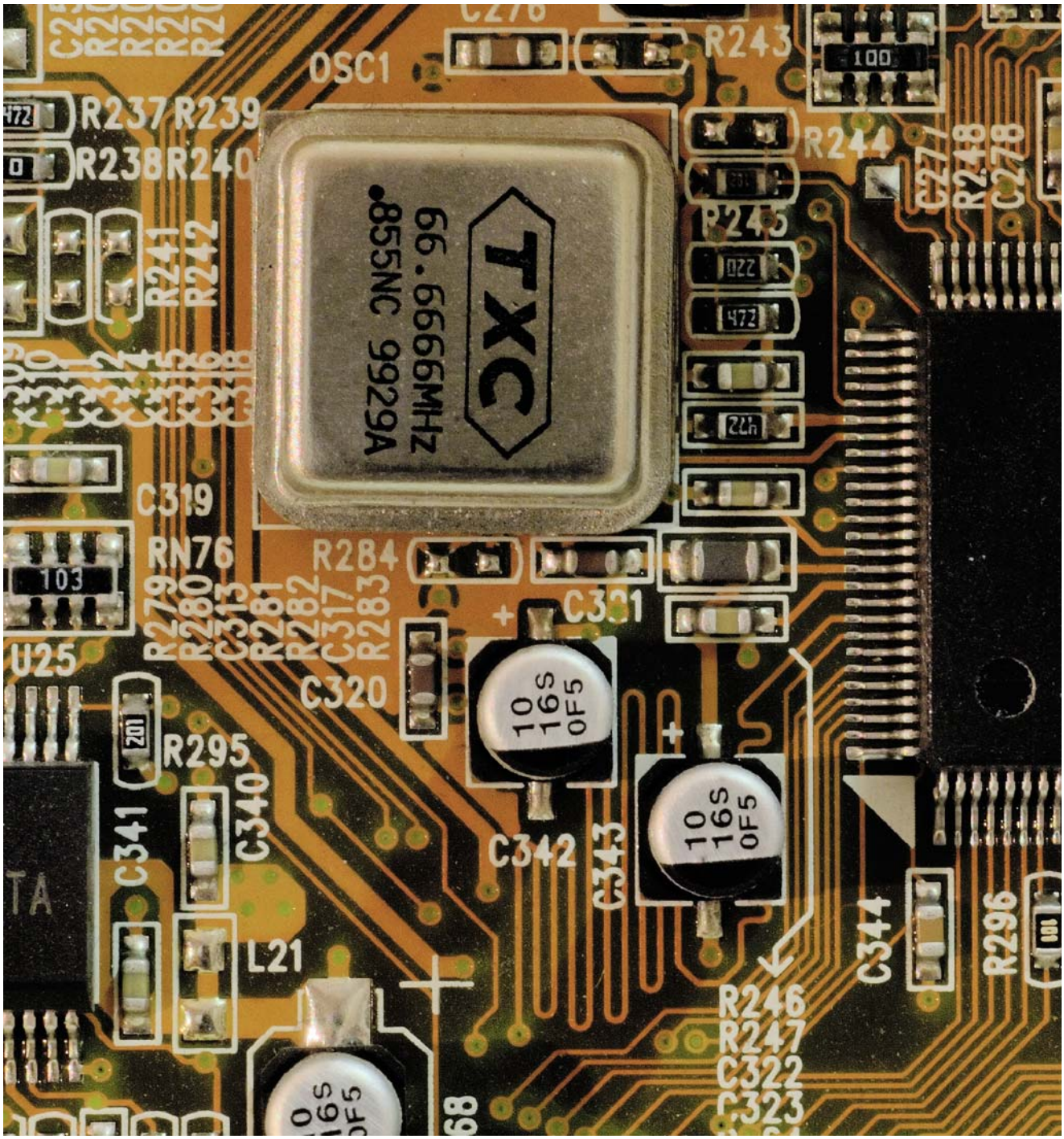

Fig. 5.2. PCI Bus mastering ATA Controller Chip (disk drive)


PROMISE®
TECHNOLOGY, INC.
PDC20267
©1999-0019
R249
R250
R252
R253
R254
R285
R286
R287
C326
C327
C328
C345
C346
C347
U23

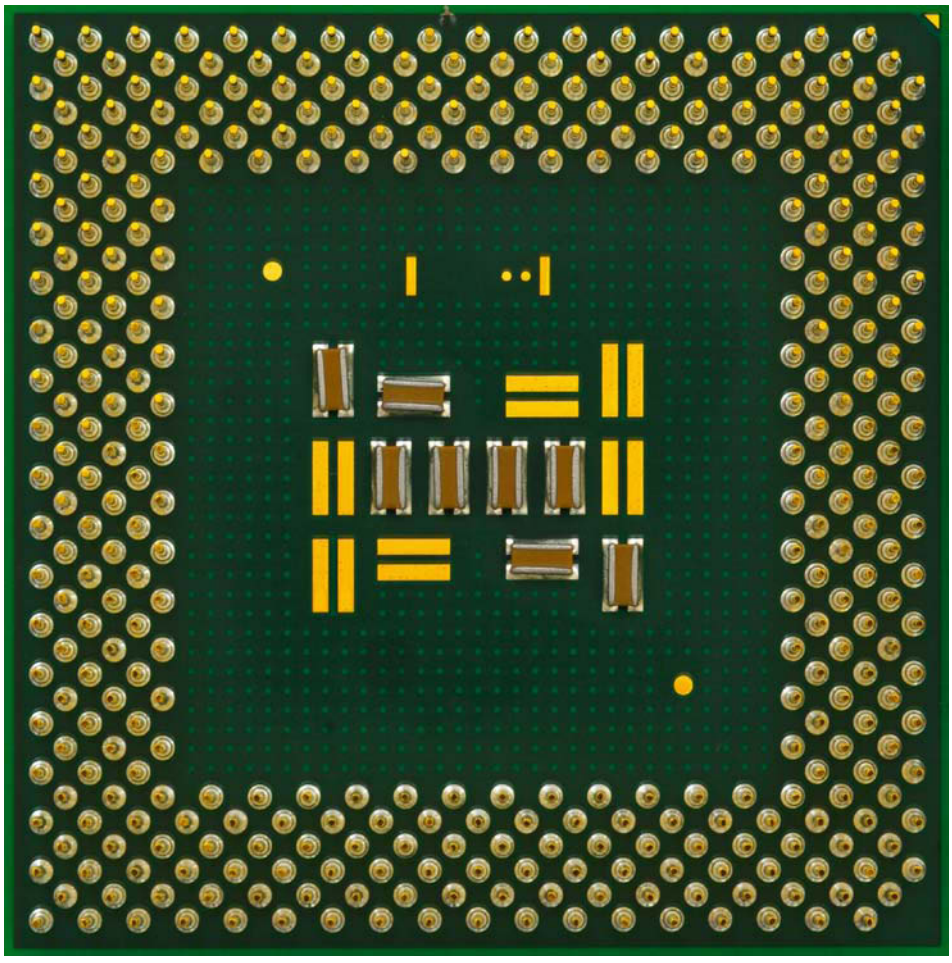

Fig. 5.3. Intel Celeron Processor (downside)

A 'closed' system of partial differential equations is obtained by coupling the current relations/continuity equations to the Poisson equation for the electric potential:

$$\lambda^2 \Delta V = n - p - C(x) \ .$$

This equation is a direct consequence of the Maxwell field equations, when magnetic and relativistic effects are neglected. Its right hand side represents the (negative and scaled) space charge density. The parameter λ, whose square multiplies the Laplace operator in the Poisson equation, is the scaled Debye length of the doped semiconductor device, determining the radius of electrical influence of an impurity ion in the semiconductor crystal. In many real life applications it is a small parameter. It is often assumed that diffusivities and mobilities are

proportional (Einstein relations), such that they may be taken equal after scaling. Then, inserting the current relations into the continuity equations gives the system of three nonlinearly coupled partial differential equations for the three unknown functions n, p and V:

$$\begin{aligned} n_t &= \operatorname{div}\left(D_n(\operatorname{grad} n - n \operatorname{grad} V)\right) + R(n,p) \\ p_t &= \operatorname{div}\left(D_p(\operatorname{grad} p + p \operatorname{grad} V)\right) + R(n,p) \\ \lambda^2 \Delta V &= n - p - C(x) \ . \end{aligned}$$

The equations for the densities n and p are parabolic (assuming for a moment that V is known) and the equation for the potential is elliptic. Note that the potential V depends linearly but in a nonlocal way on the densities n and p and

Fig. 5.4. Intel Celeron Processor (upside)

that the doping profile C, which determines the electrical characteristics of the device under consideration, only enters in the Poisson equation for the potential.

We remark that this Poisson equation models the repulsive electrical interaction between equally charged particles. A corresponding attractive (gravitational) model is obtained by reversing the sign of ΔV in the Poisson equation, as used, for example, in the modeling of biological cell motion by chemotaxis in Chapter 4.

Equilibrium states (i.e. stationary states with vanishing current densities) are Maxwell distributed:

$$n_e = \delta^2 \exp(V_e) \,, \quad p_e = \delta^2 \exp(-V_e) \,,$$

where δ is a positive device-dependent parameter. Note that, by basic solid state physics, the recombination-generation rate R vanishes in equilibrium where $n_e p_e = \delta^4$ holds. The equilibrium Poisson equation then becomes semilinear:

$$\lambda^2 \Delta V_e = \delta^2 \exp(V_e) - \delta^2 \exp(-V_e) - C(x) \,, \quad x \in D$$

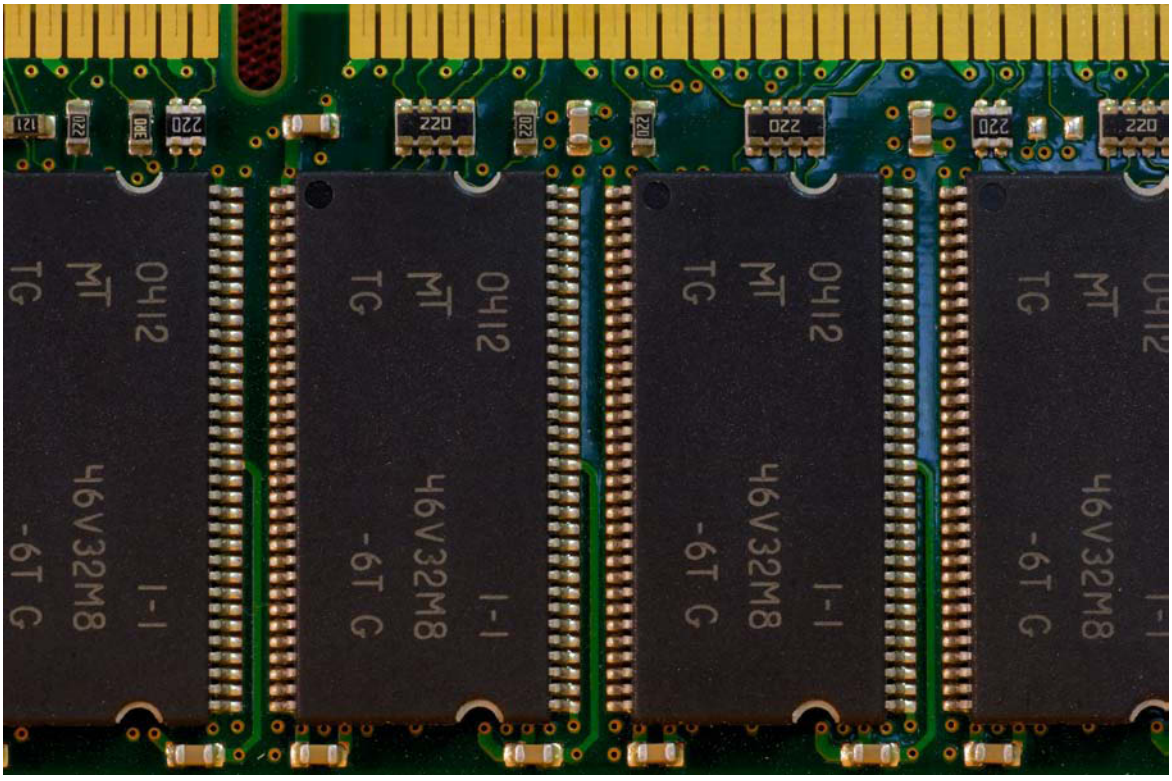

Fig. 5.5. RAM (Random Access Memory) Array

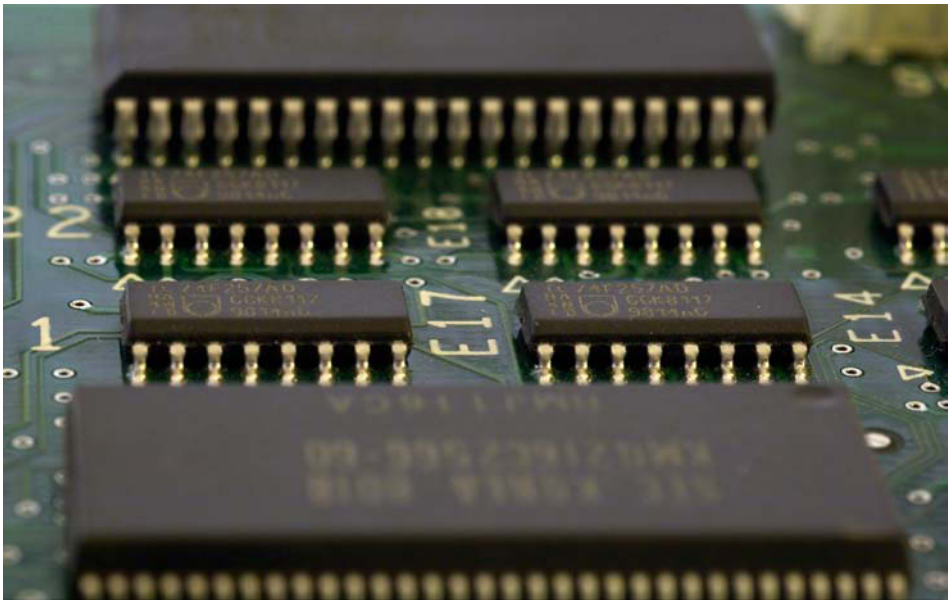

Fig. 5.6. Chipset on Graphics Card

which is a version of the so-called (repulsive) mean-field equation. Clearly, the drift-diffusion-Poisson (DDP) system has to be supplemented by initial conditions for the position densities n and p and by boundary conditions for n, p and V. The boundary of the semiconductor domain D usually splits into two parts, namely the contact segments (Ohmic, Schottky or Metal-Oxide contacts), where Dirichlet data for n, p and V are prescribed, and into insulating or artificial boundaries, where zero outflow current densities and zero outward electric field are prescribed resulting in homogeneous Neumann conditions for n, p and V. Contact voltages determine the Dirichlet condition for the potential V and Ohmic contacts are assumed to be in thermal equilibrium and to have locally vanishing space charge density. All in all, mixed Dirichlet–Neumann boundary conditions for the three unknown functions are prescribed.

Usually, equilibrium data for n and p are given at $t = 0$ (which requires the solution of the mean-field equation) and the device is driven out of equilibrium by applying contact voltages.

The mathematical analysis of the DDP system is in a rather healthy state, we refer to the references [4] and [5] for classical results and to the author's publication list[8] for more recent work, most of which focuses on various extensions of the DDP system. Under appropriate assumptions on the data there is existence and uniqueness of transient solutions, existence of stationary states with uniqueness for small contact voltages (close to equilibrium) and convergence

[8] *http://homepage.univie.ac.at/peter.markowich/publications.html*

of close-to-equilibrium transient solutions to the unique thermal equilibrium state (determined by the mean field equation) in the large-time limit. (if, say, contact voltages are turned off after some time). These qualitative results are complemented by a series of quantitative results of singular perturbation type, more specifically in the limit λ tending to zero. Note that, typically, at interfaces between positively and negatively doped device subdomains (so called pn-junctions), the doping profile has a very large gradient and, in fact, is very well approximated by a discontinuous function. When λ is set to zero in the Poisson equation, then the global charge-neutrality equation

$$0 = n - p - C(x) \,, \quad x \in D$$

results, which implies that at least one of the limiting densities n or p has to be discontinuous (it turns out that both are!). Elliptic and parabolic regularity theory implies, however, that – for λ small but nonzero – the functions n, p and V are continuous in the interior of D! This is a well-known phenomenon in singular perturbation theory, which indicates that there is a very thin layer (of width $O(\lambda)$ roughly speaking) around pn-junctions, within which the densities n and p have a very large gradient in orthogonal direction to the junction. Clearly, this interior layer structure of the solutions has to be well taken into account when numerical discretisation schemes are devised and it renders the design of discretisation schemes and grids highly nontrivial. We refer to the webpage of Paola Pietra[9] for references on this subject.

Recent mathematical/numerical efforts have gone into inverse and optimisation problems concerned with the DDP system. In particular the identification of the doping profile from current-voltage or from capacitance measurements for the sake of quality control in device manufacture and the design of doping profiles according to certain optimality criteria is of great practical importance (see the author's publication list[8] and the webpage of Martin Burger[10] for more information).

Comments on the Images 5.1–5.6 The Images 5.1–5.6 show chipsets of modern computers. Each of them consists of a huge number (many millions) of semiconductor devices, typically MOS-transistors. The continuous and rapid advance of computer technology relies on an interplay of numerical simulations and engineering insights used for the design of prototypes of new semiconductor technology, which then becomes absorbed into new mainstream chipsets. At the very basis of this is the modeling of individual semiconductor devices (typically MOS technology) using the drift-diffusion-Poisson system, energy transport and hydrodynamical models. Simulation runs of the semiconductor Boltzmann equation are often used to provide benchmarks for the macroscopic parameters like diffusivities and charge carrier mobilities. The input for the device

[9] *http://www.imati.cnr.it/∼pietra*

[10] *http://www.indmath.uni-linz.ac.at/people/burger*

model PDE systems, the so called doping profile, is obtained from process modeling (nonlinear diffusion), and device model results are then assembled into models for integrated circuits (large ODE systems). As discussed in detail the drift-diffusion-Poisson system consists of two parabolic differential equations of Fokker–Planck type for the position densities of (negatively charged) electrons and (positively charged) holes, coupled nonlinearly to a Poisson equation for the electrical potential. An important extension of the drift-diffusion equations is given by energy transport systems, which take into account convection driven by particle temperatures. The temperatures satisfy nonlinear transport equations, too, which are coupled to the drift-diffusion equations for the particle densities. We refer to [1] for detail. Further modeling detail is provided by hydrodynamic semiconductor systems [3], which are – for each carrier species – compressible Euler equations (with position density, particle velocity and temperature as unknowns) with convective forcing provided by the electric field and with momentum and energy relaxation due to the dominant inelastic collisions with the semiconductor crystal lattice (phonons). All the above mentioned charge carrier transport models are based and can be derived from the semiclassical semiconductor Boltzmann equation. This is a phase space model, posed in position-wave vector space, balancing charge carrier transport in semiconductor crystals (taking into account the crystal's energy band structure) with dominantly inelastic collisions (typically elastic particle-particle collisions are a second order effect in semiconductors). Fully quantistic models like the quantum-drift-diffusion system [3], the quantum hydrodynamics system and quantum Boltzmann equations are able to model spurious quantistic effects in current device technology as well as quantum semiconductor devices like tunnelling diodes[11]. Due to their high complexity these models were not and are still not (yet in 2006) used for general design-oriented simulations of semiconductor devices as they occur in the chipsets depicted in the Images 5.1–5.6.

References

[1] F. Brezzi, L.D. Marini, S. Micheletti, P. Pietra, R. Sacco, and S. Wang, *Finite element and finite volume discretizations of Drift-Diffusion type fluid models for semiconductors*, in Handbook of Numerical Analysis, Volume XIII: Special Volume: Numerical Methods in Electromagnetics, W.H.A. Schilders, E.J.W. ter Maten, Guest ed., P.G. Ciarlet ed., Elsevier, Amsterdam, 317–441, 2005

[2] G.F. Carey, B. Mulvaney, W.B. Richardson and C.S.Reed, *CIRCUIT, DEVICE, AND PROCESS SIMULATION: Mathematical and Numerical Aspects*, John Wiley & Sons, 1996

[11] *http://www.americanmicrosemi.com/tutorials/tunneldiode.htm*

[3] A. Jüngel, *Quasi-hydrodynamic semiconductor equations*, Progress in Nonlinear Differential Equations, Birkhäuser, Basel, 2001
[4] P.A. Markowich, *The Stationary Semiconductor Device Equations*, Springer Series: Computational Microelectronics[6], 1986
[5] P.A. Markowich, C.A. Ringhofer and C. Schmeiser, *Semiconductor equations*, Springer-Verlag, Wien, 1990
[6] P. Pichler, *Intrinsic Point Defects, Impurities, and their Diffusion*, in Silicon Springer Series: Computational Microelectronics[6], XXI, 554 p., 2004

6. Free Boundary Problems and Phase Transitions

Initial and initial-boundary value problems for systems of partial differential equations (PDEs) have functions or, more generally, distributions in the scalar case and vector fields of functions or distributions in the vector-valued case as solutions. Usually, the d-dimensional domain, on which the PDEs are posed, is given and the problem formulation is based on a fixed geometry. Obviously, there have to be compatibilities between the differential operator, particularly its differential order and certain geometric properties, and the side (initial-boundary) conditions and the geometry of the domain on which the problem is posed in order to guarantee well-posedness of the problem under consideration. In particular, for a given differential operator the number of initial-boundary conditions and the geometry of the domain boundary are crucial for solvability, uniqueness and continuous dependence on data.

Free boundary problems for PDEs have a totally different feature, namely that geometric information is an inherent part of the solution. Typically, the solution of a free boundary problem consists of one or more functions or distributions AND a set (the so called free boundary, subset of $\mathbb{R}^d$), on which certain conditions

Fig. 6.1. Layered iceberg, Lago Argentino

on the unknown function(s) are prescribed. If we assume for a moment that the free boundary is fixed, then, typically, the problem would be over-determined. So, in fact, the additional conditions are needed to determine the free boundary itself.

Regularity (smoothness) is an important issue in PDE theory. Usually, a certain degree of regularity (differentiability in the classical or weak sense) of the solutions of initial-boundary value problems is necessary to prove their uniqueness, their continuous dependence on the data, to carry out certain scaling limits, as done in singular perturbation theory, and to devise efficient numerical discretisation techniques. For free boundary problems the situation is definitely more complex. Not only the regularity of the unknown functions is important, but also the regularity of the unknown set, the free boundary. Typical questions, which arise, are: does the free boundary have empty topological interior? What are its measure theoretical properties? Is it a (finite union of) smooth manifolds? What is the optimal regularity of the free boundary? In many cases the study of the optimal regularity of the free boundary is of paramount importance for understanding the solution of the free boundary problem under consideration, to prove uniqueness, stability etc.

Obviously, the mathematical literature of free boundary problems is vast, at this point we refer to the book [4] for a review of basic analytical tools and for further references.

To start a more concrete discussion, we consider the maybe best-studied free boundary problem, the so called obstacle problem for the Laplace operator. Let us consider the classical Dirichlet functional

$$D(v) := \frac{1}{2}\int_G |\operatorname{grad} v|^2 dx\,, \tag{6.1}$$

where G is a bounded domain in $\mathbb{R}^d$ with a sufficiently smooth boundary ∂G. Also, let us fix the boundary values of v and, for the moment, the considered class of functions

$$Y := \left\{ v \in H^1(G) \,|\, v = \psi \quad \text{on} \quad \partial G \right\}\,, \tag{6.2}$$

where ψ is a prescribed function in the Sobolev space $H^1(G)$, which consists of those square integrable functions, defined almost everywhere in G with values in $\mathbb{R}$, which also have a square integrable distributional gradient.

It is an easy exercise to show that the minimum u of the functional D over the set of functions Y is the unique harmonic function on G assuming the boundary values ψ, i.e. u uniquely solves the boundary value problem:

$$\Delta u = 0 \quad \text{in} \quad G \tag{6.3}$$

$$u = \psi \quad \text{on} \quad \partial G\,. \tag{6.4}$$

The obstacle problem is obtained by a modification of this minimizing procedure. Let $\phi \in H^1(G)$ be another given function, the so called obstacle, and look

Fig. 6.2. An iceberg with a central spire, Lago Argentino

for a mimimizer of the energy functional D, which is in Y AND which nowhere (in the almost everywhere sense) in G stays below the obstacle ϕ. More formally, consider the convex set of functions:

$$X := Y \cap \{v \mid v \geq \phi\} \tag{6.5}$$

and find:

$$u := \operatorname{argmin}_{v \in X} D(v) \; . \tag{6.6}$$

Clearly, the obstacle ϕ cannot stay above the function ψ on the boundary of G, i.e. we assume:

$$\phi \leq \psi \quad \text{on} \quad \partial G \; . \tag{6.7}$$

In the two 2-dimensional case the solution of the obstacle problem can be seen as the (small amplitude) displacement of an elastic membrane, fixed at the boundary, minimizing its total energy under the constraint of having to stay above a solid obstacle.

It is actually easy to show that the obstacle problem (6.6) has a unique solution (minimizer) $u \in X$, all the technical mathematical analysis goes into the investigation of the regularity properties of its solution u and of the free boundary defined below.

We define the non-coincidence set N as

$$N := \{x \in G \mid u(x) > \phi(x)\}$$

and the coincidence set C

$$C := \{x \in G \mid u(x) = \phi(x)\} \; .$$

Then the free boundary F is defined as that part of the topological boundary of N, which lies in G, i.e.

$$F := \partial N \cap G \; ,$$

in other words it is the interface between the sets C and N.

It is a simple exercise to derive the Euler–Lagrange equations of the minimisation problem (6.6). We find, assuming sufficient regularity of the minimizer u and of the free boundary F:

$$\Delta u = 0 \quad \text{in} \quad N \, , \quad u = \phi \quad \text{in} \quad C \quad \text{and} \quad -\Delta u \geq 0 \quad \text{in} \quad G \tag{6.8}$$

$$u = \phi \quad \text{and} \quad \operatorname{grad} u \cdot n = \operatorname{grad} \phi \cdot n \quad \text{on} \quad F \, , \tag{6.9}$$

where n denotes a unit normal vector to F, and finally:

$$u = \psi \quad \text{on} \quad \partial G \; . \tag{6.10}$$

Obviously, when F is a fixed hyper-surface in G, then one of the conditions in (6.9) is redundant and the problem 6.8–6.10 is overdetermined.

In order to illustrate the difficulties of the obstacle problem, set

$$w = u - \phi\,, \quad x \in G\,.$$

Then, denoting $h(x) = -\Delta\phi(x)$, we can rewrite the Euler–Lagrange system (6.8)–(6.10) as

$$\Delta w = h(x)1_{\{w>0\}} \tag{6.11}$$

$$w = \psi - \phi \quad \text{on} \quad \partial G\,. \tag{6.12}$$

Note that the minimisation of the Dirichlet functional over the set Y defined in (6.2) leads to a simple linear problem while the minimisation over the constrained set X leads to a complicated nonlinear problem, as indicated by the right hand side of (6.11)! Assuming a smooth obstacle we conclude that the right hand side of the semilinear Poisson equation (6.11) is bounded in G, such that by classical interior regularity results of linear uniformly elliptic equations we conclude that the solution w is locally in the Sobolev space $W^{2,p}$ for every $p < \infty$ (which is the space of locally p-integrable functions with locally p-integrable weak second derivatives). By the Sobolev imbedding theorem we conclude that w (and consequently u) is locally in the space $C^{1,\alpha}$ (locally Hölder continuous first derivatives) for every $0 < \alpha < 1$. More cannot be concluded from this simple argument.

From the many results on optimal regularity of the solution of the obstacle problem we cite the review [2], where optimal local regularity for u, i.e. $u \in C^{1,1}$ is shown, if the obstacle is sufficiently smooth. Note that the optimality of this result follows trivially from the fact that Δu jumps from 0 to $\Delta\phi$ on the free boundary F! Moreover, the free boundary has locally finite $(n-1)$-dimensional Hausdorf measure and is locally a $C^{1,\alpha}$ surface, for some α in the open interval $(0, 1)$, except at a 'small' set of singular points, contained in a smooth manifold. Singularities can be excluded by assuming an exterior cone condition. Moreover, if the free boundary is locally Lipschitz continuous, then it is locally as smooth as the data, in particular it is locally analytic, if the data are analytic. We remark that the proof of the optimal regularity of the free boundary requires deep insights into elliptic theory, in particular the celebrated 'monotonicity formula' of Luis Caffarelli[1].

A more complex application of free boundary problems arises in the theory of phase transitions. A historically important example of a phase transition is the formation of ice in the polar sea, as originally investigated by the Austrian mathematician Josef Stefan[2] (1835–1893). In the year 1891 Stefan published his

[1] *http://www.ma.utexas.edu/users/caffarel/*

[2] *http://www-groups.dcs.st-and.ac.uk/~history/Mathematicians/Stefan_Josef.html*

Fig. 6.3. Melting iceberg

Fig. 6.4. Iceberg, the Stefan boundary hits the fixed boundary (water surface)

seminal paper [7], investigating the ice layer formation in a water-ice phase transition. Interestingly enough, Stefan compared his data, obtained by mathematical modeling, to measurements taken in the quest of the search of a north-west passage [11] through the northern polar sea. In his paper [7] Stefan investigated the non-stationary transport of heat in the ice and formulated a free boundary problem, which is now known as the classical Stefan problem and which has given rise to the modern research area of phase transition modeling by free boundary problems. As a basic reference we refer to [10].

Some of the photographs associated to this chapter show icebergs in lakes of Patagonia. The evolution of their water-ice phase transition free boundary is modeled by the 3-dimensional Stefan problem formulated below.

Therefore, consider a domain $G \in \mathbb{R}^d$ (of course $d = 1$, 2 or 3 for physical reasons but there is no mathematical reason to exclude larger dimensions here), in which the ice-water ensemble is contained. At time $t > 0$ assume that the domain G is divided into 2 subdomains, $G_1(t)$ containing the solid phase (ice) and $G_2(t)$ containing the liquid phase (water). These subdomains shall be separated by a smooth surface $\Gamma(t)$, where the phase transition occurs. $\Gamma(t)$ is the free boundary, an unknown of the Stefan problem. Heat transport is modeled by the linear heat equation:

$$\theta_t = \Delta\theta + f\,, \quad x \in G_1(t) \quad \text{and} \quad x \in G_2(t)\,,\ t > 0\,, \tag{6.13}$$

where f is a given function describing external heat sources/sinks. Here we assumed that the local mass density, the heat conductivity and the heat capacity at constant volume are equal and constant 1 in both phases. More realistically, piecewise constants can be used for modeling purposes. The parabolic PDE (6.13) has to be supplemented by an initial condition

$$\theta(t = 0) = \theta_0 \quad \text{in} \quad G \tag{6.14}$$

and appropriate boundary conditions at the fixed boundary ∂G. Usually, the temperature is fixed there

$$\theta = \theta_1 \quad \text{on} \quad \partial G \tag{6.15}$$

or the heat flux through the boundary is given:

$$\operatorname{grad}\theta\,.\nu = f_1 \quad \text{on} \quad \partial G\,,\ t > 0\,. \tag{6.16}$$

Here ν denotes the exterior unit normal to ∂G. Also, mixed Neumann–Dirichlet boundary conditions can be prescribed, corresponding to different types of boundary segments.

Disregarding the phase transition the problem (6.13), (6.14), (6.15) or (6.16) is well-posed. Thus, additional conditions are needed to determine the free boundary. The physically intuitive condition says that the temperature at the free boundary is the constant melting temperature θ_{m} of the solid phase. Obviously

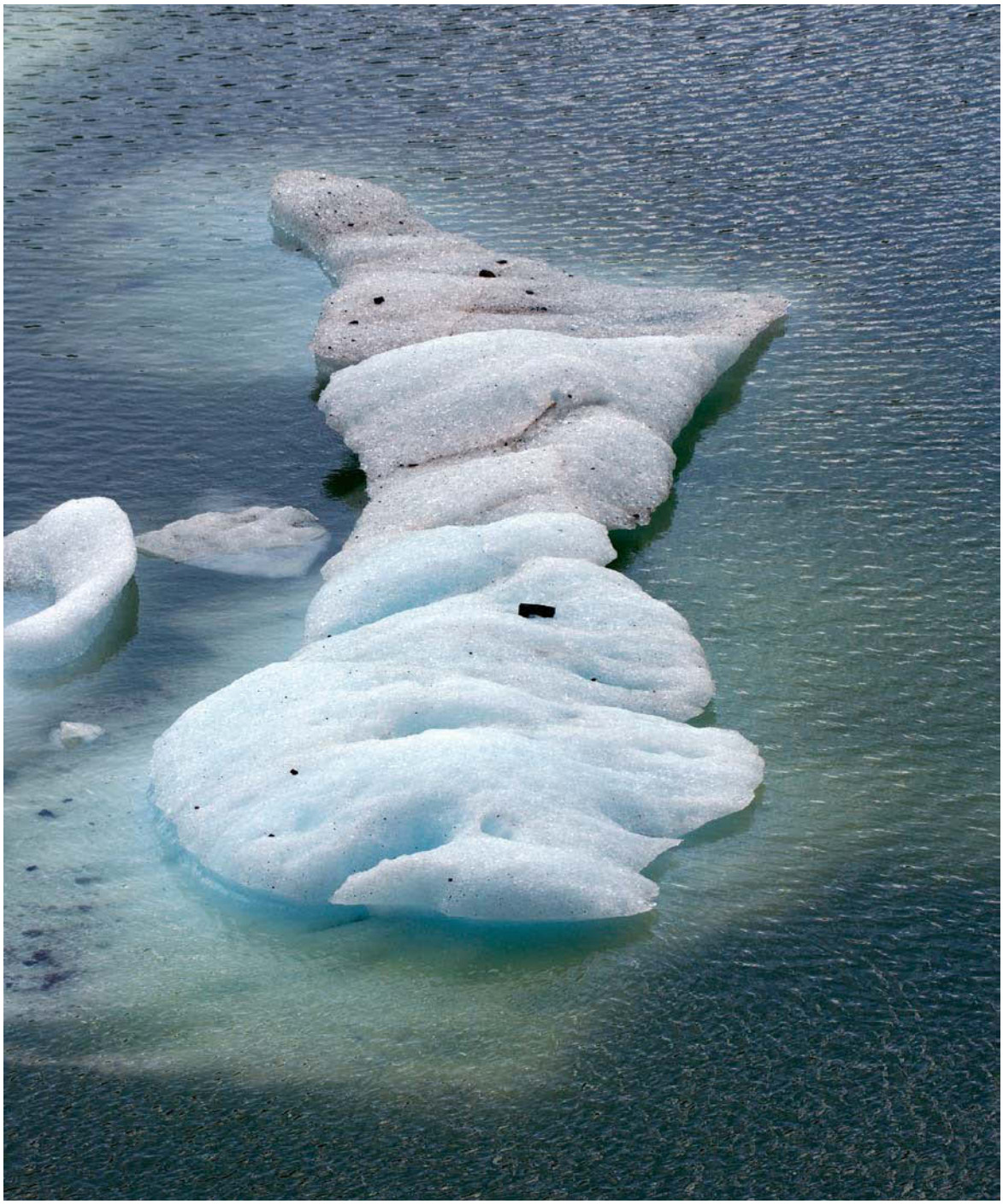

Fig. 6.5. A glimpse on the Stefan boundary under the water surface

Fig. 6.6. Complicated structure of the free boundary and its intersection with the fixed boundary

we can normalize $\theta_{\mathrm{m}} = 0$ and regard θ from now on as the difference between the local temperature and the melting temperature:

$$\theta = 0 \quad \text{at} \quad \Gamma(t)\,. \tag{6.17}$$

Note that the condition (6.17) cannot suffice to determine the free boundary. Fixing $\Gamma(t)$ arbitrarily (in a non-degenerate way) leaves us with two decoupled linear boundary value problems for the heat equation, one in each phase with Dirichlet boundary data on the interface. Both of these problems are uniquely solvable!

The second interface condition, derived from local energy balance [9], reads:

$$Lv_n = [\operatorname{grad}\theta\,.n]\,, \tag{6.18}$$

where n denotes the unit normal to the interface, [.] stands for the jump across the interface and v_n for the interface velocity in orthogonal direction. L is the latent heat parameter representing the energy needed for a phase change.

When the interface is a regular surface, given by the equation $H(x,t) = 0$, we have

$$v_n = -H_t \operatorname{grad} H \cdot n\,.$$

In (6.18) we assume that the vector n points into the liquid phase and that the jump is defined by (to get the signs right …):

$$[g] := g|_{\text{fluid}} - g|_{\text{solid}} \quad \text{on} \quad \Gamma(t) \,. \tag{6.19}$$

Note that at time $t = 0$ the interface $\Gamma(t = 0)$ is given by the 0-level set of the initial datum θ_0.

To get more insights we consider the one dimensional single phase Stefan problem, assuming that the temperature in the liquid phase is constant and equal to the melting temperature. Defining u as the difference of the melting temperature and the solid phase temperature (i.e. $u = -\theta > 0$ in the solid phase), we obtain the one-dimensional single phase problem, with interface $x = h(t)$ and fixed (Dirichlet) boundary at $x = 0$:

$$\begin{aligned} u_t = u_{xx} \,, &\quad 0 < x < h(t) \\ u(x = 0, t) = \alpha(t) \geq 0 \,, &\quad t > 0 \\ u(h(t), t) = 0 \,, &\quad t > 0 \\ u(x, t = 0) = u_0(x) \,, &\quad 0 < x < h(t) \,, \end{aligned}$$

subject to the Stefan condition:

$$L\frac{dh(t)}{dt} = -u_x(h(t), t) \,, \quad t > 0 \,.$$

This models for example the growth of an ice layer located in the interval $[0, h(t)]$. The Dirichlet boundary $x = 0$ represents the water/ice–air interface, at which the temperature variable is prescribed to be $\alpha(t)$ (below freezing). $x = h(t)$ is the ice-water interface. In order to study the onset and evolution of ice formation we assume $h(0) = 0$, i.e. no ice is present at $t = 0$. Also, external heat sources are excluded and homogeneity in the x_2 and x_3 directions (parallel to the water surface) is assumed in order to obtain a one-dimensional problem. Note that the x-variable denotes the perpendicular coordinate to the water/ice surface, pointing into the water/ice.

We remark that this problem was already stated by Stefan in his original paper [7] and that he found an explicit solution for

$\alpha = \text{const}$. The solution reads (see also [11]):

$$h(t) = 2\mu\sqrt{t}$$

$$u(x, t) = \alpha \frac{\int_{\sigma(x,t)}^{\mu} \exp(-z^2)dz}{\int_0^{\mu} \exp(-z^2)dz} \,, \quad 0 < x < h(t)$$

where

$$\sigma(x, t) = \frac{x}{2\sqrt{t}}$$

Fig. 6.7. A glacier flowing into Lago Argentino from the southern ice field

Fig. 6.8. Penitentes

and μ solves a transcendental equation:

$$\mu \exp(\mu^2) \int_0^{\mu} \exp(-z^2) dz = \frac{\mu}{2L} .$$

Note that the thickness of the ice layer behaves like $\sqrt{t}$. Stefan found coincidence of this theoretical result with the experimental data available to him.

There is a convenient reformulation of the Stefan problem in terms of a degenerate parabolic equation, making use of the enthalpy formulation of heat flow. The physical enthalpy e is related to the temperature θ by

$$\theta = \beta(e) , \tag{6.20}$$

where

$$\begin{aligned} \beta(e) &= e + \frac{L}{2} , && \text{for} \quad e < 0 \\ \beta(e) &= 0 , && \text{for} \quad -\frac{L}{2} < e < \frac{L}{2} \\ \beta(e) &= e - \frac{L}{2} , && \text{for} \quad e > 0 \end{aligned} \tag{6.21}$$

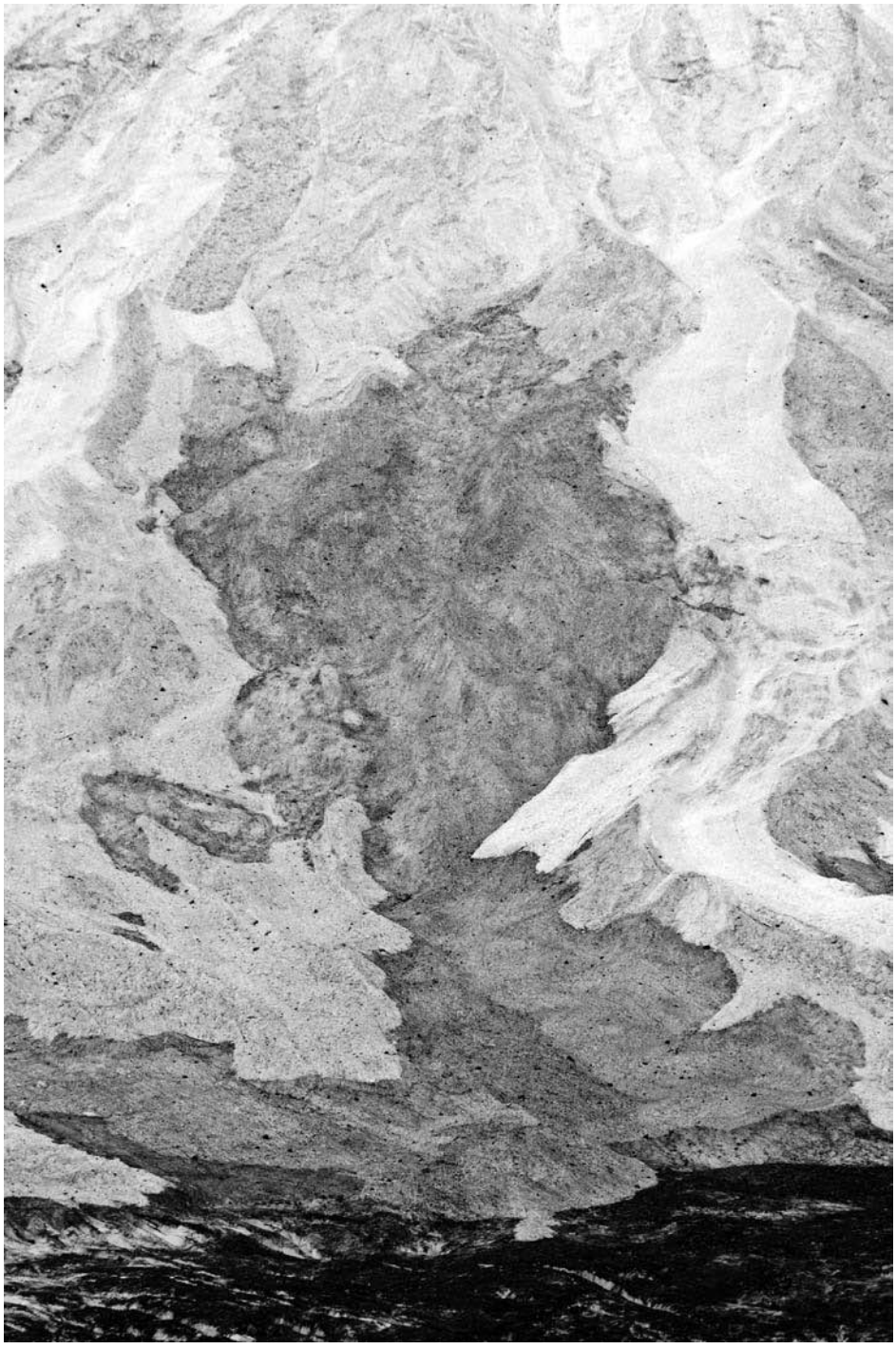

Fig. 6.9. Glacier in Chilean Patagonia

Fig. 6.10. Free boundary of glacier flow, Patagonia

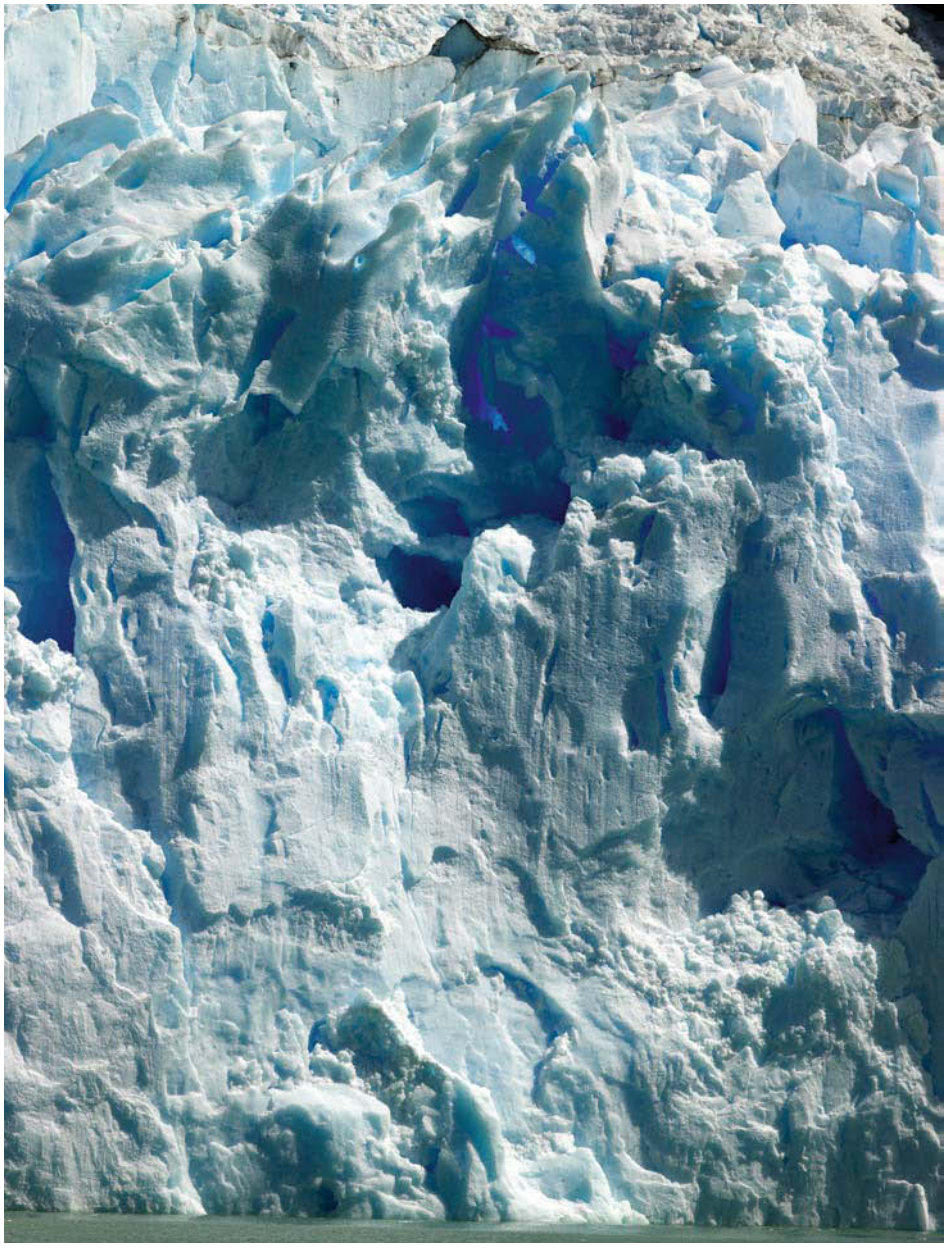

Fig. 6.11. A glacier front entering Lago Argentino

(see [9]). Now consider the degenerate parabolic PDE for the enthalpy:

$$e_t = \Delta\beta(e) + f\ , \quad x \in G\ ,\ t > 0 \tag{6.22}$$

subject to an initial condition

$$e(t = 0) = e_0 \tag{6.23}$$

which is such that $\theta_0 = \beta(e_0)$. Note that the temperature can be calculated uniquely from the enthalpy but not the other way around! Also we prescribe appropriate boundary conditions of Dirichlet or Neumann type (in correspondence to the boundary conditions (6.15)) on the fixed boundary ∂G:

$$e = e_1 \quad \text{on} \quad \partial G\ ,\ t > 0 \tag{6.24}$$

where, again, e_1 is such that $\theta_1 = \beta(e_1)$, or, resp.

$$\operatorname{grad} e.\nu = f_1 \quad \text{on} \quad \partial G\ ,\ t > 0\ . \tag{6.25}$$

It is a simple exercise in distributional calculus to show that a smooth solution e of (6.22)–(6.25), which is such that its 0-level set is a smooth surface in G for $t > 0$, gives a smooth solution θ of the Stefan problem (6.13)–(6.18), simply by defining the temperature $\theta = \beta(e)$ and the free boundary $\Gamma(t)$ as the 0-level set of $e(\cdot, t)$. The nice feature of the nonlinear initial-boundary value problem for the degenerate parabolic equation (6.22) is the fact that the phase transition boundary $\Gamma(t)$ does not appear explicitely. This allows for somewhat simpler analytical and numerical approaches.

For a collection of analytical results and references on the Stefan problem and its variants we refer to [8].

Comments on the Images 6.1–6.8 The Images 6.1–6.7 show icebergs in Patagonian lakes. Clearly, the free Stefan boundary is not visible itself, since it is the ice-water phase transition under the water surface. In Image 6.5 and in Image 6.6 we get a glimpse of it, though … What we see on the other images is – at least in part – the intersection of the free (Stefan) boundary with the fixed boundary (water surface). Note that about 7/8 of the mass of a typical iceberg is under water[3]!

Also the air-ice interface of icebergs, which is very well visible in most of the Images 6.1–6.7 is determined by a free boundary problem, however, of much more complicated nature than the Stefan Problem determining the ice-water phase transition. Clearly, various mechanisms enter in the formation of the above-water surface of an iceberg: the formation process of the iceberg itself (mostly through calving from a glacier) giving the initial condition, the wind pattern, erosion by waves, ablation (through solar radiation), melting …[4].

[3] *http://www.wordplay.com/tourism/icebergs*

[4] *http://www.wordplay.com/tourism/icebergs*

For a mathematical model of ablation see [1], where an integro-differential equation for the snow/ice surface is derived, based on the heat equation with a self-consistent source term accounting for ablation through solar radiation. We remark that in this reference the flow of melt water along the surface and refreezing effects are neglected (the paper deals with glacier surface modeling), which are important in iceberg surface modeling. In reference [1] it is argued that the derived nonlinear model, which takes into account surface light scattering, is able to describe typical glacier surface structures like penitents (resembling a procession of monks in robes), as can be seen in the Image 6.8.

Comments on the Images 6.9–6.11 For most macroscopic modeling purposes the flow of glaciers and ice fields is assumed to be slow and incompressible, taking into account a specific relationship between the strain tensor and the ice viscosity [6]. Assuming isothermal flow and shallow ice, a time-dependent highly nonlinear version of the obstacle roblem, based on a quasilinear diffusion equation for the local height (over ground) of the ice is obtained, known as a classical model of glaciology (see [6] for a physical derivation and references). The free boundary is represented by the edge of the glacier or ice field (the obstacle is the ground level surface!). In its most simple form, assuming 2-dimensional flow of an ice sheet over its bed surface $z = H(x)$, with small variations in x and uniform in the second spatial coordinate y, the model reads:

$$h_t = \left(\frac{(h-H)^5 h_x^3}{5} - u_b(x,t)(h-H) \right)_x + a(x,t) \quad \text{on} \quad \{h(x,t) > H(x)\} \ .$$

The unknown h denotes the height over ground, assuming uniformity of the flow in y, and u_b the given sliding velocity in x direction. Clearly, the cross-section of the ice sheet at time t is the set in the (x,z)-plane, where $H(x) < z < h(x,t)$. The flow is assumed to be driven by gravity, caused by the variation of the weight of the ice depending on its height, and by sliding at the ice-bed interface. For realistic glacier modeling large variations of the bed $z = H$ have to be taken into account to describe mountain slopes, e.g. by tilting the geometry. We remark that this problem becomes particularly interesting when source terms $a = a(x,t)$ are present, e.g. modeling snowfall on the glacier or ablation by solar rays. A mathematical analysis of properties of the free boundary (in one space dimension) can be found in [3]. We refer to [5] for an excellent account of glacier physics.

References

[1] M.D. Betterton, *Theory of Structure Formation in Snowfields motivated by Penitentes, Suncups, and Dirt Cones*, Physical Review E, Vol. 63, 2001

[2] L. Caffarelli, *The Obstacle Problem*, Fermi Lectures, Scuola Norm. Sup. di Pisa, 1998[5]

[3] N. Calvo, J.I. Diaz, J. Durany, E. Schiavi and C. Vazquez, *On a Doubly Nonlinear Parabolic Obstacle Problem modeling large Ice Sheet Dynamics*, SIAM J. Appl. Math., Vol. 63, No. 2, pp. 683–707, 2002

[4] A. Friedman, *Variational Principles and Free-Boundary Problems*, Wiley-Interscience, New York, 1982

[5] W.S.B. Paterson, *Physics of Glaciers*, Elsevier, 2000

[6] C. Schoof, *Mathematical Models of Glacier Sliding and Drumlin Formation*, Ph.D. thesis, University of Oxford, 2002

[7] J. Stefan, *Über die Theorie der Eisbildung, insbesondere über die Eisbildung im Polarmeere*, Annalen der Physik und Chemie, 42, pp. 269–286, 1891

[8] A.M. Meirmanov, *The Stefan Problem*, de Gruyter Expositions in Mathematics 3, 1992

[9] M. Paolini, *From the Stefan Problem to Crystalline Evolution*, Lecture Notes, 2002[6]

[10] A. Visintin, *Models of Phase Transitions*, Birkhäuser-Boston, Series: Progress in Nonlinear Differential Equations, Vol. 28, 1996

[11] C. Vuik, *Some historical notes about the Stefan problem, Nieuw Archief voor Wiskunde*, 4e serie, 11, pp. 157–167, 1993

[5] can be downloaded from *http://www.ma.utexas.edu/users/combs/Caffarelli/obstacle.pdf*

[6] can be downloaded from *http://www.dmf.bs.unicatt.it/cgi-bin/preprintserv/paolini/Pao02A*

7. Reaction-Diffusion Equations – Homogeneous and Heterogeneous Environments

Many physical, chemical, biological, environmental and even sociological processes are driven by two different mechanisms: on one hand there is diffusion, a random particle (= chemical molecule, biological cell or biological specimen) movement microscopically described by Brownian motion[1], and on the other hand there are chemical, biological or sociological reactions representing instantaneous interactions, which depend on the state variables themselves and possibly also explicitely on the particles' position. Typical examples are flame propagation, movement of biological cells in plants and animals (see Chap. 4 on chemotaxis and biological pattern formation), spread of biological species in homogeneous or in heterogeneous environments (for example in the three dimensionally terraced rice paddies in the southern Chinese Guanxi province depicted in the Images 7.1–7.3) etc.

For the mathematical modeling, let $u = u(x, t)$ be the d-dimensional concentration vector of the interacting particle species, where x in $\mathbb{R}^n$ denotes the position variable (typically $n = 1, 2$ or 3) and $t > 0$ time. Then the diffusion part of the motion is (in a quasilinear context) described by the parabolic evolution equation:

$$u_t = \operatorname{div}(D \operatorname{grad} u) \ ,$$

where D is a positive definite symmetric diffusion matrix, which may depend on x describing inhomogeneous diffusion, on t or/and even on the unknown vector u itself. Note that in the vector-valued case $\operatorname{grad} u$ denotes the Jacobi matrix of the vector field u. If D is a positive scalar valued function, then the direction of the diffusive flux is parallel to the gradient of the concentration function u, pointing in the direction of smaller values of u.

In the reaction-diffusion framework the reaction process is modeled by a 'local' dynamical system of the form

$$u_t = F(x, t, u) \ .$$

F is independent of the position variable x, if the process occurs in an unstructured (homogeneous) environment and x-dependent if spatial structure interacts instantaneously with the reaction. The t-dependence can be used to account for external time dependent driving forces.

[1] see, e.g., the excellent out-of-print book downloadable from *http://www.math.princeton.edu/∼nelson/books/bmotion.pdf*

Fig. 7.1. Terraced Rice Paddies in Guanxi Province, China

A classical example for F in the scalar case (one species only) is the so-called Fisher logistic nonlinearity:

$$F = u(1-u) \ .$$

The exact solution of the initial value problem for the so called logistic ordinary differential equation (ODE)

$$u_t = u(1-u) \ , \quad u(0) = u_0 \geq 0$$

is easily calculated:

$$u(t) = \frac{u_0}{\exp(-t) + u_0 \left(1 - \exp(-t)\right)} \ .$$

Note that there are two stationary states $u = 0$ (total extinction of the species, unstable) and $u = 1$ (total saturation, exponentially stable).

In order to describe the interaction of both types of processes, namely diffusion and reaction, we can imagine that on small time intervals the diffusion process and the reaction process happen consecutively. Then, when the lengths of the considered time intervals tend to zero, at least on a formal level, this time-splitting scheme turns into the so-called reaction-diffusion system

$$u_t = \operatorname{div}(D(x,t,u) \operatorname{grad} u) + F(x,t,u) \ .$$

If the process occurs in a spatially confined domain G, then boundary conditions have to be imposed, e.g. the Dirichlet condition

$$u = 0 \quad \text{on} \quad \partial G \, (\text{zero density outside } G)$$

or the Neumann condition

$$\operatorname{grad} u \cdot n = 0 \quad \text{on} \quad \partial G \, (\text{no outflow through the boundary}) \ .$$

Clearly, inhomogeneous boundary conditions may occur, as well as linear combinations of Dirichlet and Neumann conditions. Note that diffusion per se does not change the total number of particles (unless the boundary conditions interfere, as is the case, e.g., with homogeneous Dirichlet conditions) while the reaction term describes local generation and annihilation of particles of the considered species.

A different way of deriving reaction-diffusion equations proceeds by local mass balance. Therefore, denote by V an arbitrary subdomain of the domain G,

Fig. 7.2. Terraced Rice Paddies in Guanxi Province, China

with boundary S. Clearly, the (temporal) rate of change of the mass of the particles in V is equal to the mass created in V plus the net flow of material into V through S. In mathematical terms this law of local mass balance reads:

$$\frac{d}{dt}\int_V u(x,t)dx = -\int_S J(x,t)ds(x) + \int_V F\left(x,t,u(x,t)\right)dx\ ,$$

where $ds(x)$ denotes the $(n-1)$-dimensional surface element. The first term on the right hand side stands for the incoming flux through the boundary S, with flux density J, and the second term denotes the local mass production in V, with production per unit volume $F(x,t,u)$. The divergence theorem can be applied to the boundary integral and we obtain:

$$\int_V (u_t + \operatorname{div} J - F)dx = 0\ ,$$

such that, since V is arbitrary in G, we conclude that the integrand is zero, assuming its continuity:

$$u_t = -\operatorname{div} J(x,t) + F(x,t,u)\ , \quad x \in G, t > 0\ .$$

Assuming a Fick-type law, connecting the flux density with the concentration vector:

$$J(x,t) = -D(x,t,u)\operatorname{grad} u(x,t)$$

with a symmetric, positive definite diffusion matrix D, we obtain the reaction-diffusion equation already derived above. Note that the minus sign in the definition of the flux density accounts for the equilibrating tendency of diffusion, creating a flow from high densities to low ones.

Reaction-diffusion systems have been introduced by Fisher[2] in the year 1937 [4] and at the same time by Kolmogorov[3] et al. [5].

Classical examples of reaction-diffusion systems are the so called predator-prey models, often referred to as Lotka[4]–Volterra[5] equations, see [8]. Assuming that there is one species of prey, whose concentration is denoted by u, and one

[2] *http://www-groups.dcs.st-and.ac.uk/~history/Mathematicians/Fisher.html*
[3] *http://www-groups.dcs.st-and.ac.uk/~history/Mathematicians/Kolmogorov.html*
[4] *http://users.pandora.be/ronald.rousseau/html/lotka.html*
[5] *http://www-groups.dcs.st-and.ac.uk/~history/Mathematicians/Volterra.html*

Fig. 7.3. Terraced Rice Paddies in Guanxi Province, China

Fig. 7.4. Fields in Guanxi Province, China

species of predators with concentration v (here u and v are scalar variables, note the change of notation!), their interaction dynamics is modeled by:

$$u_t = d_1 \Delta u + au - buv - fu^2$$
$$v_t = d_2 \Delta v - dv + cuv - ev^2 \ ,$$

where a, b, f, d, c, e, d_1 and d_2 are positive constants or parameter functions. These reaction parameters can easily be interpreted. In the absence of predators and without diffusion, the prey species satisfies a logistic equation, predicting saturation at the value $\frac{a}{f}$, occuring with exponential speed at the rate a. Moreover, in the absence of prey and without diffusion, the predators die out exponentially, with exponential rate d. We remark that the parameters f and e account for the strength of intra-species friction among prey and predators resp. This friction, caused for example by competition for nutrients, stabilizes the prey population even without predators. If both species are present initially, then their respective rates of change are supposed to be influenced by the number of their encounters, typically ending badly for the prey, i.e. $b > 0$, and good for the predator, i.e. $c > 0$. Note that due to the quadratic nature of the Lotka–Volterra system, only two-body interactions prey-prey, predator-predator and predator-prey are taken into account by this model.

The coefficients d_1 and d_2 determine the strength of diffusion of prey and predators, resp. Obviously, the environment dependence can be accounted for by making the coefficients x-dependent in an appropriate way.

The mathematical literature on reaction-diffusion equations is vast. As a standard text we reference the textbook [9].

Typical mathematical questions in the theory of reaction-diffusion equations deal with existence of solutions, global boundedness of solutions by means of maximum and invariant region methods, large-time asymptotics, travelling waves and geometry and topology of attracting sets, singular limits etc.

The maybe most basic mathematical question refers to the stability properties of the reaction-diffusion system under consideration. For this, assume that, for simplicity's sake, D is independent of u and t, F independent of t and that $u_0 = u_0(x)$ is a stationary state of the reaction-diffusion system, i.e.

$$0 = \operatorname{div}(D(x) \operatorname{grad} u_0) + F(x, u_0) \ .$$

An important question concerns the behaviour of solutions of the nonlinear system in comparism with the solutions of the linearized system, when the linearization is performed at the stationary state u_0, in direction of a function v:

$$v_t = \operatorname{div}(D(x) \operatorname{grad} v) + D_u F(x, u_0) v \ .$$

Clearly, this is still a difficult problem in full generality (and also for many particularly interesting cases). Thus, it seems intruiging to neglect diffusion and to analyse the linear ODE system instead

$$w_t = D_u F(x, u_0) w \ .$$

At least in the homogeneous case, where D, F and consequently u_0 are independent of x, it suffices to calculate the eigenvalues of $DF(u_0)$ to decide about linearized, diffusionless stability. If all eigenvalues have negative real parts, then only exponentially decaying modes of w exist, eigenvalues with positive real parts generate exponential instabilities and more information is required if eigenvalues with zero real part occur. In the first two cases the linearized behaviour carries over to the diffusionless nonlinear ODE system locally around stationary points.

For example, take the predator-prey model formulated above. Then, neglecting diffusion, a simple calculation shows the existence of two stationary states, namely $(0, 0)$ corresponding to extinction of both species and a state (u_0, v_0) with

$$u_0 = \frac{ae + db}{ef + bc}$$
$$v_0 = \frac{ac - df}{ef + bc} \ .$$

Note that the predator-equilibrium value becomes negative unless $ac - df > 0$.

Fig. 7.5. Fields in Chiapas, Mexico

A simple calculation shows that the extinction state is the intersection of a 1-dimensional stable manifold corresponding to the predator species and an unstable one corresponding to the prey species. The other stationary state is stable (in the linearized sense when diffusion is neglected and when $ac - df > 0$).

A very interesting phenomenon happens when diffusion is taken into account in the stability analysis. Although, intuitively speaking, diffusion stabilizes particle flow, there are cases of reaction-diffusion vector systems ($d > 1$!) with stationary points, which are exponentially stable in the diffusionless case AND feature unstable modes if appropriate diffusion is taken into account. This so called Turing instability (see [11]) is generated by sufficiently different diffusivities for the different components of the vector u. An example is given in Chapter 4, in the context of biological pattern formation.

For analytical results on diffusive predator-prey models in heterogeneous environments we refer to [3].

While modeling and analysis of reaction-diffusion systems in spatially unstructured environments (i.e. the nonlinearity of F and the diffusion matrix D are

independent of the position variable x) is by now a classical subject, the study of the interaction of the spatial structure with reaction and diffusion has only started recently, particularly in biological/environmental/population dynamics models. In this respect we cite [10]:

> In the last two decades, it has become increasingly clear that the spatial dimension and, in particular, the interplay between environmental heterogeneity and individual movement, is an extremely important aspect of ecological dynamics.

In many cases when persistence of species or invasion of species into environments are analyzed, the standard assumption of homogeneity of the environment is obsolete and position dependent nonlinear reaction terms and diffusion matrices have to be considered. Local environmental properties very often influence individual survival and macroscopic persistence of species. For mathematical results on reaction-diffusion equations in periodic media we refer to the re-

Fig. 7.6. Namibian savanna

cent papers of Henri Berestycki (and coworkers), which (among others) can be downloaded from his webpage[6].

Also, we point out the work of S.A. Levin[7], in particular the review paper [6].

As an important and mathematically interesting example for the interaction of heterogeneity and reaction-diffusion we mention homogenisation problems. Consider a periodically fragmented environment, with a periodicity scale which is small compared to the total characteristic dimension of the environment and denote by the small positive parameter ε the dimensionless ratio of these two length scales, i.e. the microscopic-macroscopic ratio.

Then it is reasonable to assume that the diffusion matrix and the reaction nonlinearity F are periodic in the position variable, with periodicity of the order ε. In precise terms, let

$$D = D(y) \,, \quad F = F(y, u) \,,$$

where D and F are periodic with respect to an n-dimensional lattice L (i.e. the set of n-vectors with integer components) in y, define the fast scale

$$y = \frac{x}{\varepsilon}$$

[6] *http://www.ehess.fr/centres/cams/person/berestycki/*
[7] *http://www.eeb.princeton.edu/∼slevin/*

and consider the reaction-diffusion system

$$u_t = \operatorname{div}\left(D\left(\frac{x}{\varepsilon}\right)\operatorname{grad} u\right) + F\left(\frac{x}{\varepsilon}, u\right)$$

either on the whole space $\mathbb{R}^n$ or on a bounded domain with appropriate boundary conditions. For the sake of simplicity, we neglected slow scale effects in D and in F.

The main question is whether slow scale 'averaged' dynamics can be extracted from the fast scale problem without actually resolving the fast scale features. In

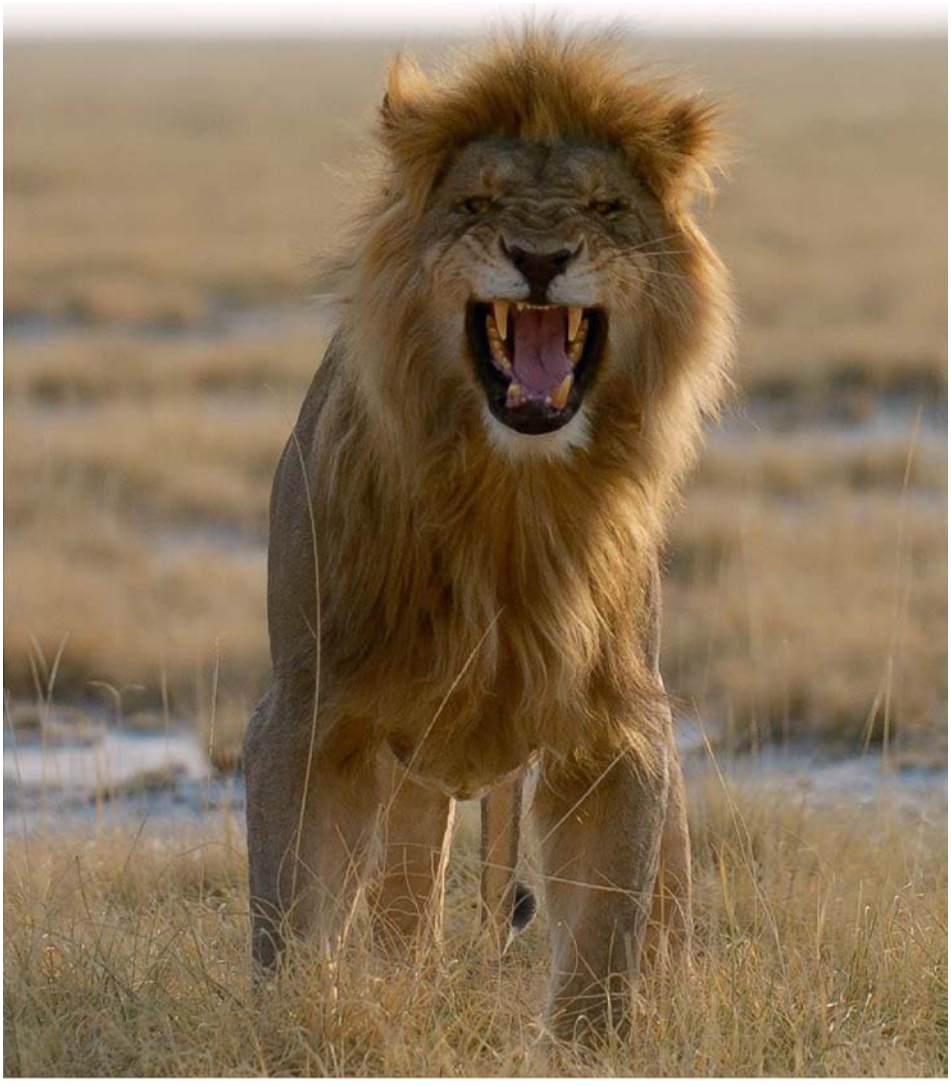

Fig. 7.7. Male lion

Fig. 7.8. Eagle

other words, does the solution u converge to a limit as ε converges to zero? If yes, how can we characterize this limit?

For 'good' nonlinearities we expext a homogenized reaction-diffusion equation to hold for the limit u^0, of the form:

$$u_t^0 = \operatorname{div}(D^0 \operatorname{grad} u^0) + F^0(u^0) \ .$$

Here the 'homogenized' (constant coefficient) diffusion matrix D^0 is obtained in analogy to the linear case by solving a cell problem (see [7], [2]) and F^0 is obtained by computing the average of $F(., u)$ over a lattice cell C:

$$F^0(u) = \frac{1}{\operatorname{vol} C} \int_C F(y, u) dy \ .$$

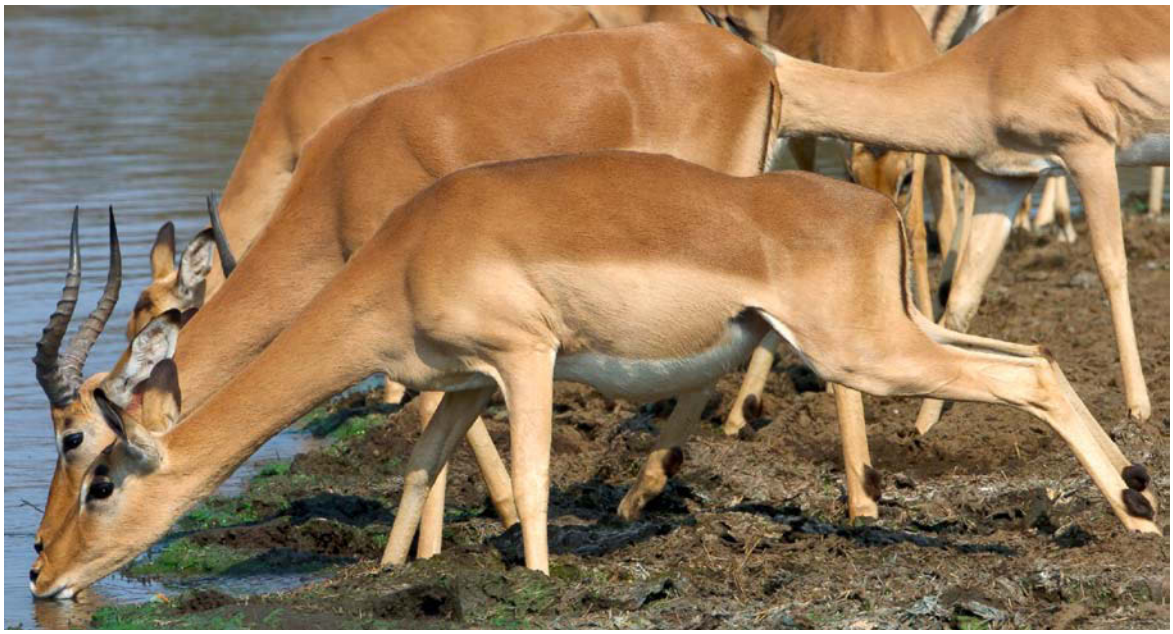

Fig. 7.9. Impala

Fig. 7.10. Predator and Prey

The theory becomes more involved, when slow scale dependence of D and/or F is considered, too. Then double scale convergence techniques have to be applied.

Comments on the Images 7.1–7.5 The Images 7.1–7.3 show three dimensionally terraced rice paddies[8] in the Chinese province Guanxi, close to the city of Guilin. Clearly, these are excellent examples for heterogeneous biological environments, where heterogeneity is introduced through the topography of the hillside on which the paddy is located and through the walls separating the paddies, which inhibit the global spread of certain (invading or intentionally introduced) species

[8] *http://en.wikipedia.org/wiki/Paddy_field*

or at least change their invasion patterns. Also we remark that the paddies are connected by irrigation, which has to be included as a convection term into the reaction diffusion system modeling biological populations in a terraced rice

Fig. 7.11. Lagoa Rodrigo de Freitas, from Corcovado. Rio de Janeiro, Brazil

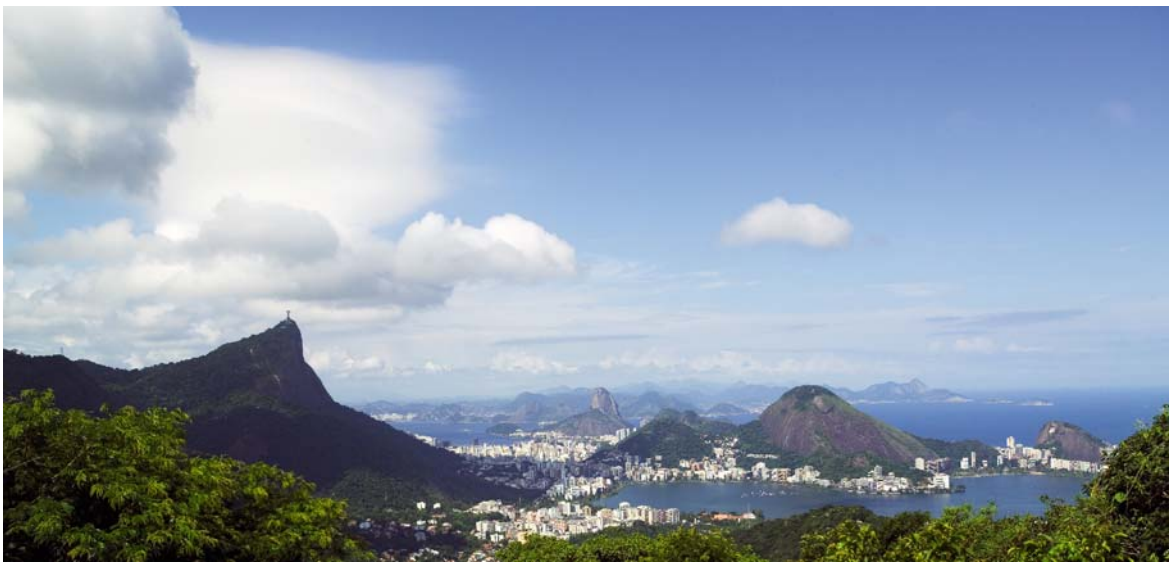

Fig. 7.12. Lagoa Rodrigo de Freitas (*foreground*) and Guanabara bay, Rio de Janeiro, Brazil

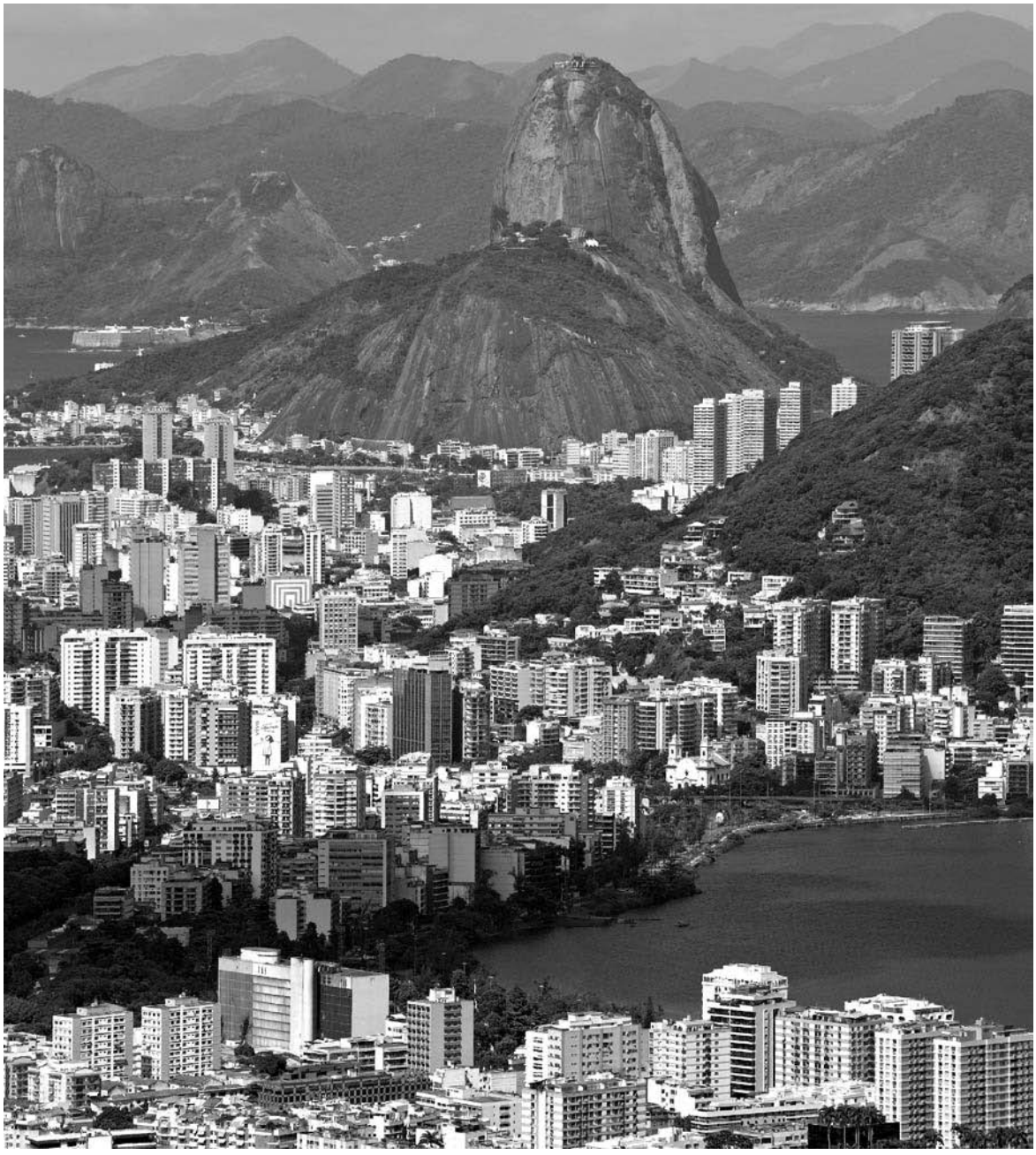

Fig. 7.13. Lagoa Rodrigo de Freitas (*foreground right side*) and Sugar Loaf Mountain, Rio de Janeiro, Brazil

paddy field, with a downhill pointing drift vector field representing the water flow pattern.

The Images 7.4, 7.5 show patches of fields of different crop, another classical example of heterogeneous biological environments. An important question, which mathematics can strive to answer is how to do the patching in an optimal way in order to minimise the success of invasion of detrimental biological species into agricultural systems. For more information of the distinctive features of species invasion in heterogeneous environments (compared to homogeneous environments) we refer to the work of Tom Robbins[9].

Comments on the Images 7.6–7.10 African savanna environments[10] are classical examples, where Lotka-Volterra predator-prey models can be applied. Typical well studied examples are lion-wildebeest or lion-zebra interactions. Clearly, savannas are highly complex ecosystems and the degree of accuracy in the modeling of savanna population dynamics can only be increased at the cost of enormously growing complexity. For example, when the interaction of a number of predator species with a number of prey species is considered in a realistic context, then large systems of reaction-diffusion equations are obtained. Typically, a number of predator species compete for the same prey species, e.g. lions, hyenas and leopards feed on impalas, kudus, zebras, wildebeest etc. Even more accuracy can be achieved by taking into account the social behaviour of predators and prey species, by self-consistently coupling the predator-prey systems with reaction-diffusion equations modeling savanna vegetation and by incorporating seasonal/climatic changes.

The Images 7.7–7.10 were shot in national parks of South Africa and Namibia. Note that population dynamics in national parks have to take various specific effects into account. Often parks in Africa are fenced giving rise to zero-outflow boundary conditions (homogeneous Neumann boundary conditions) for the wildlife population densities satisfying predator-prey equations (idealizing a no-penetration/escape situation, which is often unrealistic as in the case of lions escaping through holes in the fence of Etosha National Park in northern Namibia). Also, in some parks culling of certain animal species is done in order to counteract the roaming restrictions imposed by fencing (as it was done with elephants in South African parks) and in many cases animals are introduced into parks by the National park biologists. These processes have to be described by annihilation/generation terms in the reaction-diffusion equations. Savannas also carry typical features of heterogeneity. Animal interactions statistics vary according to geographical features and predator-prey encounters have different statistical outcomes in different locations (e.g. on a waterhole compared to open savanna grassland), animals tend to diffuse more into their preferred habitat (often vegetation dependent) etc., such that the encounter and diffusion coefficients in the Lotka–Volterra systems depend strongly on position.

[9] *www.math.utah.edu/∼robbins/*

[10] *http://www.blueplanetbiomes.org/savanna.htm*

Comments on the Images 7.11–7.13 The Images 7.11–7.13 show the Lagoa (Portugese for Lagoon) Rodrigo de Freitas in the city of Rio de Janeiro in Brazil. Obviously, the ecological management of this lagoon is of significant importance for the economy and overall ecology of the city. The same can be said about other lagoons in urban or semi-urban environments (think of the lagoon of the city of Venice in Italy, for example).

The ecological balance of a lagoon is to a large extent represented by the phytoplankton-zooplankton-nutrient-oxygen interaction, which is typically of predator-prey type. We refer to [1], where a convection-diffusion-predator-prey model for a prototypical shallow lagoon is presented and mathematically analysed, in particular with respect to the existence of time-periodic solutions (assuming period inputs), which represent long-term coexistence states.

References

[1] W. Allegretto, C. Mocenni and A. Vicino, *Periodic Solutions in Modeling Lagoon Ecological Interactions*, to appear in J. Math. Biology, 2006
[2] A. Bensoussan, J.L. Lions and G. Papanicolaou, *Asymptotic Analysis for Periodic Structures*, Studies in Mathematics and its Applications 5, North Holland Publishing Co., 1978
[3] Y. Du and S.-B. Szu, *A diffusive Predator-Prey model in heterogeneous Environment*, JDE, Vol. 203, 331–364, 2004
[4] R.A. Fisher, *The advance of advantageous genes*, Ann. Eugenics 7, 335–369, 1937
[5] A.N. Kolmogorov, I.G. Petrovsky, and N.S. Piskunov, *Étude de l'équation de la diffusion avec croissance de la quantité de matière et son application à un problème biologique*, Bulletin Université d'État à Moscou (Bjul. Moskowskogo Gos. Univ.), Serie internationale A 1, 1–26, 1937
[6] S.A. Levin, *Population Dynamics Models in Heterogeneous Environments*, Ann. Rev. Ecol. Syst., Vol. 7, 287–310, 1976
[7] P.A. Markowich and C. Sparber, *Highly Oscillatory Partial Differential Equations*, in: Applied Mathematics Entering the 21st Century: Invited Talks from the ICIAM 2003 Congress, James M. Hill and Ross Moore, Editors, SIAM Proceedings in Applied Mathematics 116, 2004
[8] J.D. Murray, *Mathematical Biology*, Springer, Berlin, 1993
[9] J. Smoller, *Shock Waves and Reaction Diffusion Equations*, Springer-Verlag, Grundlehren Series, 258, 608 pp, 1982
[10] P. Turchin, *Qualitative Analysis of Movement*, Sinauer Assoc. Inc., Sunderland, Mass., 1998
[11] A.M. Turing: *The Chemical Basis of Morphogenesis*, Philosophical Transactions of the Royal Society (B) 237, 37–72, 1952

8. Optimal Transportation and Monge–Ampère Equations

Assume that a construction entrepreneur faces the following problem: there is a pile of soil, sand or rubble (deblais) which has to be moved into a hole or fill (remblais) of equal volume. Or imagine a farmer, who has to move a pile of grain into a silo. Of course, for simple economic reasons, in both cases, the transportation of the materials should be carried out at the least possible transportation cost or labor. Typically, this cost is related to the distance, which (point) masses have to travel during the transportation process and intuitively it is clear that the optimal transportation plan (if it exists) will depend decisively on the geometries of the material pile and the volume to be filled by it, or more generally, on the local mass densities of the pile and of its desired allocation, if non-uniform mass distributions are considered.

This problem was originally formulated and analysed by the French civil engineer Gaspard Monge[1] in the year 1781 [13], initiating a profound mathematical theory, which connects the seemingly different areas of differential geometry, linear programming, nonlinear partial differential equations and probability theory. At this point we already remark that numerous other applications of the so called Monge–Kantorovich optimal mass transportation theory (we shall see in a moment how the Nobel laureate L.V. Kantorovich[2] came into this field) and its variants exist, many of them within the realm of our daily lives and of the nature that surrounds us. Here we mention optimal water distribution in irrigation channel systems, optimal urban planning (allocation of housing, service and office locations in cities), traffic network planning in cities, internet traffic optimisation, blood vessel branching in the human arterial/venous system, optimal branching in the growth of trees, structuring of arteries in leaves, branching of rivers systems, shape optimisation, meteorological fluid dynamics (semigeostrophic equations) … For an overview of these (and other) applications we refer to the survey [9] and to the references [5], [1]. Note that all these applications have one common feature: they deal with the transport of a supply measure (representing e.g. a mass density, density of residential areas in a city, bit density etc.) into a demand measure under the condition of minimizing an associated cost or work functional. In some cases there is an additional minimisation problem involved, typically determining some optimal geometry along which the transport is affected or an optimal graph, e.g. an urban transportation system or internet nodes. The photographs associated with this Chapter illustrate some modeling applications of

[1] *http://www-groups.dcs.st-and.ac.uk/~history/Mathematicians/Monge.html*
[2] *http://nobelprize.org/economics/laureates/1975/kantorovich-autobio.html*

Fig. 8.1. 'Deblais', modern Mass Transportation

the Monge–Kantorovich theory, as discussed in more detail in the comments to the Images 8.1–8.11.

Before we discuss the mathematics of optimal mass transportation we want to mention the excellent book [14], which to our knowledge is the most complete and readable mathematical account of the Monge–Kantorovich mass transportation problem and its link to the above mentioned other areas of modern mathematics.

To start the technical discussion, let f and g be two nonnegative Radon measures on $\mathbb{R}^n$, where f represents the original mass density supported in the deblais (denoted by X in the sequel) and g the desired mass density supported in the remblais (denoted by Y in the sequel), after transportation (clearly, $n = 3$ in most applications). We assume that both f and g are bounded measures with the same total mass. In mathematical terms the transportation is affected by a map $S\colon X \to Y$, which is one-to-one, measurable and pushes the measure f into the measure g, i.e.

$$f\left(S^{-1}(A)\right) = g(A) \quad \text{for all Borel sets} \quad A \subseteq Y\,. \tag{8.1}$$

For a given mass point $x \in X$, $y = S(x)$ denotes its location after transportation. Note that for measures f, g which are uniform in the deblais X and remblais Y resp., the condition (8.1) is – for smooth maps S – equivalent to

$$\det |DS(x)| = \frac{\mathrm{vol}(Y)}{\mathrm{vol}(X)} \quad \text{for all} \quad x \in X\,,$$

Fig. 8.2. 'Deblais', old fashioned Mass Transportation

where $DS(x)$ denotes the Jacobian of the map $S = S(x)$. Now let $c = c(x, y)$ be the transportation cost (or work), given by a nonnegative measurable function c, which maps $X \times Y \to \mathbb{R}^+$. We can think of the value $c(x, y)$ as the cost or work it takes to move the mass point x in X into the point y in Y. Then the total transportation cost (or work) is defined by:

$$C_c(f, g; S) := \int_X c\left(x, S(x)\right) df \ . \tag{8.2}$$

As already mentioned above, intuitively speaking, c typically is a function of the Euclidean distance $|x - y|$. Actually, very important classical cases are

$$c(x, y) := |x - y| \tag{8.3}$$

used by Monge, assuming that the transportation cost is equal to the distance of a mass point before and after transportation, and the quadratic case

$$c(x, y) := \frac{|x - y|^2}{2} \ . \tag{8.4}$$

In non-standard applications as in urban transportation network planning or in irrigation networks other, more complicated cost functions arise.

The Monge formulation of the optimal transportation problem reads:

$$O_c(f, g) = \inf C_c(f, g; S) \ , \tag{8.5}$$

where the infimum is taken over all transportation maps S, which are one-to-one on from X to Y, measurable and push the measure f into g. Obviously, this is a very difficult optimisation problem, mainly due to the highly nonlinear constraint (8.1) on S and due to the seemingly total lack of compactness of minimizing sequences. No derivative of S is involved in C_c, which might give coercivity!

A big step forward was taken by L.V. Kantorovich in the '40 s (see [11], [12]). He introduced the following relaxed version of the Monge problem: Consider the functional

$$R_c(f,g,\pi) := \int\limits_{X\times Y} c(x,y)\pi(dx,dy)\ , \tag{8.6}$$

where π is a bounded nonnegative Borel measure on $X \times Y$ with marginals f and g, i.e. loosly speaking

$$\int\limits_X \pi(dx,y) = g(y) \tag{8.7}$$

$$\int\limits_Y \pi(x,dy) = f(x) \tag{8.8}$$

and minimize $R_c(f,g,\pi)$ over all those measures π:

$$P_c\,(f,g) := \min R_c\,(f,g,\pi)\ . \tag{8.9}$$

In fact the functional R_c is linear in π and there is enough compactness to proof that minimizing sequences converge to a minimizer. But how are these two problems related? First of all, we note that for all admissible transportation maps S the measure

$$\pi(x,y) := f(x)\,\delta\left(y - S(x)\right) \tag{8.10}$$

satisfies (8.7) and (8.8). However, generally, a minimizer π of (8.9) may not be of the form (8.10) such that it does NOT in general correspond to a transportation map and thus to a solution of the Monge problem.

Now let us consider the case, where f and g are absolutely continuous with respect to the Lebesgue measure on $\mathbb{R}^n$, represented by smooth functions (which, sloppily, we denote by the same symbols) of compact supports X and Y, resp., and that the transportation cost is given by the quadratic function (8.4). In this case the problem of constructing an optimal transportation plan was basically resolved by Yann Brenier[3] in [3] who proved a striking polar decomposition theorem of smooth vector fields as composition of a gradient map (of a convex scalar potential) and a Lebesgue measure preserving map. This very remarkable

[3] *http://math1.unice.fr/∼brenier*

theorem can be regarded as a nonlinear version of the Helmholtz decomposition theorem, which additively decomposes a smooth vector field into a divergence free vector field, tangential to the boundary of the domain, and a gradient map. It turns out, by using a dual formulation by Kantorovich of the Monge problem (which is a continuous version of linear programming) that the optimal transportation map is the gradient of a convex potential, i.e.

$$S_{\text{opt}}(x) = \text{grad}\, V(x)\,, \quad V \text{ convex on } X\,. \tag{8.11}$$

Since (8.1) implies (after a weak formulation using test functions), assuming sufficient smoothness of S:

$$g\left(S(x)\right) \det\left(DS(x)\right) = f(x), \tag{8.12}$$

we conclude that V is a (weak) solution to the following Monge–Ampère equation:

$$\begin{gathered} g(\text{grad}\, V) \det(D^2 V) = f(x),\ x \in X \\ \text{grad}\, V : X \to Y \end{gathered} \tag{8.13}$$

($D^2 V$ stands for the Hessian of V). This links the Monge–Kantorovich mass transportation theory to the area of partial differential equations. We remark that the Monge–Ampère equation is a fully nonlinear elliptic differential equation, which has only recently been investigated in a detailed mathematical way. In particular we refer to the work of Luis Caffarelli[4] [6], [7], [8], which presents a deep regularity theory for the Monge–Ampère equation, basically giving results analogous to the Schauder theory for linear elliptic equations. Note that even the interpretation of the equation (8.13) is not obvious since convex functions in general do not have pointwise second derivatives, in full generality $D^2 V$ is – due to convexity of V – a matrix of signed measures only!

The solution of the Monge–Kantorovich optimisation problem is even more complicated if the cost function $s = s(|x - y|)$ is not uniformy convex, e.g. in the original case of Monge (8.3). Here we only mention that, again under the above assumptions on the measures f and g, the optimal transportation map exists and satisfies:

$$S_{\text{opt}}(x) = x - a(x)\text{grad}\, u(x)\,, \tag{8.14}$$

where u is again a scalar potential with $|\text{grad}\, u(x)| = 1$ and a is nonnegative. We refer to [9] on how to recover u and the distance a from the measures f and g.

Obviously, for more complex realistic applications the cost functional has to be adapted, in particular when there are (geometrical or other) constraints on the transportation trajectories. Heuristically speaking, the Monge–Kantorovich problem corresponds to the case where all possible transportation roads exist

[4] *http://rene.ma.utexas.edu/users/caffarel/*

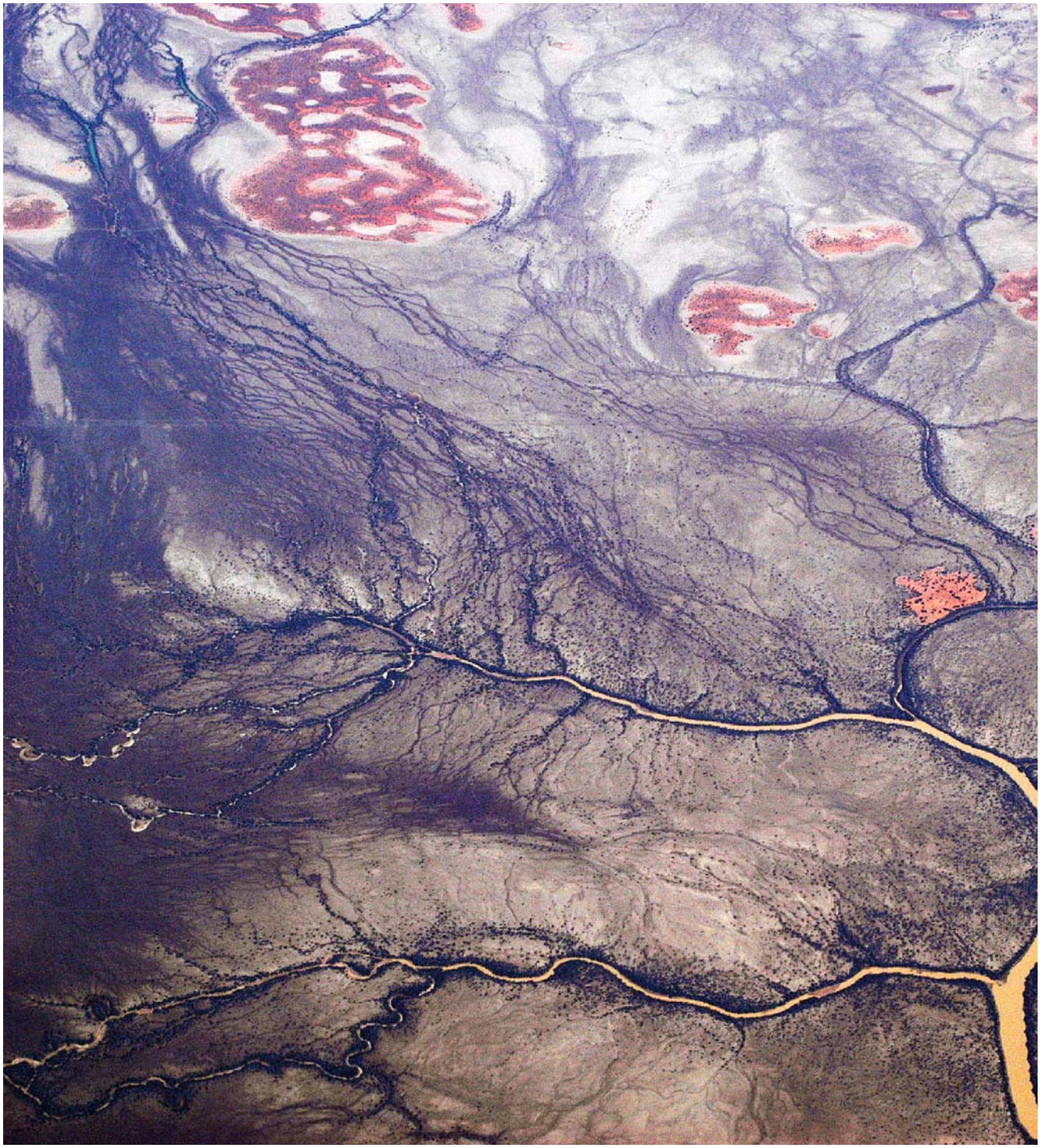

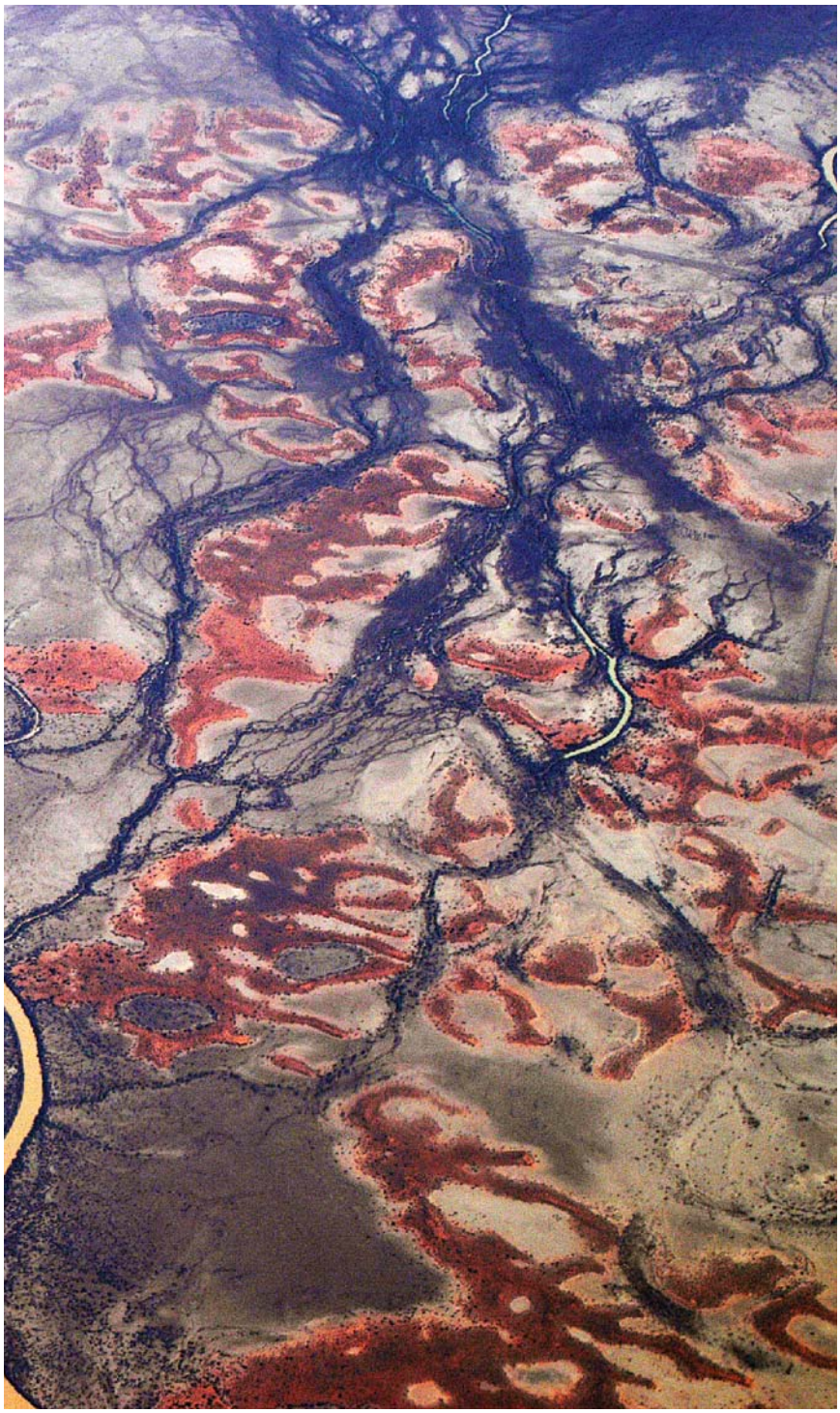

Fig. 8.3. River Bed Branching, Central Australia

Fig. 8.4. Branching of Vessels in Lotus Leafs

Fig. 8.5. Branches of a tree, Kalahari Desert

and do not enter in the minimisation process. In many applications, however, the construction of the transportation roads is really part of the transportation problem itself. For example, Buttazzo and Stepanov in [5] analyse the problem of constructing an optimal public transportation network in a city, based on Monge–Kantorovich mass (measure) transportation theory. They let f represent the density of housing locations, g the density of work places and define a cost function, which expresses the fact that an inhabitant of a city either can walk from the point x to the point y, or, if altogether shorter, walk from x to the nearest point in the transportation network (represented by a closed connected subset U of the city), use the network until the closest point to y and then walk from there to y. Then they define a Kantorovich functional in analogy to (8.6), and minimise again over all transportation network sets U with a one-dimensional Hausdorff measure less than or equal to a prescribed maximal network length.

Comments on the Images 8.1–8.11 The Images 8.1–8.11 show classical and modern applications of the Monge–Kantorovich mass transportation theory.

In the Images 8.1 and 8.2 we can see piles of construction material ('deblais') to be moved, most likely to a fill ('remblais') on the same or on a different construction site. This is the application which G. Monge had in mind in the 1780's, when he gave the now classical (original) Monge-formulation [7] of the Monge–Kantorovich mass transportation problem. Clearly, the means of realizing the transportation map differ in Images 8.1 and 8.2 and the importance for minimizing the transportation cost is quite evident, particularly in Image 8.2 …

The Images 8.3 to 8.7 feature examples of branching and irrigation flow networks, in particular river branching in Image 8.3, leaf vessel branching in Image 8.4 and branches of trees in the Images 8.5–8.7. These examples and many others can be regarded as supply-demand systems, where goods (nutrient fluids or river water) are transported from the supply location (e.g. the base of the leaf or an upstream location in the riverbed) to the demand location (e.g. the leaf's perimeter or a downstream location in the riverbed). It is clear that the original versions of the Monge–Kantorovich optimal mass transportation cannot be applied directly, particularly since their solutions are transference plans of minimal cost, which do not take possible infrastructures and 'infrastructure costs' into account, i.e. there is no biasing of transportation trajectories in the Monge–Kantorovich problem. The trajectories are simply geodesics (straight lines in the Euclidean setting). Various generalisations, taking into account network costs by differentiating the transportation costs on low and high capacity edges, were suggested by E.N. Gilbert [10], Q. Xia [15] and M. Bernot, V. Caselles and J.-M. Morel [2] (among others). For a review of the existing literature and a wealth of new results on irrigation plans (not taking into account 'who goes where', only prescribing the supply and demand measures) and traffic plans (taking into account 'who goes where', prescribing a transportation plan) we refer to [2]. Most generally, traffic plans are defined as probability measures on spaces of transport paths (connected and piece-

Fig. 8.6. Branches of trees, Dead Vlei, Namibian Desert

Fig. 8.7. Branches of a tree, Dead Vlei, Namibian Desert

Fig. 8.8. Urban planning in Buenos Aires, for the living …

wise smooth curve segments). Associated transportation plans are measures representing the mass transported THROUGH a given traffic plan, connecting the irrigating (source) measure with the irrigated (demand) measure. The cost functional of traffic plan is set up according to infrastructural expenses and constraints. In analogy to the Kantorovich cost functional a minimisation over irrigation plans connecting a given supply to a given demand measure or, resp., over traffic plans with a given transportation plan is carried out, leading to the simultaneous construction of the transport paths and the transportation plan. Note that a major difference to the Kantorovich problem lies in the fact that the cost function generally depends on the whole transportation path and not only on its endpoints!

The Images 8.8–8.11 depict urban areas in Buenos Aires, Quito and Rio de Janeiro. Recently, urban planning models based on Monge–Kantorovich mass transportation have been introduced in the literature. We cite [4], where a very interesting model of optimal distribution of residential areas (density f) and service areas (density g) in an urban environment is presented, which we shall discuss in some detail thereafter. The model is based on the propositions that there is a transportation cost for moving between residential and service areas, that overcrowding of residential areas is typically avoided by city dwellers and that concentration of services is desirable for increasing efficiency. Obviously,

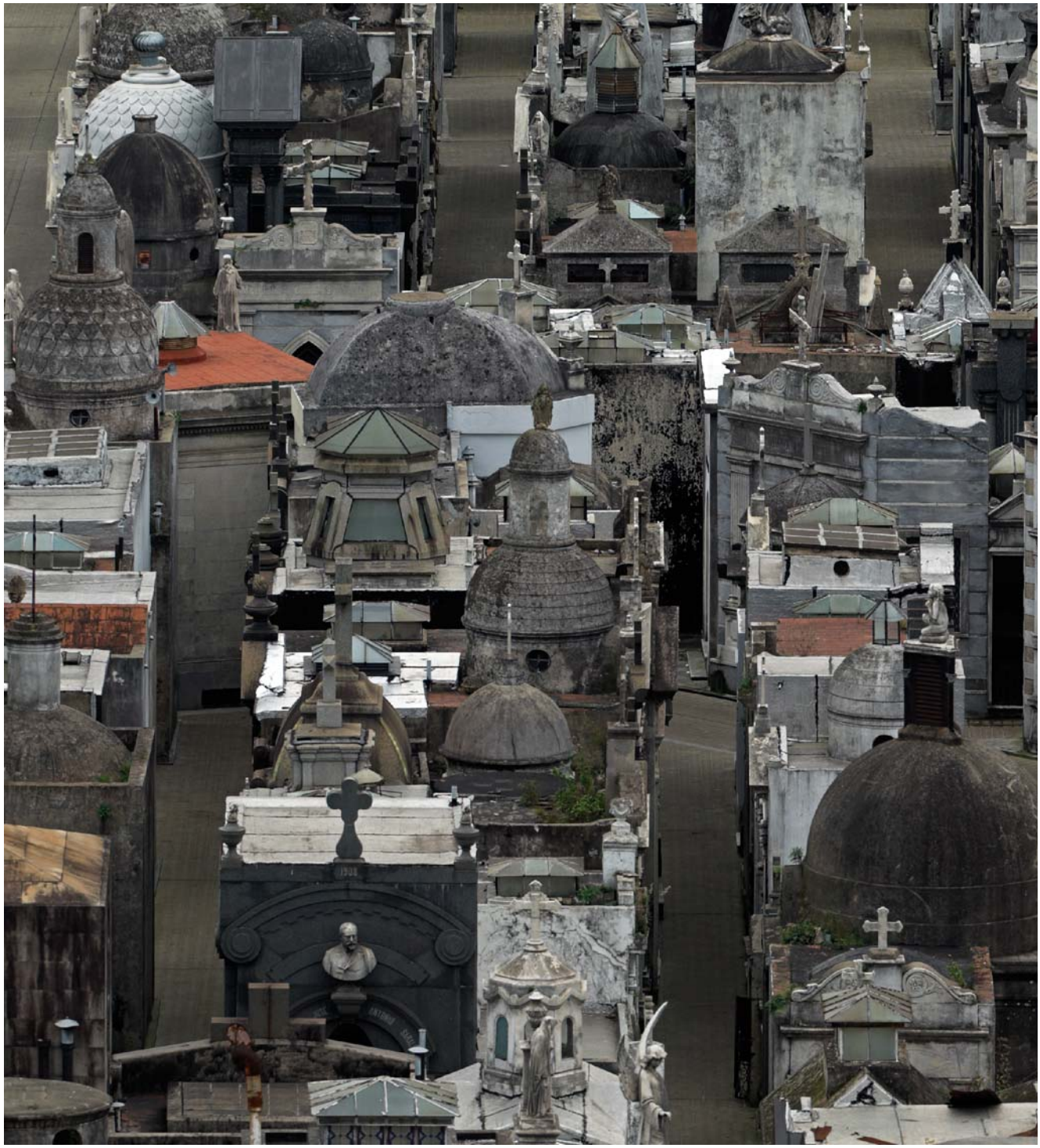

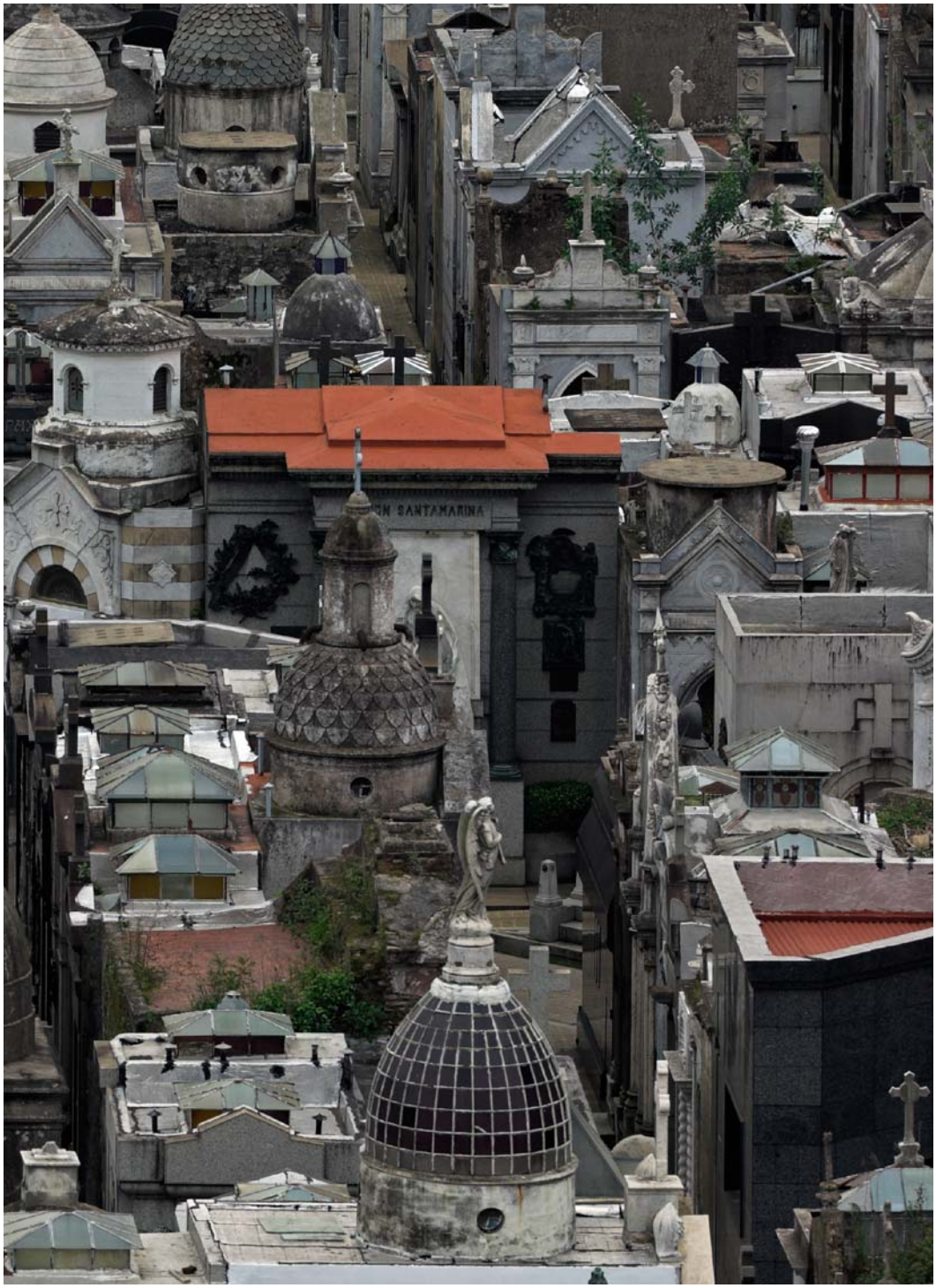

Fig. 8.9. Urban planning in Buenos Aires, for the deceased …

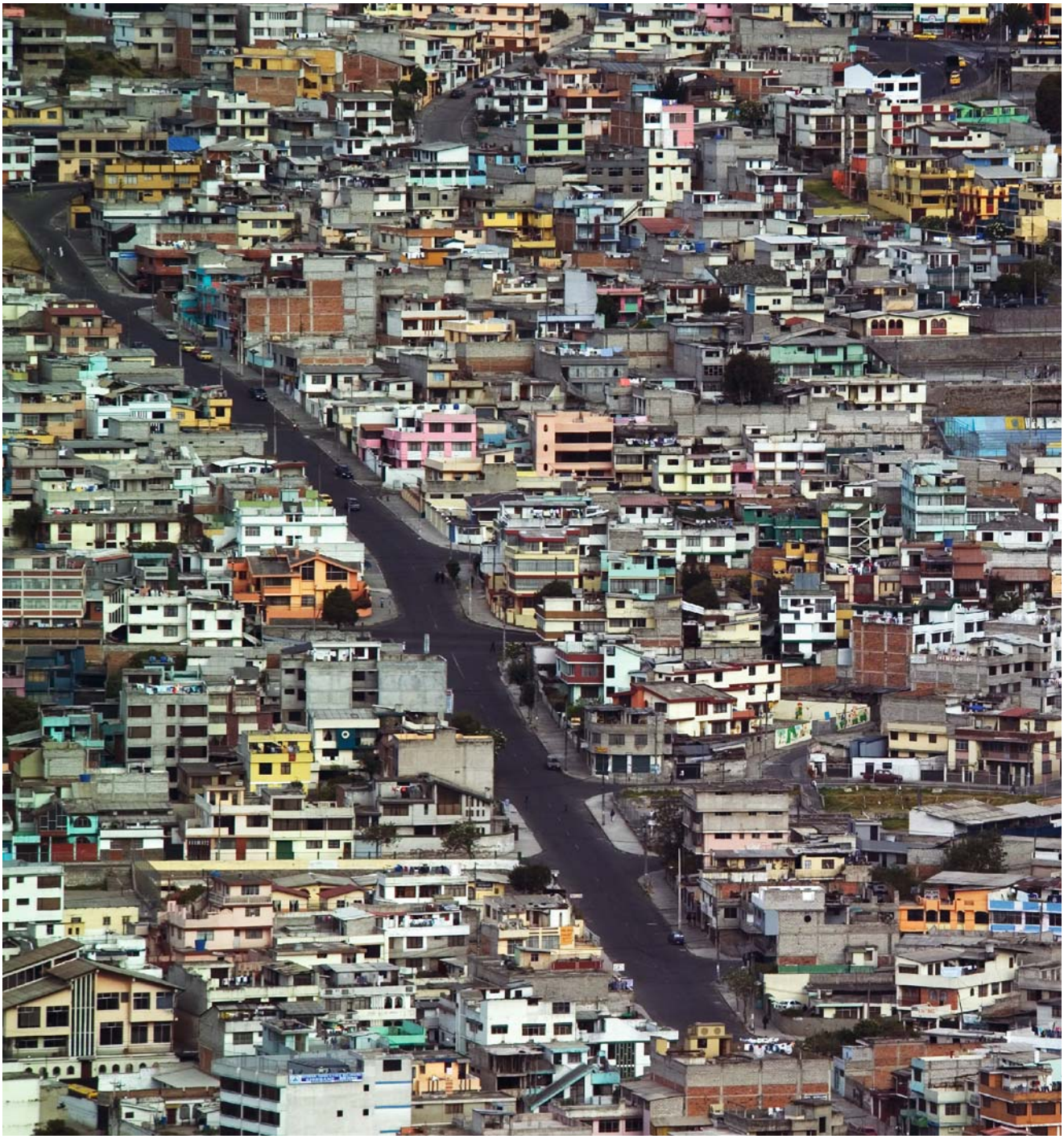

Fig. 8.10. Urban planning in Quito (Ecuador), or lack of it …

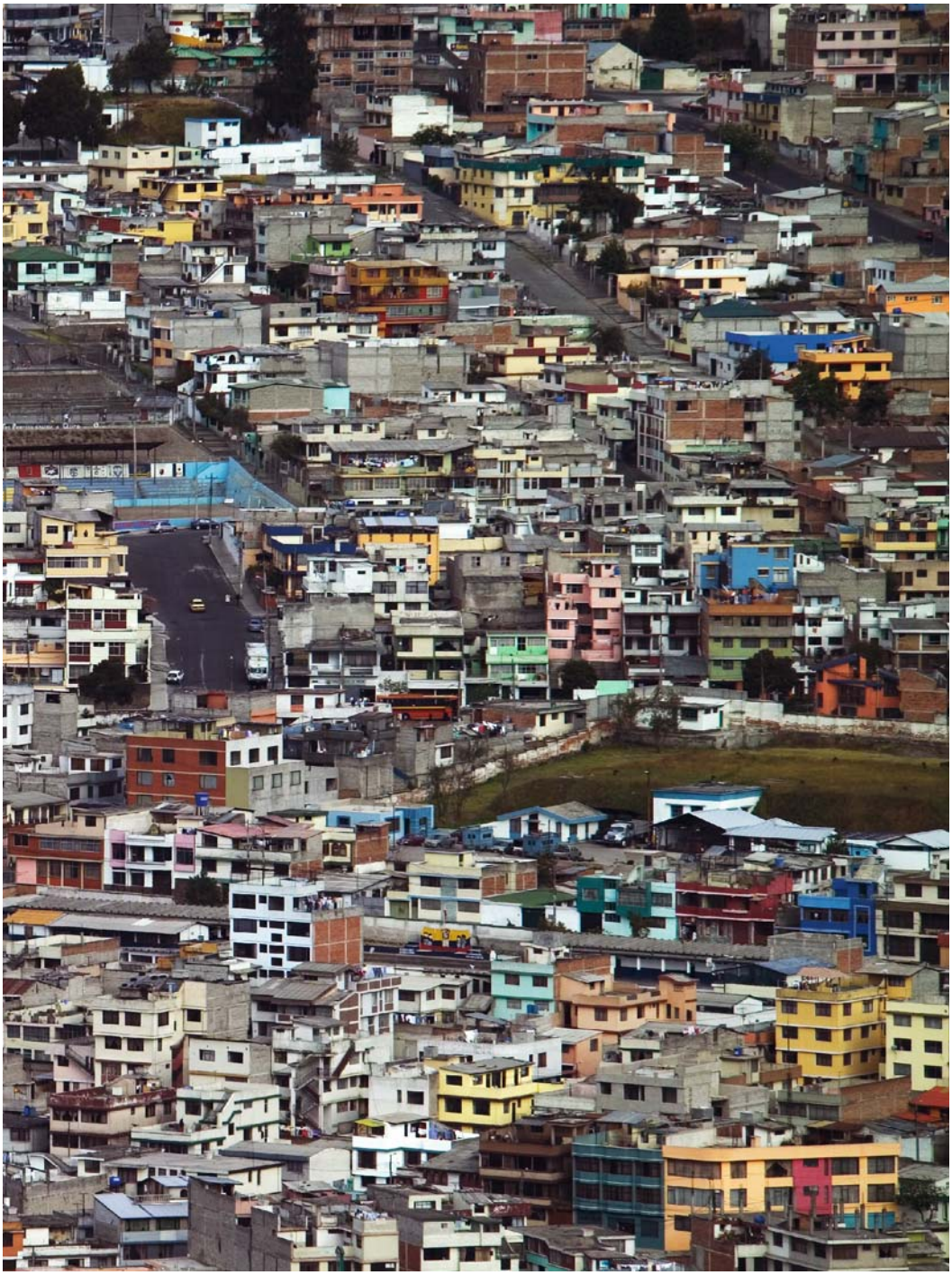

Fig. 8.11. Favela in Rio de Janeiro. No urban planning whatsoever …

many collateral issues in urban planning are neglected by the model (like the historic growth situation of cities, formation of low income and slum areas by uncontrolled immigration into urban areas, city topography etc.). No existing city has yet been planned by this model (and most likely never will be) but nevertheless it serves as an interesting starting point for further modeling and as an educational tool for city planners. In the Buttazzo–Santambrogio model the transportation cost is accounted for by a Wasserstein distance of the densities f and g , overcrowding is avoided by penalising with an 'unhappiness' functional of f heavily penalizing population densities f, which are not absolutely continuous with respect to the Lebesgue measure, and service concentration is built in by heavily penalizing non-atomic service measures g. Then, a total cost functional is defined by summing up these three terms and minimizing densities f and g are sought (with equal prescribed total mass). Note that a classical Monge–Kantorovich mass transportation problem appears here only as a subproblem defining the transportation cost between residential and service areas!

Typical minimizers (f, g) have the form of a certain number of circular residential areas with a service pole (atom of g) in the center. The radial population density in these 'subcities' decreases away from the service pole.

References

[1] M. Bernot, *Optimal Transport and Irrigation*, Thesis, Ecole Normale Supérieure Cachan, 2005
[2] M. Bernot, V. Caselles and J.-M. Morel, *Traffic Plans*, Publ. Math., Vol. 49, pp. 417–451, 2005
[3] Y. Brenier, *Polar factorization and monotone rearrangement of vector-valued functions*, Comm. Pure Appl. Math. 44 , pp. 375–417, 1991
[4] G. Buttazzo and F. Santambrogio, *A Model for the Optimal Planning of an Urban Area*, SIAM J. Math. Anal., Vol. 37, Nr. 2, pp. 514–530, 2005
[5] G. Buttazzo, E. Stepanov, *Optimal Transportation Networks as Free Dirichlet Regions for the Monge–Kantorovich Problem*, CVGMT, preprint, 2003[5]
[6] L. Caffarelli, *A localization property of viscosity solutions of the Monge-Ampère equation*, Annals of Math. 131, pp. 129–134, 1990
[7] L. Caffarelli, *Interior $W^{2,p}$ estimates for Solutions of the Monge-Ampère equation*, Annals of Math. 131, pp. 135–150, 1990
[8] L. Caffarelli, *Some regularity properties of solutions to the Monge-Ampère equation*, Comm. in Pure Appl. Math. 44, pp. 965–969, 1991
[9] L.C. Evans, *Partial Differential Equations and Monge–Kantorovich Mass Transfer*, In: Current Developments in Mathematics 1997, ed. by S.T. Yau[6]
[10] E.N. Gilbert, *Minimum cost communication networks*, Bell System Tech. J. 46, pp. 2209–2227, 1967
[11] L.V. Kantorovich, *On the transfer of masses*, Dokl. Akad. Nauk. SSSR 37, pp. 227–229, 1942 (in Russian)
[12] L.V. Kantorovich, *On a problem of Monge*, Uspekhi Mat. Nauk. 3, pp. 225–226, 1948
[13] G. Monge, *Mémoire sur la Théorie des Deblais et des Remblais*, Histoire de l'Acad. des Sciences de Paris, 1781
[14] C. Villani, *Topics in Optimal Transportation*, American Mathematical Society, in: Graduate Studies in Mathematics Series, vol. 58, 2003
[15] Q. Xia, *Optimal paths related to transport problems*, Commun. Contemp. Math. 5(2), pp. 251–279, 2003

[5] downloadable from the Preprint Server - *http://cvgmt.sns.it/papers/gbuest03/*
[6] downloadable from *http://www.math.berkeley.edu/∼evans/*

9. Wave Equations

Waves occur in many aspects of our daily lives and in the nature which surrounds us. Just take a stone and throw it into a resting water surface: you will observe a surface wave, spreading in concentric circles around the impact point on the water. Or think of the high breaking waves in the ocean which are so highly desirable for surf champions. Less pleasantly, there are the energy waves generated by potent seaquakes, which travel under the ocean surface with the speed of about thousand kilometres per hour and turn into deadly tsunami water waves close to beaches. Other examples are the sound waves, generated by our speech, propagating in the air to the partner of our conversation, electromagnetic waves described by the Maxwell[1] equations, light propagating in spherical waves from a source and, even more fundamentally, as established by quantum mechanics [19][2], there is a matter-wave duality which basically states that even particles with positive mass (say, electrons) have wave-like features (e.g. delocalisation).

So how is wave motion characterized? Webster's dictionary gives the following definition:

> a disturbance or variation that transfers energy progressively from point to point in a medium and that may take the form of an elastic deformation or of a variation of pressure, electric or magnetic intensity, electric potential, or temperature.

Clearly, this refers to the time-dependent transport of some physical quantity (e.g. energy) in certain spatial directions of a medium, such that typical characteristics of the quantity are maintained during the transport process. We remark that the transport of, say, energy is typically affected WITHOUT significant transport of particles of the medium.[3]

As maybe the most simple example, consider a (possibly) complex-valued function $w = w(x)$, defined on $\mathbb{R}^n$, and set

$$u(x,t) = w(x - vt)\,, \quad x \in \mathbb{R}^n,\ t \in \mathbb{R}\,, \tag{9.1}$$

where v is a given n-dimensional parameter vector, x denotes the spatial variable and t represents time. Obviously, this function in space-time can be interpreted in the following way: take $w = w(x)$ and move it with speed $|v|$ in the direction $\frac{v}{|v|}$.

[1] *http://www-groups.dcs.st-and.ac.uk/~history/Mathematicians/Maxwell.html*

[2] see *http://www.kfunigraz.ac.at/imawww/vqm/* for a visualisation attempt

[3] For enlightening animations of wave motion we refer to the webpage *http://www.kettering.edu/~drussell/demos.html*

Then, at time t, the function $w(x)$ is transported into $u(x, t)$. u is called a travelling wave with velocity v and profile w. When we set:

$$w_k(x) = \exp(ik \cdot x) \,, \tag{9.2}$$

where k is a given n-dimensional parameter vector, then by the above transport process we obtain the so called plane wave:

$$u_k(x, t) = \exp\left(ik \cdot (x - vt)\right) \tag{9.3}$$

representing harmonic oscillations. The parameter vector k is called wave vector of the plane wave u_k , its j-th component k_j determines the periodicity

$$p_j = \frac{2\pi}{k_j}$$

of the wave profile w_k in direction x_j.

Note that a travelling wave of the form (9.1) solves the first (differential) order linear transport equation

$$u_t = -v \cdot \operatorname{grad}_x u \,, \tag{9.4}$$

out of which by differentiation we can easily obtain the second order linear anisotropic wave equation:

$$u_{tt} = \sum_{j,l} a_{j,l} u_{x_j x_l} \,, \tag{9.5}$$

where in this case $a_{j,l} = v_l v_j$. For general wave motions, the real-valued coefficient matrix $A = (a_{j,l})_{j,l}$ is assumed to be symmetric and non-negative definite such that the total wave energy

$$E(u) = \frac{1}{2} \int_{\mathbb{R}^n} \left((u_t)^2 + (\operatorname{grad} u)^T A \ \operatorname{grad} u\right) dx \tag{9.6}$$

is a time-conserved quantity, with two nonnegative contributions stemming from the kinetic and potential energies. Equations of the form (9.5) model, for example, the motion of thin elastic chords (in one dimension), of thin membranes (two dimensions) and of three dimensional elastic objects under the assumption of small oscillation amplitudes (which allows to use linear models). In these applications the solution u represents the displacement and u_t the velocity. Clearly, appropriate initial-boundary conditions have to be imposed. Other applications include propagation of small amplitude sound waves in gases and fluids.

In one spatial dimension the linear wave equation reads:

$$u_{tt} = v^2 u_{xx} \,, \quad x \in \mathbb{R} \,, \, t \in \mathbb{R} \,, \tag{9.7}$$

where v is a positive parameter. This equation is particularly easy to solve. We introduce characteristic coordinates $r = x - vt$, $s = x + vt$ and rewrite (9.7) as:

$$u_{rs} = 0 \,. \tag{9.8}$$

The general solution of (9.8) is the sum of a function of r and a function of s such that after back-transformation we obtain:

$$u(x,t) = f(x+vt) + g(x-vt) \tag{9.9}$$

for the general solution of (9.7), where f and g are arbitrary smooth functions. Thus, the general solution of the one dimensional linear wave equation is the sum of two travelling waves, one travelling to the left and the other travelling to the right. Consider now the one dimensional wave equation (9.7) with initial data given by a point source with vanishing initial velocity:

$$u(x,t) = \delta(x) \,, \quad u_t(x, t=0) = 0 \,, \quad x \in \mathbb{R} \,.$$

Fig. 9.1. Circular Waves in a Kyoto Zen Garden

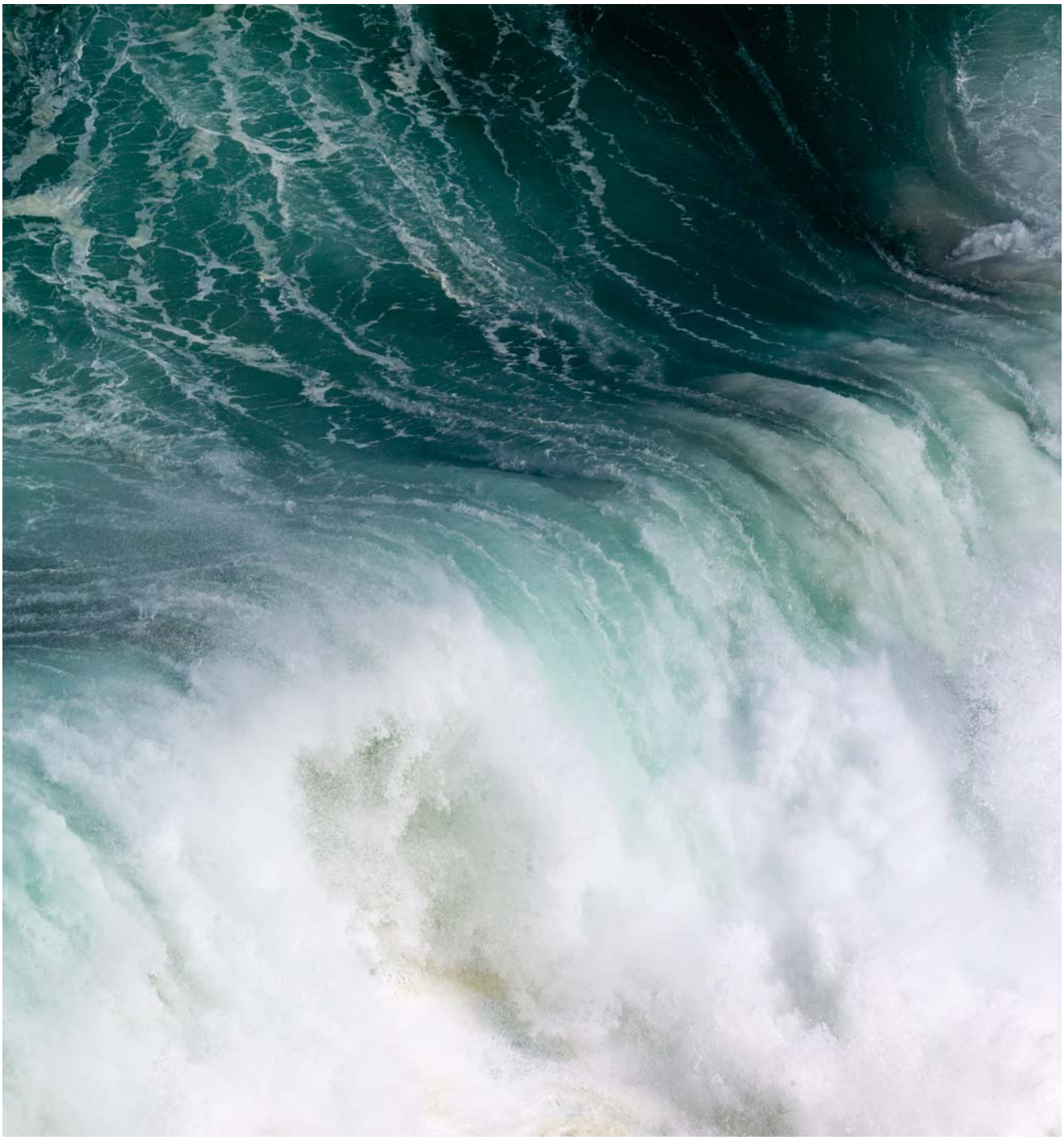

Fig. 9.2. Ocean Wave hitting the Beach

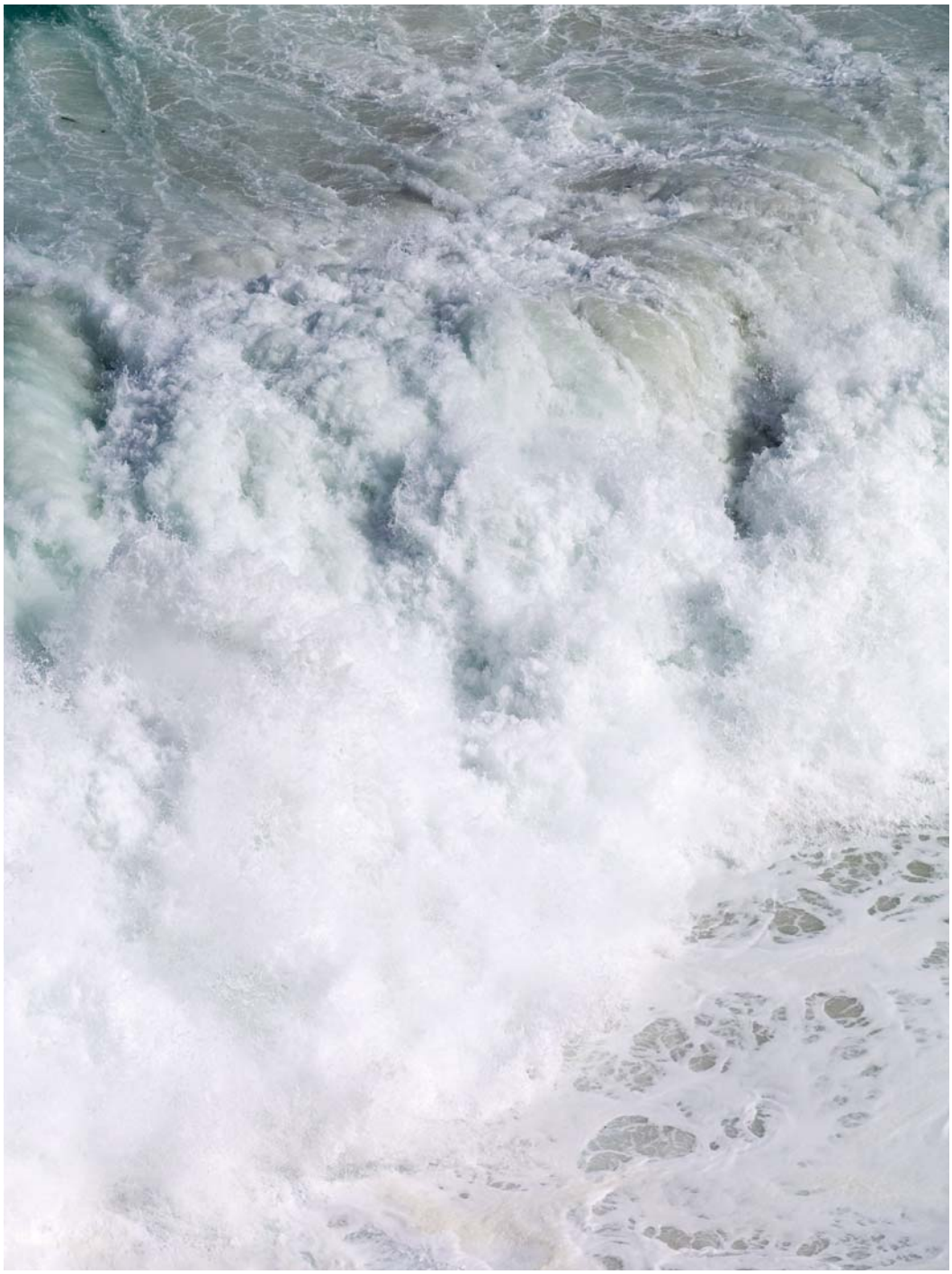

Fig. 9.3. Wave Breaking

Then a straightforward application of the formula (9.9) gives the solution of the initial value problem:

$$u(x,t) = \frac{1}{2}\delta(x+vt) + \frac{1}{2}\delta(x-vt)\,, \tag{9.10}$$

i.e. the initial delta mass is split into two equal parts, each of which is transported along a characteristic in x,t-space. In particular this means that every point x in $\mathbb{R}$ 'feels' the effect of the point source at only one moment in time. In two and more dimensions the corresponding solution is not compactly supported anymore, but it decays to zero as $|x|$ tends to infinity, in particular as $\frac{1}{\sqrt{|x|}}$ in two dimensions and as $\frac{1}{|x|}$ in three dimensions. Note that in a one dimensional world a sound emitted from a source can only be heard at one instant of time, not 'continuously' (with loudness decaying with distance from the source and with time) as in our three dimensional world!

A simple computation shows that the function

$$u_k(x,t) = \exp\left(\mathrm{i}k\cdot\left(x \pm v\frac{k}{|k|}t\right)\right)$$

is a special plane wave solution of the n-dimensional wave equation

$$u_{tt} = v^2\Delta u\,, \quad x\in\mathbb{R}^n\,,\ t\in\mathbb{R}$$

where v denotes again a real positive parameter. Clearly, the velocity of propagation of this plane wave is $\pm v\frac{k}{|k|}$. Therefore, in more than one dimension the propagation velocities of plane wave solutions of the wave equation lie on the sphere with radius v, but their directions depend on the wave vector. This is a weak dispersion effect.

Quantum mechanics [19] is governed by a very particular wave equation, named after the Nobel price winning Austrian theoretical physicist Erwin Schrödinger[4]. The Schrödinger equation, in its most basic form modeling the quantistic transport of an elementary particle (say, an electron) with positive mass m, is a linear partial differential equation for a complex valued function u, the so called wave function of the particle. The equation reads:

$$\mathrm{i}\hbar u_t = -\frac{\hbar^2}{2m}\Delta u + V(x)u\,, \quad x \in \mathbb{R}^n,\ t \in \mathbb{R} \tag{9.11}$$

where $\hbar$ is the so called normalized Planck constant[5] and $V(x)$ the real valued electric potential field driving the motion of the electron. The wave function u is an auxiliary quantity, the important physical observables are computed from u by 'post-processing'. They are quadratic in the wave function, e.g.

$$\varrho(x,t) = |u(x,t)|^2 \tag{9.12}$$

is the (probabilistic) position density of the particle,

$$j(x,t) = \hbar\mathrm{Im}\left(u(x,t)\mathrm{grad}\,u^*(x,t)\right) \tag{9.13}$$

its current density (* denotes complex conjugation) and

$$e(x,t) = \frac{\hbar^2}{2m}|\mathrm{grad}\,u(x,t)|^2 + V(x)|u(x,t)|^2 \tag{9.14}$$

its energy density. Note that the total mass

$$M := \int_{\mathbb{R}^n} \varrho dx$$

and the total energy

$$E := \int_{\mathbb{R}^n} e dx$$

are time-conserved by the Schrödinger equation.

[4] *http://nobelprize.org/physics/laureates/1933/schrodinger-bio.html*
[5] *http://scienceworld.wolfram.com/physics/PlancksConstant.html*

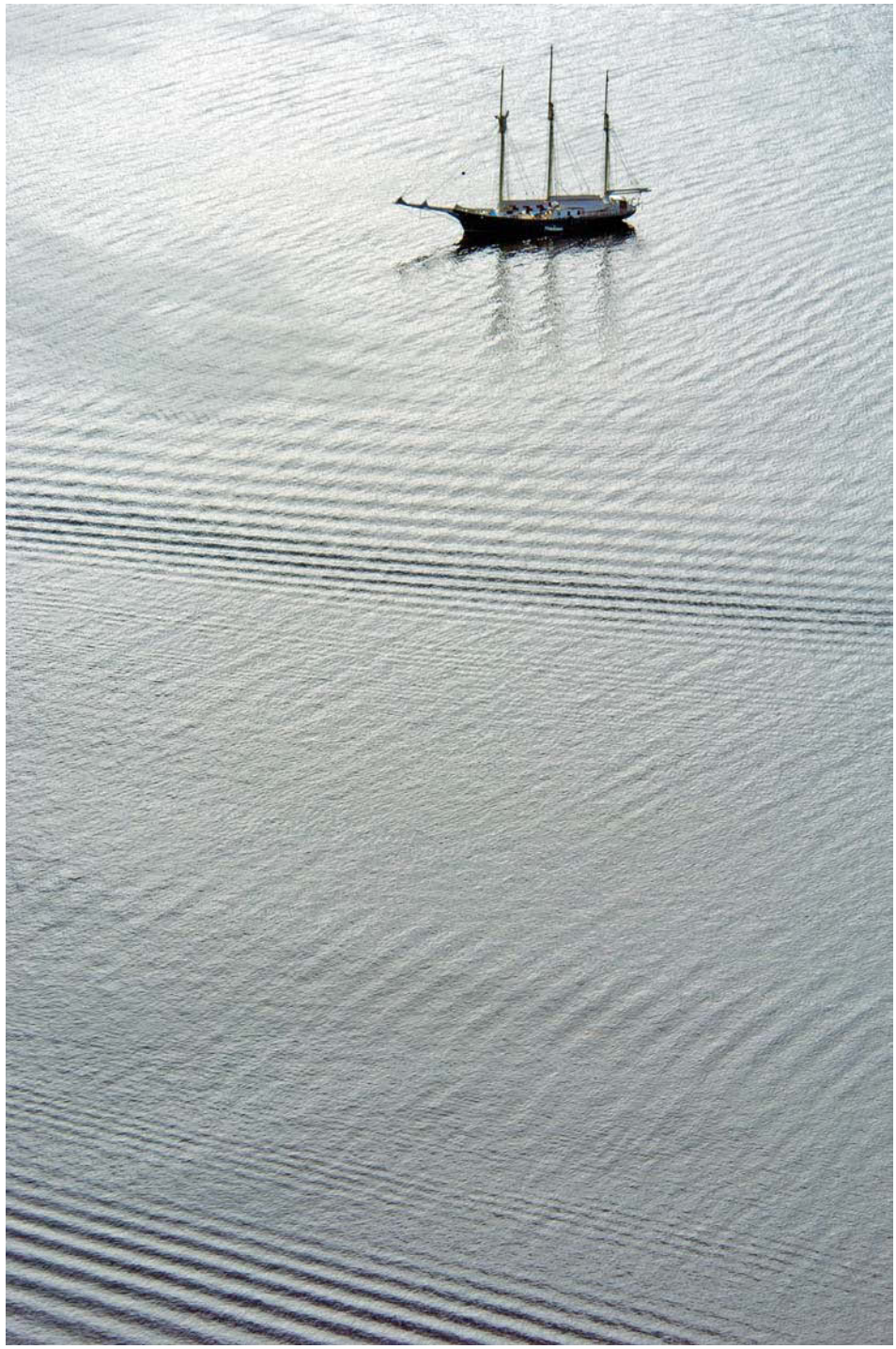

Fig. 9.4. Plane and transversal Waves

For many mathematical purposes it is convenient to scale the Schrödinger equation by introducing macroscopic space-time coordinates. Denoting by ε the microscopic/macroscopic aspect ratio, we obtain:

$$\mathrm{i}\varepsilon u_t = -\frac{\varepsilon^2}{2}\Delta u + V(x)u\,, \quad x \in \mathbb{R}^n\,,\ t \in \mathbb{R}\,. \tag{9.15}$$

In many applications, e.g. in quantum effect semiconductor devices, Bose–Einstein condensates[6] etc., ε is a small parameter. In order to understand the dispersion property and the transport of oscillations property of the Schrödinger equation consider the free quantistic transport case $V = 0$ and prescribe an ε-oscillatory plane wave initial wave function:

$$u(x, t = 0) = \exp\left(\mathrm{i}k \cdot \frac{x}{\varepsilon}\right)\,. \tag{9.16}$$

It is an easy exercise to show that the solution of the initial value problem (9.15), (9.16) in this case is given by the function:

$$u(x, t) = \exp\left(\mathrm{i}k \cdot \frac{x}{\varepsilon} - \frac{\mathrm{i}}{2}|k|^2\frac{t}{\varepsilon}\right)\,. \tag{9.17}$$

Two issues are apparent:

a) The initial spatial oscillations with frequency of order of $\frac{1}{\varepsilon}$ are propagated in space and oscillations in time with frequency of the same order are generated. This is a typical property of linear wave equations.
b) The velocity of the wave with initial wave vector $\frac{k}{\varepsilon}$ is equal to $\frac{k}{\varepsilon}$. Thus waves with different wave vectors move with different velocity vectors and possible wave speeds are not restricted. This is a dispersion property, much stronger than in the case of the linear second order wave equation discussed above.

Of particular interest is the so called classical limit of the Schrödinger equation $\varepsilon \to 0$, which corresponds to observing particle motion on larger and larger scales. Intuitively, quantistic effects should diminish in this process and the motion should become dominated by classical mechanics, i.e. by Newton's second law. This was verbalized by the German Nobel Prize winning physicist Max Planck[7], who stated in the year 1900:

Classical mechanics is the limit of quantum mechanics as $\hbar$ tends to zero.

[6] *http://www.colorado.edu/physics/2000/bec/*
[7] *http://www.dhm.de/lemo/html/biografien/PlanckMax/*

The classical mathematical technique for carrying out the classical limit of the Schrödinger equation is the so called WKB high frequency method[8]. The method is based on the following ansatz (Madelung transform) for the wave function:

$$u(x,t) = a(x,t)\exp\left(\mathrm{i}\frac{S(x,t)}{\varepsilon}\right) \tag{9.18}$$

where $a = a(x,t)$ is a real valued modulation and $S = S(x,t)$ a real valued phase variable. Obviously, the ansatz is based on the hypothesis that the phase is of order $\frac{1}{\varepsilon}$. After inserting (9.18) into the Schrödinger equation (9.15), separating real and imaginary parts and neglecting terms which tend to 0 as ε tends to 0, we obtain the following system of partial differential equations, called the WKB system:

$$\varrho_t + \operatorname{div}(\varrho \operatorname{grad} S) = 0 \quad \text{(transport equation)} \tag{9.19}$$

$$S_t + \frac{|\operatorname{grad} S|^2}{2} + V(x) = 0 \quad \text{(eikonal Hamilton–Jacobi equation)} \tag{9.20}$$

(see [14], [3]). It is well known that solutions of the Hamilton–Jacobi equation (9.20) develop – in general – singularities in finite time. Even for smooth potential V and for smooth initial datum $S(x, t = 0)$ the solution S will generally be only Lipschitz continuous in x and t, thus not more than almost everywhere differentiable [2]. The sets of singularities of S in position-time space are called caustics. The formal limiting procedure, which leads to the WKB system can be justified rigorously only locally in time, more precisely before caustic onset! After the occurrence of singularities in the phase variable S the formal procedure is not correct anymore. This is due to the fact that the $O(\varepsilon^2)$-term which was neglected for obtaining (9.20) depends on derivatives of ϱ, which become very large at caustics. A different limit approach is called for if caustics are to be crossed. This is achieved by introducing the so called phase space Wigner[9] transform of the wave function u

$$W(x,\xi,t) := \frac{1}{(2\pi)^n}\int\limits_{\mathbb{R}^n} u\left(x+\frac{\varepsilon}{2}z,t\right)u^*\left(x-\frac{\varepsilon}{2}z,t\right)\exp(\mathrm{i}\xi\cdot z)dz$$

(see [20], [13], [4]). Note that the quadratic observables can be easily computed from the Wigner transform, which itself is quadratic in the wave function. For example, the position density ϱ defined in (9.12) is the zeroth order velocity moment of W:

$$\varrho(x,t) = \int\limits_{\mathbb{R}^n} W(x,\xi,t)d\xi\ .$$

Also, the Wigner transform satisfies a first order transport equation, nonlocal in the velocity variable, which can be taken to the limit $\varepsilon \to 0$ in a rigorous

[8] *http://webphysics.davidson.edu/Faculty/wc/WaveHTML/node38.html*

[9] *http://www-gap.dcs.st-and.ac.uk/~history/Mathematicians/Wigner.html*

way under mild conditions on the initial wave function. By this limit process the Vlasov equation of classical mechanics (see Chapter 1) is obtained:

$$w_t + \xi \cdot \mathrm{grad}_x\, w - \mathrm{grad}_x\, V(x) \cdot \mathrm{grad}_\xi\, w = 0\,, \quad x \quad \text{and} \quad \xi \in \mathbb{R}^n\,, \tag{9.21}$$

where the positive measure w denotes a weak limit point of the sequence W as $\varepsilon \to 0$. We remark that the equation (9.21) can be interpreted in the following way: the measure w is constant along the characteristics of the linear hyperbolic equation (9.21), which are precisely the Newtonian trajectories of classical mechanics:

$$\frac{dx}{dt} = \xi\,, \quad \frac{d\xi}{dt} = -\mathrm{grad}_x\, V(x)\,. \tag{9.22}$$

This dynamical system is a formulation of Newton's second law, which states that force (here given by the field $-\mathrm{grad}_x\, V(x)$) is equal to mass (has been scaled to 1) times acceleration $\frac{d^2x}{dt^2}$. In this way the fundamental law of classical mechanics is recovered from the quantistic Schrödinger equation. This limiting process, here carried out formally, has been justified rigorously in the references [13], [4].

Many important wave phenomena are inherently nonlinear and cannot be described by linear wave equations. A typical example is the motion of ocean waves before and after breaking.

Here we mention the cubically nonlinear Schrödinger equation as an often used model for nonlinear wave motion:

$$\mathrm{i}\varepsilon u_t = -\frac{\varepsilon^2}{2}\Delta u + V(x)u + a|u|^2 u\,, \quad x \in \mathbb{R}^n\,,\ t \in \mathbb{R}\,. \tag{9.23}$$

If the real parameter a is positive, the equation is defocusing, i.e. all energy contributions are non-negative, and if a is negative, the equation is focusing, i.e. the energy contribution stemming from the nonlinearity (the so called interaction energy) is non-positive. The cubic nonlinearity models binary particle interactions, higher order interactions are neglected here. The cubic Schrödinger equation has various applications, ranging from tsunami modeling to a quantistic phenomenon called Bose–Einstein condensation[10], represented by a temperature phase transition in the nano-Kelvin range, occurring in boson gases, leading to the formation of a 'super-atom'. In the latter case V is typically a harmonic (quadratic) potential representing the laser confinement of the condensate, and the nonlinear Schrödinger equation is referred to as Gross–Pitaevski equation [15], [1].

We remark that the mathematical features of focusing and defocusing nonlinear Schrödinger equations are totally different. Focusing nonlinearities often lead to finite time blow-up of solutions, depending on the space dimension, the polynomial order of the nonlinearity and the initial datum. In this case the position density $\varrho = \varrho(x, t)$ features a concentration (i.e. formation of a Dirac mass)

[10] *http://www.colorado.edu/physics/2000/bec/*

at some finite blow-up time. Defocusing equations are typically better behaved, do not exhibit blow-up and in many cases have global-in-time solutions [18].

Another important nonlinear problem is represented by the so called KdV-equation (named after D.J. Korteweg[11] and G. de Vries, [9]), modeling the one-dimensional wave motion in shallow water, i.e. shallow water waves in a channel[12]. It is a quadratically nonlinear partial differential equation of third differential order for the real-valued function $u = u(x, t)$, representing the wave profile:

$$u_t + \left(\frac{u^2}{2}\right)_x + \varepsilon^2 u_{xxx} = 0\,, \quad x \in \mathbb{R}\,, \quad t > 0\,. \tag{9.24}$$

Here the equation is presented already in dimensionless, scaled form, and ε represents an aspect ratio parameter.

Of particular interest is the zero-dispersion limit of the KdV equation, obtained by taking ε to 0 in the solution of (9.24), subject to appropriate initial data. Note that setting ε to 0 in (9.24) leads to the inviscid Burgers equation[13]

$$U_t + \left(\frac{U^2}{2}\right)_x = 0\,, \quad x \in \mathbb{R}\,, \, t > 0\,, \tag{9.25}$$

which is the prototype for a one-dimensional hyperbolic conservation law. The Burgers equation has straight line characteristics in time-position space, along which the value of the initial state $U(t = 0)$ is transported. Thus, this equation exhibits solutions, which become discontinuous in finite time (at points of intersection of characteristics), unless the initial datum $U(t = 0)$ is a nondecreasing function of the spatial variable x. Similarly to the WKB limit of the Schrödinger equation, the term which was neglected when passing from the KdV to the Burgers equation, is a third order derivative of u and the formal limit procedure breaks down at the onset of shock-type singularities of the Burgers solution. In fact, for sufficiently smooth initial data, the KdV equation has smooth solutions and, for ε small, breakdown of regularity is migitated by the onset of fast oscillations with frequency of order $\frac{1}{\varepsilon}$ when the derivatives of u get large. In other words, the nonlinear convection term $\left(\frac{u^2}{2}\right)_x$ tends to create discontinuities in the solution and the third derivative term $\varepsilon^2 u_{xxx}$ tends to smooth the solution. The latter wins the competition but at the prize of developing high frequency oscillations if ε is small. This limit process was made mathematically rigorous in a series of three deep papers [10], [11], [12] by the Abel Prize recipient Peter Lax[14] and his then Ph.D. student David Levermore[15]. Their mathematical methodology was based on the fact that the KdV equation can be written as an infinite

[11] *http://staff.science.uva.nl/~janwieg/korteweg/*
[12] *http://mathworld.wolfram.com/Korteweg-deVriesEquation.html*
[13] *http://en.wikipedia.org/wiki/Burgers'_equation*
[14] *http://mathworld.wolfram.com/news/2005-03-18/abelprize/*
[15] *http://www.math.umd.edu/~lvrmr/*

dimensional integrable dynamical system, just as the one-dimensional cubically nonlinear Schrödinger equation. Integrability implies the existence of infinitely many invariants which lead, by so called inverse scattering, to a representation of the solution u, which can be directly exploited for the passage to the limit $\varepsilon \to 0$. Actually, the same approach was applied for the classical limit of the defocusing cubic one-dimensional Schrödinger equation in [6]. The methodology for carrying out dispersive limits in non-integrable nonlinear partial differential equations is not developed well, yet. Only few results exist in the literature so far.

Many nonlinear dispersive equations have explicit travelling wave solutions (so called solitons), of the form (9.1) with a given wave form w. A particularly interesting feature of the KdV equation is that solitons with opposite velocities interact only over a finite time interval and then survive the interaction practically unchanged.

Finally we mention the KP (Kadomtsev–Petviashili) equation [7] which models two dimensional shallow water waves, with one-dimensional directional motion, and only weak transverse effects. Numerical simulations were reported in [8].

Comments on the Image 9.1 The Image 9.1 shows ritual interpretations of circular waves in a Zen garden in Kyoto, Japan. A classical example for the occurrence of circular waves is a water surface (say, a lake), which experiences a point source perturbation (say, a pebble thrown into it). The mathematical form of a circular wave is:

$$\psi(r,t) = A(r)\exp\left(\mathrm{i}(kr-\omega t)\right) \ ,$$

where the amplitude A is a function of the radial spatial variable $r = |x|$, ω is the frequency and k the radial wave vector. Here we assume that the phase of the wave is zero. For point sources, $A(r)$ decays as $\frac{1}{\sqrt{r}}$ as r increases. The image also shows a not-too-realistic attempt of the Zen artist to describe the interaction of circular waves with each other and with plane waves. We refer to the webpage[16] for a computational simulation of circular wave interaction. Interesting animations of circular waves can be found in the webpages[17].

In three dimensions, sound waves spreading from a point source are spherical, with $A(r) = \frac{\text{const}}{r}$. They are special solutions of the linear wave equations in three space dimensions:

$$\psi_{tt} = c^2 \Delta \psi \ ,$$

where $c = \frac{\omega}{k}$. For more information on spherical waves see the webpage[18].

[16] *http://members.aol.com/nicholashl/waves/circular_reflection.html*
[17] *http://www.walter-fendt.de/ph11e/interference.htm*
http://members.aol.com/nicholashl/waves/circularwaves.html
[18] *http://scienceworld.wolfram.com/physics/SphericalWave.html*

Fig. 9.5. 'Waves' in Belem, Lisbon

Comments on the Images 9.2–9.4 The Images 9.2–9.4 show ocean waves. The motion of waves in oceans is obviously influenced by many factors, like bottom and shore topography, wind and other surface disturbances (like ships on the ocean), tides etc. We refer to the webpage[19] and to [17] as reference on the mathematical-physical modeling. A particularly interesting nonlinear phenomenon is the breaking of ocean waves close to the beach (see Image 9.3, upper right hand corner). To understand the basic mechanism of wave-braking, which in mathematical terms can be considered as a folding catasthrophy of the wave's height function U (free air-water surface), consider the classical initial value problem for the one-dimensional inviscid Burgers equation (9.25) as a basic model:

$$U_t + \left(\frac{U^2}{2}\right)_x = 0\,, \quad x \in \mathbb{R}\,, \quad t > 0$$
$$U(x, t = 0) = U_0(x)\,, \quad x \in \mathbb{R}\,.$$

Here, external effects like wind and topography are excluded to keep the discussion simple.

By carrying out the differentiation in the nonlinearity of the Burgers equation, it becomes apparent that the solution u is constant along the characteristics, which are straight lines in the (x, t)-plane given by:

$$X(t; x) = x + tU_0(x)\,.$$

Here x is the starting point of the characteristic and the solution u along the characteristic is:

$$U\big(X(t; x), t\big) = U_0(x)\,, \quad t > 0\,.$$

Obviously, (at least two) characteristics starting at different points x will intersect in finite time unless the initial datum U_0 is non-decreasing. If they intersect, they transport different initial data leading to a shock-type discontinuity in the solution U. This singularity can be interpreted as the onset of wave breaking. The typical approach of hyperbolic equations is to continue the solution U beyond breaking time as a so called weak solution, which dissipates entropy and which can be obtained as a limit of solutions of the viscous Burgers equation in the vanishing viscosity limit [16]. Clearly, this is not the correct approach, when wave breaking is to be modeled. Instead, a different solution concept has to be invoked, namely so called multi-valued solutions. A good way of introducing multi-valued solutions is to consider the Newtonian phase-space $(R_x \times R_v)$ flow, given by:

$$\frac{dX}{dt} = V\,, \quad X(t = 0; x) = x$$
$$\frac{dV}{dt} = 0\,, \quad V(t = 0; v) = v$$

[19] *http://en.wikipedia.org/wiki/Ocean_surface_wave*

and apply this flow to the Lagrangian phase-space manifold:

$$L_0 = \{(x, v) \mid v - U_0(x) = 0\}$$

Before the onset of shocks, the Newtonian flow maps the initial Lagrangian manifold L_0 into the graph of a function in the (x, v)-plane with $v = U(x, t)$ being the smooth solution of the Burgers equation. After the onset of singularities, the image manifold L_t of L_0 is not a graph of a single-valued function anymore, it represents the multi-valued wave surface after breaking. A nice way to see this is via kinetic theory. Consider the free streaming kinetic equation:

$$f_t + v.\mathrm{grad}_x f = 0$$
$$f(t = 0) = \delta\big(v - U_0(x)\big) \ .$$

Its solution is given by

$$f(x, v, t) = \delta(L_t) \ , \quad t > 0 \ .$$

For more information on multi-valued solutions of conservation laws and Hamilton–Jacobi equations we refer to [5].

Image 9.4 shows two fronts of (almost) plane waves propagating away from the ship at rest. Most likely these wave fronts are caused by winds close to the ocean surface. Between the two plane wave fronts there is a transversal wave of even smaller amplitude.

References

[1] W. Bao, D. Jaksch and P.A. Markowich, *Numerical solution of the Gross–Pitaevskii Equation for Bose–Einstein condensation*, JCP, Vol. 187, No. 1, pp. 318–342, 2003

[2] L.C. Evans, *Partial Differential Equations*, AMS, 2002

[3] I. Gasser and P.A. Markowich, *Quantum Hydrodynamics, Wigner Transforms and the Classical Limit*, Asympt. Analysis, Vol. 14, No. 2, pp. 97–116, 1997

[4] P. Gerard, P.A. Markowich, N.J. Mauser and F. Poupaud, *Homogenization Limits and Wigner Transforms*, Comm. Pure and Appl. Math., Vol. 50, pp. 323–378, 1997

[5] S. Jin and S. Osher, *A Level Set Method for the Computation of multivalued Solutions to quasi-linear Hyperbolic PDEs and Hamilton–Jacobi Equations*, Comm. Math. Sci. Vol. 1(3), pp. 575–591, 2003

[6] S. Jin, C.D. Levermore and D.W. McLaughlin, *The Semiclassical Limit of the Defocusing Nonlinear Schroedinger Hierarchy*, Comm. Pure & Appl. Math. 52, pp. 613–654, 1999

[7] B.B. Kadomtsev and V.I. Petviashili, *On the Stability of Solitary Waves in weakly dispersive Media*, Sov. Phys. Dokl., 15, pp. 539–541, 1970
[8] C. Klein, P.A. Markowich and C. Sparber, *Numerical Study of Oscillatory Regimes in the Kadomtsev–Petviashili Equation*, submitted, 2006
[9] M.D. Kruskal and N.J. Zabusky, *Interaction of Solitons in a Collisionless Plasma and the Recurrence of Initial States*. Phys. Rev. Lett. 15, pp. 240–243, 1965
[10] P.D. Lax and C.D. Levermore, *The Small Dispersion Limit for the Korteweg–deVries Equation I*, Comm. Pure & Appl. Math. 36, pp. 253–290, 1983
[11] P.D. Lax and C.D. Levermore, *The Small Dispersion Limit for the Korteweg–deVries Equation II*, Comm. Pure & Appl. Math. 36, pp. 571–593, 1983
[12] P.D. Lax and C.D. Levermore, *The Small Dispersion Limit for the Korteweg–deVries Equation III*, Comm. Pure & Appl. Math. 36, pp. 809–830, 1983
[13] P.-L. Lions and T. Paul, *Sur les mesures de Wigner*. Rev. Mat. Iberoam. 9, pp. 553–618, 1993
[14] P. A. Markowich, N. Mauser and C. Sparber, *Multivalued Geometrical Optics: Wigner Functions versus WKB-Methods*, Asymptotic Analysis 33 (2), pp. 153–187, 2003
[15] L.P. Pitaevskii, Zh. Eksp. Teor. Fiz 40, 646, 1961 (Sov. Phys. JETP 13, 451, 1961
[16] J. Smoller, *Shock-Waves and Reaction-Diffusion Systems*, Springer, 1983
[17] J.H. Stocker, G.J. Komen, L. Cavaleri, *Dynamics and Modelling of Ocean Waves*, Cambridge University Press, 2006
[18] C. Sulem and P.-L. Sulem, *The Nonlinear Schroedinger Equation: Self-focusing and Wave Collapse*, Appl. Math. Sciences, Volume 139, Springer, 1999
[19] W. Thirring, *Lehrbuch der Mathematischen Physik 4-Quantenmechanik grosser Systeme*. Springer Wien-New York, 1980
[20] E. Wigner, *On the Quantum Correction for Thermodynamic Equilibrium*, Phys. Rev. 40, pp. 749–759, 1932

10. Digital Image Processing and Analysis – PDEs and Variational Tools

Most digital photographic still cameras have CCD (Charge-Coupled-Device) or CMOS (Complementary-Metal-Oxide-Semiconductor) image capturing sensors. Typically, these semiconductor chips feature a rectangular array of devices – so called photosites – each of which being sensitive to either red (R), green (G) or blue (B) light. Technically, the sensitivity to only one of the RGB colors is achieved by filtering, such that only photons of a certain frequency range pass through the filter (corresponding to R, G or B resp.). Thus, each individual photosite acts as a counter of photons corresponding to red, green or blue color light. These sites are organised in a so-called RGB Bayer matrix:

$$
\begin{array}{l}
\ldots\ldots\ldots\ldots\ldots\ldots\ldots\ldots\ldots\ldots \\
\ldots R\ G\ R\ G\ R\ G\ R\ G\ R\ G \ldots \\
\ldots G\ B\ G\ B\ G\ B\ G\ B\ G\ B \ldots \\
\ldots R\ G\ R\ G\ R\ G\ R\ G\ R\ G \ldots \\
\ldots G\ B\ G\ B\ G\ B\ G\ B\ G\ B \ldots \\
\ldots R\ G\ R\ G\ R\ G\ R\ G\ R\ G \ldots \\
\ldots G\ B\ G\ B\ G\ B\ G\ B\ G\ B \ldots \\
\ldots\ldots\ldots\ldots\ldots\ldots\ldots\ldots\ldots\ldots
\end{array}
$$

Note that more 'green' sites (actually, half of the total number) occur in the Bayer matrix, which accounts for the human eye's greater sensitivity with respect to the green color.

The Image 10.1 shows a diffractive pattern of the CCD sensor of the P25 digital back (22 million photosites, produced by PhaseOne[1]), to be attached on a Hasselblad[2] H1 or H2 medium format camera. This was the high end of commercially available sensor technology until December 2005, when 39-megapixel sensors became available!

After image capturing the Bayer matrix data are read out directly into the image processing engine – the so called imager – of the camera (note that the read-out method is precisely where CCD and CMOS imaging sensors differ). Then, the procedure varies according to the chosen image format. If the user has opted for a jpg-image, then the three colours are first interpolated by the so called Bayer algorithm[3] such that finally after interpolation full RGB data are available at EACH pixel (corresponding to a photosite). Afterwards the imager performs certain processing tasks, typically an estimate of the grey-balance,

[1] *http://www.phaseone.com*
[2] *http://www.hasselblad.com*
[3] *http://de.wikipedia.org/wiki/Bayer-Sensor*

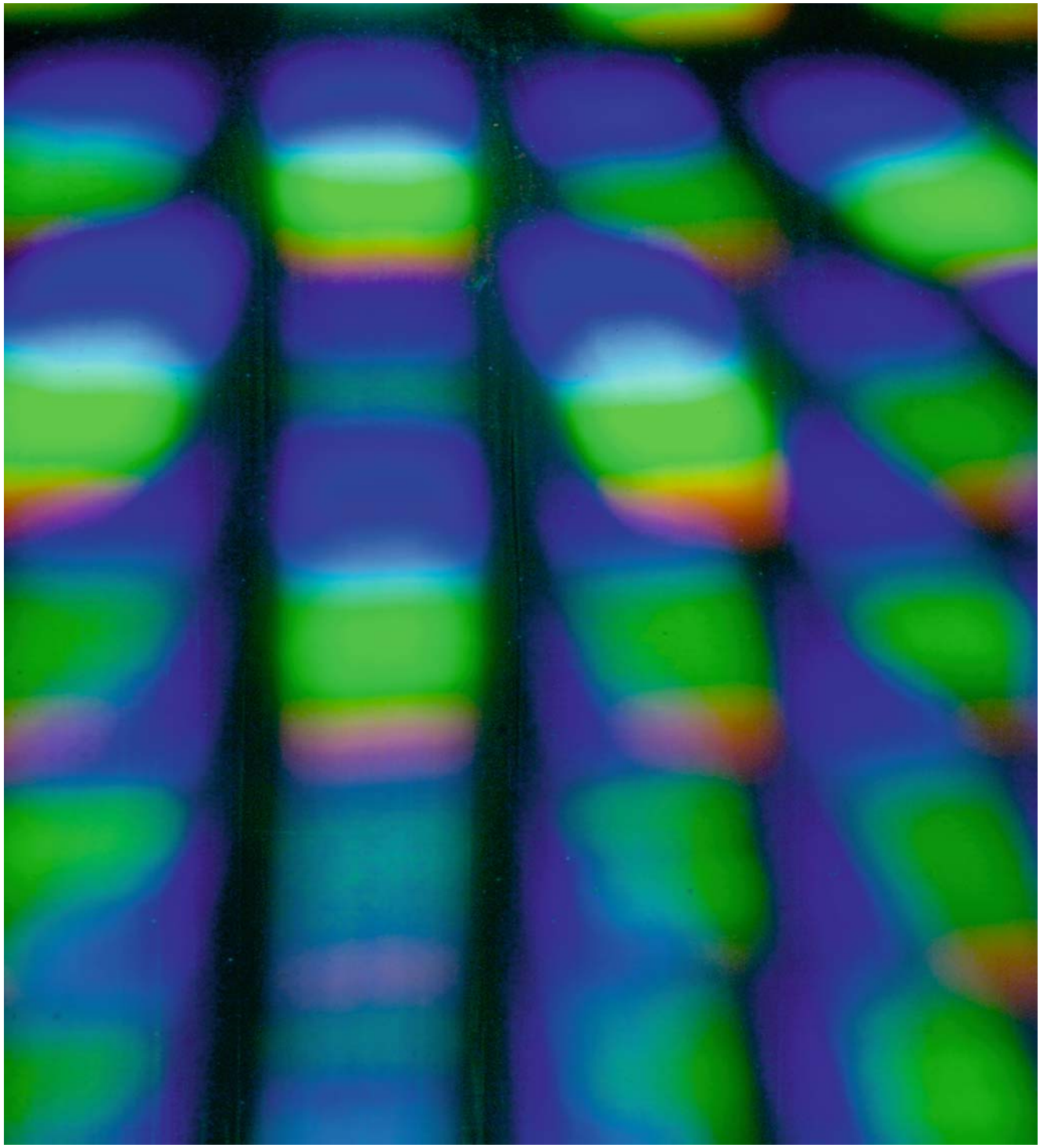

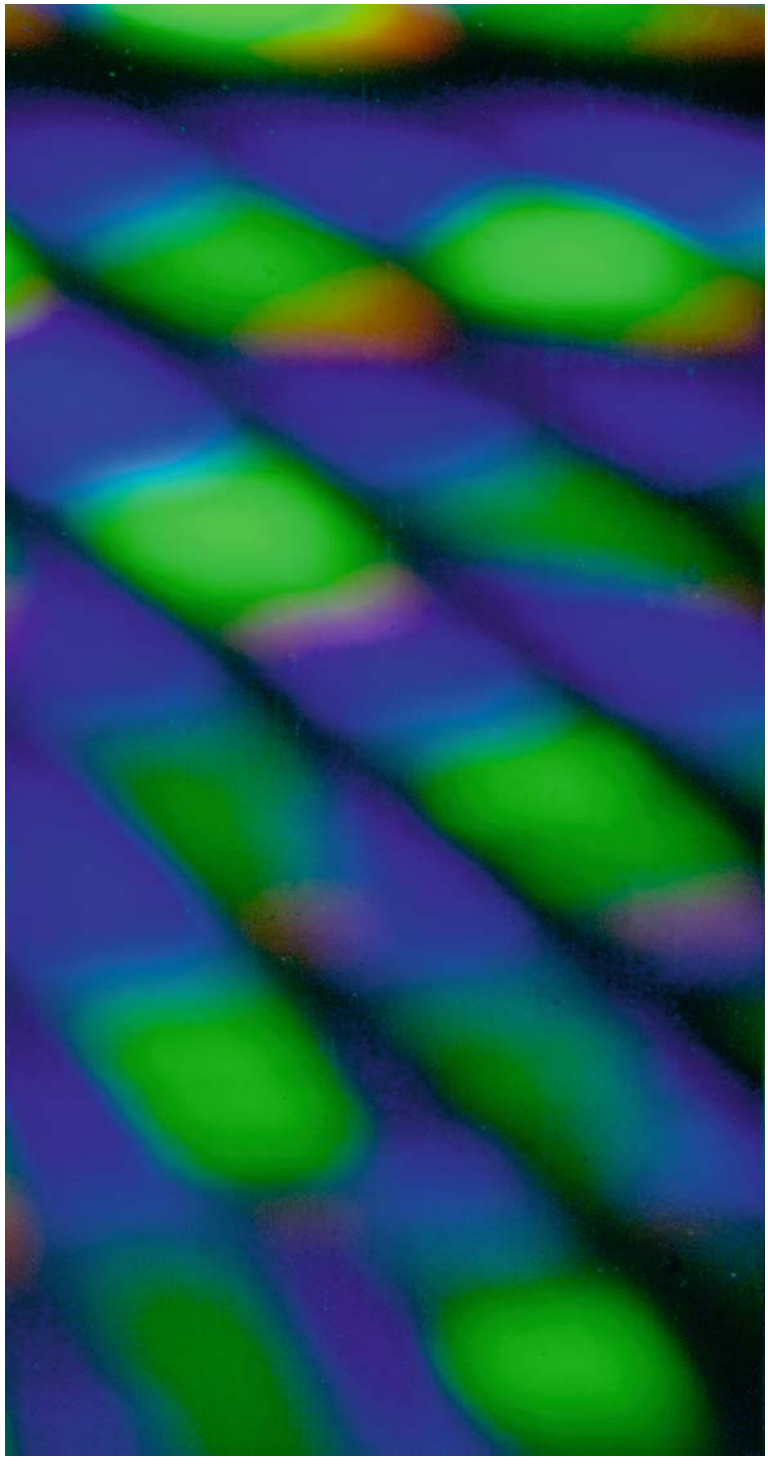

Fig. 10.1. Diffraction from the CCD-sensor of Phase One's P25 digital back

some contrast enhancement, sharpening, noise-reductionand data compression. If the user has decided instead to acquire a so called RAW image, then the full RGB data file is tagged with user-specified camera settings and immediately stored into the internal memory of the camera and finally onto some sort of memory card, which acts as 'digital film'. The Bayer algorithm is then performed in a software on the user's computer called RAW converter (typically available from the camera manufacturer) and the user thereafter has to perform the image processing himself according to his own preferences, instead of according to the preferences of the programmer of the camera imager, as in the case of jpg-images. We remark that there are also digital imaging sensors used in commercially available cameras, whose functioning is based on different concepts[4], e.g. the FOVEON[5] sensor and the Fujitsu Super CCD.

A digital still image is a set of three matrices, representing the intensities of the colours red, green and blue. In the following, we shall perform a simplification: we shall assume that each of the three colour intensity matrices has been interpolated onto the image domain G (say, by piecewise constant interpolation, associating a 'small' square domain to each pixel, whose union fills up the whole image) to give a pointwise almost everywhere defined function. Thus, a colour image in the following is assumed to be represented by a three dimensional vector field of the RGB intensities, defined a.e. on a two dimensional domain G (typically rectangular) representing the image. Thus, we shall deal here with image processing on the 'continuous' level instead of the 'discrete' pixel level. Obviously, this simplification allows us to explain image processing by using 'continuous' vector field techniques employing partial differential equation and variational methods. Clearly, in actual numerical computations the 'continuously' defined functions, obtained by mathematical image processing have to be discretized again, but this issue will not be discussed here.

As already mentioned, there are various issues involved in image processing and in image analysis. Typically, images have to be grey balanced, contrast enhanced, sharpened, denoised, and maybe segmented for object recognition. In some cases imaging artifacts due to limitations of the CCD or CMOS technologies have to be eliminated and sometimes an image size adjustment or/and a data compression is desired.

In the following we shall concentrate on the subsequent issues:

- denoising
- de-blurring, edge detection and sharpening
- image segmentation.

For a synthetic overviev of image processing techniques we refer to the book [3].

Very often all three color channels (i.e. vector field component intensity functions) are processed equally and independently, or only a linear combination

[4] *http://www.photozone.de/3Technology/digital_3.htm*

[5] *http://www.foveon.com/*

of them is processed. Here, again simplifying, we shall deal with single channel images only, which is equivalent to treating black and white images. Thus, for what follows, we assume to have a black and white image, represented by a real valued intensity function u_0, defined pointwise almost everywhere on the image domain G.

In most practical applications digital images are processed in spaces of functions of bounded variation, however, there have been serious recent objections to this claim. These objections are based on the prevailing idea that natural images have a very strong multi-scale feature such that, generally, their total variation may become unbounded [1].

For most image processing tasks it is of paramount importance to analyse the principal features and structures of the image under consideration. It is intuitively clear that these features are independent of high frequencies contained in the intensity function u_0. Thus, it seems natural to try to extract significant image information by smoothing the intensity function. In particular, think of the problem of detecting edges in images. It seems natural to think of edges as those curves in the image domain, where the (Euclidean norm of the) gradient of the intensity function assumes maximal values, or – as used in many applications – where the Laplacian of the intensity function (which is the trace of its Hessian matrix) becomes 0. Thus, edge detection requires the computation of pointwise derivatives of the intensity function, which cannot be done without smoothing the piecewise constant intensity obtained from digital imaging. Moreover, the gradient of the piecewise constant function u_0 is – trivially – singular at ALL pixel edges (gradients of piecewise constant functions are singular measures concentrated on the partition edges)! Obviously, the 'significant' image specific edges can only be distinguished from the 'insignificant' pixel edges by smoothing. Thus, we deduce that image structure is, maybe somewhat counter-intuitively, revealed by discarding detail in a coherent way. Also, currently available digital imaging sensors are known to introduce noise into RGB images, which typically gets worse when the nominal sensitivity (iso value) is increased. Digital high-iso noise is patchy and ugly, much worse than the grain we all got used to (and even got to like) in analog images. Thus, efficient and non-destructive image denoising is of utmost importance to the photographic community.

The most basic smoothing technique is the convolution of u_0 by a Gaussian function with mean value zero and a fixed variance $t > 0$:

$$u(x,t) := (u_0 * G_t)(x) \,, \tag{10.1}$$

where the 2-dimensional Gaussian reads:

$$G_t(x) := \frac{1}{2\pi t} \exp\left(-\frac{|x|^2}{2t}\right) \,. \tag{10.2}$$

For carrying out the convolution in (10.1) the image has to be appropriately extended to all of $\mathbb{R}^2$, say, either by 0 outside G or periodically. Both approaches

avoid the need of dealing with boundary conditions. Clearly, the Gaussian density (10.2) is the fundamental solution of the linear heat equation in $\mathbb{R}^2$, such that the function $u = u(x, t)$ can also be obtained by solving the linear heat equation with initial datum u_0 on the time interval $[0, t]$ (linear scale space):

$$u_t = \Delta u \tag{10.3}$$

$$u(t = 0) = u_0 \ . \tag{10.4}$$

Thus, to the image of origin u_0 this linear diffusion process associates a scale of smoothed images $\{u(x, t) \mid t \geq 0\}$. A mathematically trivial but practically important remark is in order: As t becomes progressively larger, more and more detail – and eventually also significant image structure – is destroyed. The reason for this is that the solution of the heat equation tends to a constant (0 in the whole space case) as t tends to infinity. This convergence holds uniformly on bounded sub-domains of $\mathbb{R}^2$, i.e. also on the image domain G. Thus, in practice, only not-too-large values of t are important for image analysis.

In principle, the heat equation (10.3), (10.4) can be regarded as a (primitive) denoising algorithm for the image u_0. However, there are two main problems involved with this. Firstly, the Laplacian generates isotropic diffusion of equal strength in all directions, independent of the local image structure. This is not what is desired in image de-noising: we would like to diffuse/denoise uniformly in those image subdomains, where no edges occur. In particular, we do not want to have too much local diffusion in direction orthogonal to edges. In short, edges should not be smeared out too much. Secondly, the smoothing (10.3), (10.4) does not commute with image contrast changes represented by strictly monotonically increasing functions of the image intensity u_0. It is desirable to have a smoothing algorithm, which is such that changing the contrast of the original image first and consecutive smoothing gives the same result as changing the contrast after smoothing the original image (morphological invariance). Obviously, the linear diffusive smoothing (10.3), (10.4) does not satisfy this principle, since in general $F\left(u(\cdot, t)\right)$ is NOT the solution of the heat equation with initial datum $F(u_0)$ for every strictly increasing function F.

The first issue was originally addressed by P. Perona and J. Malik [7] by introducing image dependent diffusivities. In particular, they considered nonlinear diffusion equations of the form:

$$u_t = \operatorname{div}\big(g(|\operatorname{grad} u|^2) \operatorname{grad} u\big) \ , \tag{10.5}$$

where $g = g(s)$ is a nonnegative decreasing function, which converges to 0 as s tends to infinity and $g(0+) = 1$. It is easy to show that (10.5) introduces linear-like diffusive smoothing in regions where $|\operatorname{grad} u|$ is small while there is a competition between diffusion in the tangential and orthogonal directions (relative to level sets $L_a(t) := \{x \in G \mid u(x, t) = a\}$) in regions with edges (where $|\operatorname{grad} u|$ is large). In particular, the equation (10.5) can be written as:

$$u_t = g(p^2) u_{ll} + \left(g(p^2) + 2p^2 g'(p^2)\right) u_{nn} \tag{10.6}$$

where we denoted $p = |\text{grad } u|$, u_{ll} the second tangential derivative and u_{nn} the second normal derivative relative to a level curve $L_a(t)$. Obviously, the ratio

$$R := \frac{g(p^2)}{g(p^2) + 2p^2 g'(p^2)}$$

determines the relative strength of diffusion parallel to and across level curves. Actually, the nonlinearity of g can also be tuned to give backward diffusion across level curves, thus performing localized smoothing in regions without edges AND localized edge sharpening. As a classical example, consider

$$g(s) := \frac{1}{1 + \lambda^2 s} .$$

Then the coefficient of u_{nn} in (10.6) becomes negative when $|\text{grad } u| > \lambda$.

An efficient choice of a nonlinear smoothing algorithm is based on the idea of diffusion ONLY in direction tangential to level curves, i.e. on the degenerate diffusion equation:

$$u_t = u_{ll} . \tag{10.7}$$

After back transformation to the original $x = (x_1, x_2)$ coordinates we obtain:

$$u_t = |\text{grad } u| \, \text{div}\left(\frac{\text{grad } u}{|\text{grad } u|} \right) . \tag{10.8}$$

Since

$$\kappa(x,t) := \text{div}\left(\frac{\text{grad } u(x,t)}{|\text{grad } u(x,t)|} \right)$$

is the curvature of the level curve $L_a(t)$ of the function u through the image point x at time t, the nonlinear non-divergence form degenerate parabolic equation (10.8) is referred to as the (mean) curvature equation. Also, the equation (10.8) satisfies the morphological invariance condition, since, given a strictly increasing nonlinear contrast change F, multiplication of (10.8) by $F'(u)$ shows that $F(u)$ solves the curvature equation with initial datum $F(u_0)$, i.e. smoothing by (10.8) and contrast changes commute. Note that the equation (10.8) can be rewritten in an intruiging way. Clearly, the vector

$$o(x,t) := -\frac{\text{grad } u(x,t)}{|\text{grad } u(x,t)|}$$

is the unit vector orthogonal to the level curve $L_a(t)$ passing through the point x at time t, pointing into the direction of steepest decay of u. Then (10.8) can be written as first order transport equation:

$$u_t + \kappa(x,t) o(x,t) \cdot \text{grad } u = 0 . \tag{10.9}$$

By standard theory of first order PDEs, smooth solutions u are constant along the characteristic curves, which satisfy the ODEs:

$$\frac{dx}{dt} = \kappa(x,t)o(x,t)\ . \tag{10.10}$$

Therefore, the speed of the motion is equal to the local curvature and the direction of the velocity vector is orthogonal to the level curves, pointing into the direction of decay of u. The smoothing effect of the curvature equation is based on equilibrating the curvature of the level sets of the solution.

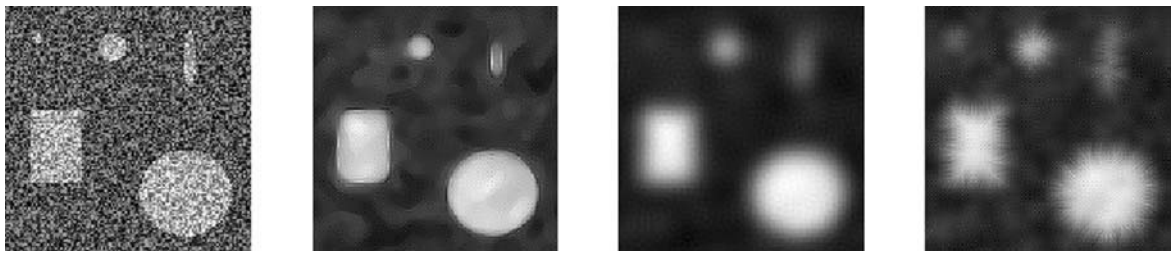

Fig. 10.2. Diffusive Smoothings (courtesy of Arjan Kuijper)

Image 10.2 shows the effect of different diffusive smoothings. From the left to the right we can see: The original noisy image with equidistributed noise, image smoothing by the curvature equation, by the heat equation and by directional diffusion along the orthogonals to level curves. All diffusions were performed up to the same final 'time'. Clearly, the curvature equation maintains the sharpness of the edges, while the heat equation destroys edge sharpness completely. Isotropic diffusion can be seen very well in the latter case. It is, however, interesting to note that the heat equation creates a somewhat uniform background out of the equidistributed noise while the curvature flow tries to extract information out of noise. Diffusion along the orthogonals of the level curves (worst possibility…) creates very visible artifacts in the form of spikes originating from the edges.

A somewhat different approach is represented by smoothing of Fatemi–Rudin–Osher type [5]. They consider the total variation of the intensity function as decisive for the state of an image and propose to minimize the following functional, over the space of functions with bounded total variation:

$$T(u) := \int_G \left(|\mathrm{grad}\, u| + \frac{\lambda}{2}(u-u_0)^2 \right) dx\ , \tag{10.11}$$

where λ is a positive parameter. Clearly, the second term under the integral penalises smoothed images u which are too far away from the original image u_0,

i.e it decides the relative importance of keeping total image variation small and of not moving away too far from the original image. The Euler–Lagrange equation (which is a necessary condition for the minimizer) of the functional (10.11) reads:

$$-\mathrm{div}\left(\frac{\mathrm{grad}\, u}{|\mathrm{grad}\, u|}\right) + \lambda(u - u_0) = 0\,, \quad x \in G\,, \tag{10.12}$$

subject to the homogeneous Neumann boundary condition:

$$\mathrm{grad}\, u \cdot \gamma = 0 \text{ on } \partial G\,, \tag{10.13}$$

where γ is the unit outer normal vector of ∂G.

The corresponding gradient flow (steepest descent method) is given by the parabolic equation:

$$u_t = \mathrm{div}\left(\frac{\mathrm{grad}\, u}{|\mathrm{grad}\, u|}\right) - \lambda(u - u_0)\,, \tag{10.14}$$

again subject to homogeneous Neumann boundary conditions. For appropriate initial data we expect the solutions of (10.14) to converge to the minimizer of (10.11).

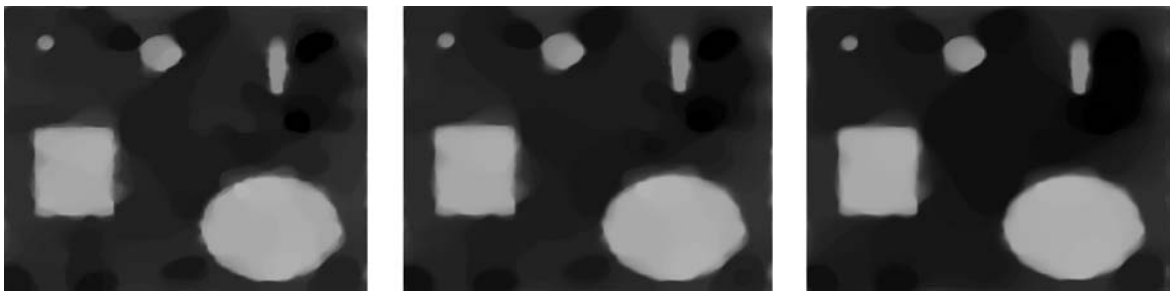

Fig. 10.3. Rudin–Osher–Fatemi Smoothing (courtesy of Martin Burger)

A generic modification of the Rudin–Osher–Fatemi functional is obtained by replacing the penalizing term by a multiple of the L^1 norm (instead of the square of the L^2 norm) of the difference of the original and the smoothed image intensity functions. In Image 10.3 we show the minimizing intensities of this modified functional for decreasing values of the penalization parameter (from left to right), where the original image is the same as the left image in Image 10.2. When the penalisation becomes weaker, edge sharpness decreases slightly, the algorithm extracts less information out of the noise but – clearly – overall smoothness of the image increases.

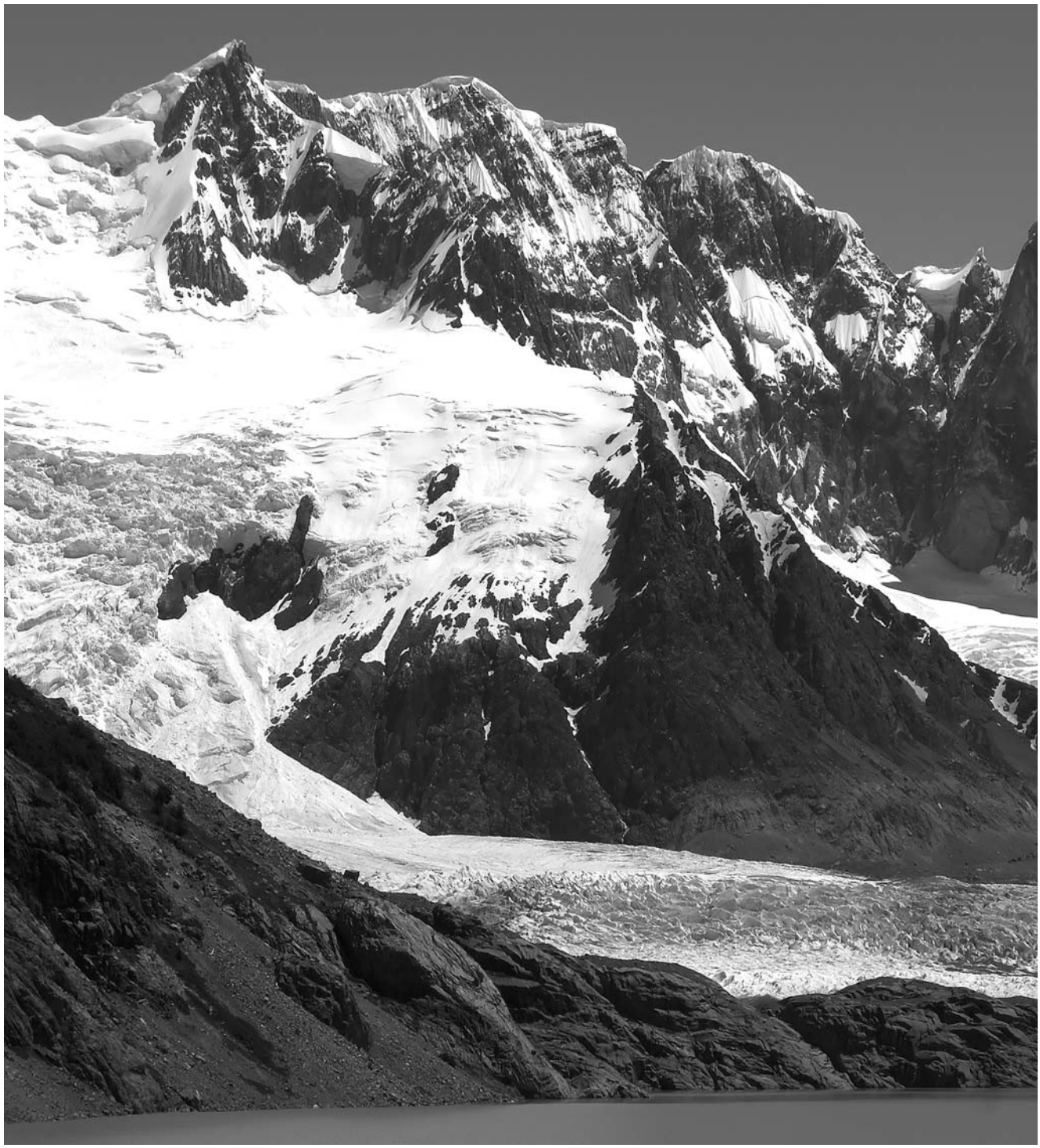

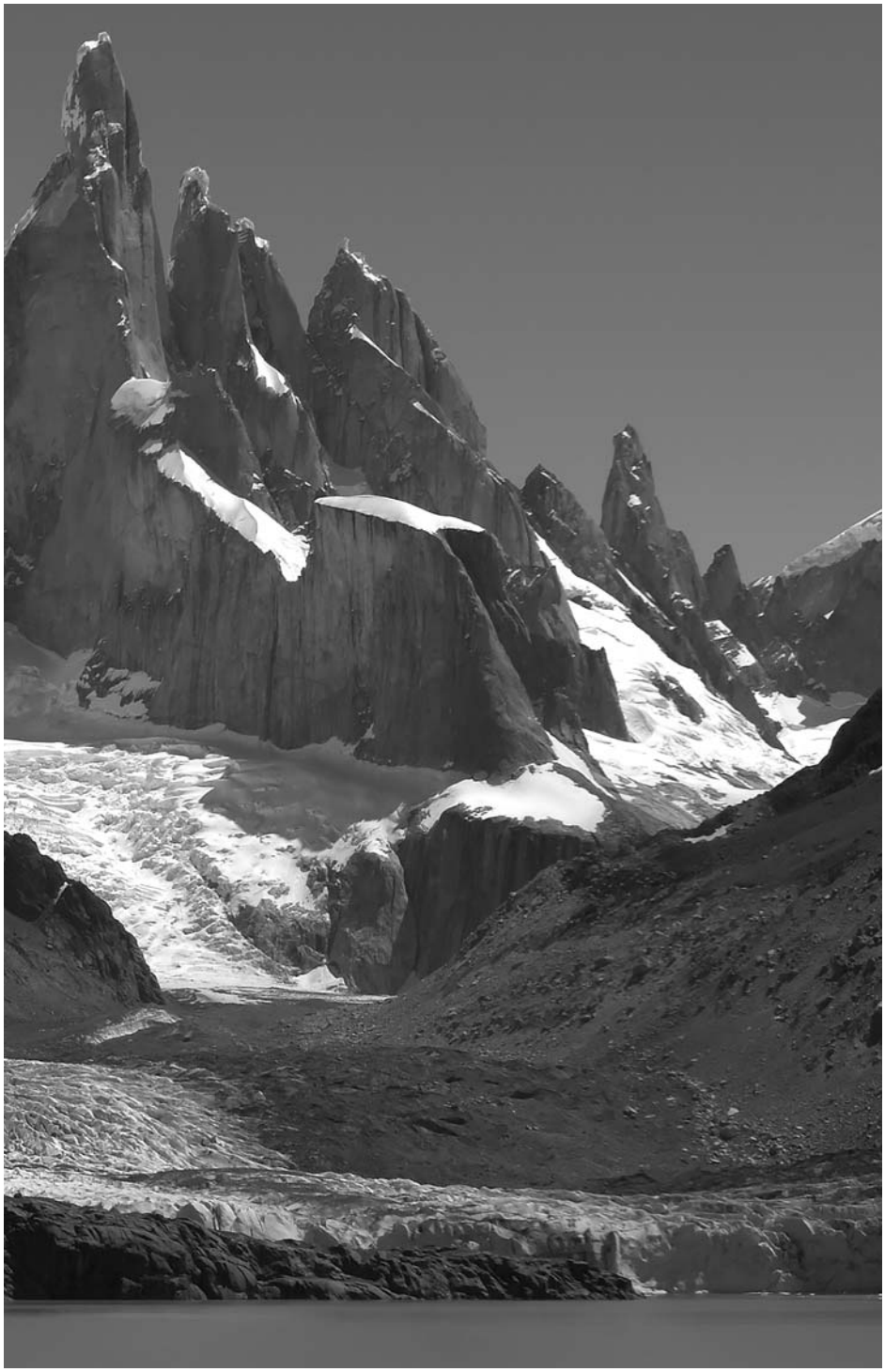

Fig. 10.4. Natural image, Cerro Torre seen from Laguna Torre in Argentinian Patagonia

The Perona–Malik equations, the curvature equation and the Rudin–Osher–Fatemi equation are important examples of the class of so-called geometric PDEs, which are typically analyzed by viscosity solution theory [4] or, resp., by BV-solution theory.

Digital image sensors have – in most commercially available cameras – so called anti-aliasing filters[6] mounted in front of them, which remove frequency components above the Nyquist frequency. By Nyquist's and Shannon's sampling theory[7] these frequencies are not correctly representable by the sensor anymore. In practical terms, anti-aliasing filters reduce the dreaded Moirée effect[8], which occurs when an image pattern resonates with the pixel matrix or exceeds the sensor resolution. These anti-aliasing filters also have a negative effect: they reduce the sharpness of digital images, which then has to be restored by image processing. Also, sharpening (or de-blurring) of images has to be performed to eliminate/reduce camera shake, motion blur, atmospheric disturbances etc.

Contrarily to smoothing, image sharpening is an inverse problem, with the typical instability associated with backward diffusion. Intuitively though, it seems natural to sharpen (or de-blur) an image u_0 by just running the backward heat equation on it:

$$u_t = -\Delta u \,, \quad t > 0 \tag{10.15}$$

$$u(t=0) = u_0 \,. \tag{10.16}$$

This method actually has its merits, when the sharpening scale t is chosen appropriately. If, however, t becomes too large, the image decomposes due to the inherent instability of backward diffusion. Various possibilities to overcome this instability issue arise, e.g. stabilisation of the linear backward heat equation by nonlinearities like the curvature equation, employing Hamilton–Jacobi type image motions or taking the generic inverse problem viewpoint with the classical philosophy of stabilisation by penalisation.

An 'unstabilised' Hamilton–Jacobi-type attempt was given by L.I. Rudin and S. Osher, called now the shock filter:

$$u_t + \operatorname{sgn}(\Delta u)|\operatorname{grad} u| = 0 \,. \tag{10.17}$$

An improved version, the so called edge detector PDE, reads:

$$u_t + \operatorname{sgn}\left((\operatorname{grad} u)^T D^2 u \operatorname{grad} u\right)|\operatorname{grad} u| = 0 \,. \tag{10.18}$$

Note that both equations involve second order derivatives in a very non-standard way! The Rudin–Osher PDE is related to the Hildreth–Marr edge detector, which defines edges of a smoothed digital image as those subsets of the image domain, where Δu changes sign, while the PDE (10.18) is related to Canny's

[6] *http://en.wikipedia.org/wiki/Anti-aliasing_filter*

[7] *http://en.wikipedia.org/wiki/Nyquist-Shannon_sampling_theorem*

[8] *http://www.dpreview.com/learn/?/Glossary/Digital_Imaging/Moire_01.htm*

Fig. 10.5. Billboard, artificial Image (or sort of …)

edge detector (see, e.g., [6]), defining edges as sets where $(\operatorname{grad} u)^T D^2 u \operatorname{grad} u$ changes sign. In both cases the direction of propagation is changed locally when an edge is crossed. Although these equations are numerically stable and seem to converge to a steady state, stabilised algorithms are preferable for practical purposes. The maybe most efficient de-blurring algorithm is stabilized BV de-blurring, suggested by Rudin, Osher and Fatemi [5], [9]. The main idea is similar to BV-denoising based on the functional (10.11), i.e. the total variation of the image intensity function shall be minimised under a penalisation. In the case of denoising the penalisation was that the denoised image should not be too far from the original one in the L^2 norm, while for de-blurring we require that the original image shall be close to the blurred version of the restored one. Obviously, this leaves us with the definition of the blur operator. Usually, a linear blur is assumed, of convolution form:

$$B(u) = k * u \,, \tag{10.19}$$

where $k = k(x)$ is a given nonnegative function (or measure), depending on the specific image blur under consideration (see [3] for examples). Note that either u has to be extended appropriately to the full space $\mathbb{R}^2$ or boundary conditions

have to be imposed in order to give mathematical sense to the convolution (10.19). Then, the de-blurred image u, obtained from the blurry original image u_0, is given by:

$$u = \operatorname{argmin}\left(\int_G \left(|\operatorname{grad} v| + \frac{\lambda}{2}(k * v - u_0)^2 \right) dx \right) , \tag{10.20}$$

where the minimisation is performed over the space of real-valued functions v defined on G with bounded total variation. Again, the positive parameter λ controls the relative importance of BV minimization and of the penalisation.

At this point a word of caution is in order. In imaging science there is a distinction between natural images and artificial ones. The former class refers to digital images of objects (trees, bushes, human faces etc.), and scenes (sceneries…) which occur in nature, while the second class refers to digital images of man-made structures (typically images of two-dimensional artificial structures). Figure 10.4 shows a typical natural image, namely a landscape in Argentinian Patagonia and Figure 10.5 an artificial image. Statistical analysis of image banks has shown that natural images have significant multi-scale features (as can be seen clearly in Figure 10.4), much more than artificial images. Recent research [1] has led to the conjecture that – typically – natural images are 'not of bounded variation'. This statement has to be understood that – by the conjecture – the total variation becomes unbounded when a sequence of digital images with increasing sensor resolution of the same natural scene is taken. We expect more insight into these questions in the near future, now that digital imaging sensor technology has improved significantly, particularly in megapixel count and in non-destructive low-iso noise control. Of course, a possible implication of this is that we have to be very careful using – or even have to abandon – BV-techniques for the processing and analysis of natural images, particularly when they were acquired by a high resolution digital sensor.

The deep connection between smoothing and sharpening is also illustrated by the most popular sharpening technique of the digital photography community, referred to as 'sharpening by unsharp masking', as used for example in the benchmark image processing software 'Photoshop CS' by ADOBE[9]. Let u_0 be the original digitally acquired image and denote by $u(t)$ a smoothed version of it (the so called unsharp mask), obtained by running the heat equation from time 0 to t, as done in Photoshop by using the convolution (10.1) with the Gaussian (10.2), or some nonlinear smoothing algorithm. Then compute the difference

$$w(x,t) := u_0(x) - u(x,t) . \tag{10.21}$$

Clearly, w can be regarded as an image of the edges of u_0, since it 'concentrates' there while being small away from edges, at least for t not too large. Then choose

[9] *http://www.adobe.com*

another positive parameter σ and set:

$$u_{\text{enhanced}}(x,t) := u_0 + \sigma w(x,t)\ . \tag{10.22}$$

Actually, in Photoshop CS there is a third parameter, which decides on the minimal contrast difference of adjacent pixels such that sharpening is actually applied to the pixels under consideration. In practice, this technique leads to increasing the intensity function u_0 on the darker side of the edge and decreasing it on the brighter side such that a visual impression of gain of sharpness is achieved.

Image 10.6 of this gallery shows the edges of the landscape shown in Image 10.4 and Image 10.7 the edges of Image 10.5. The great complexity of the edge set of the natural Image 10.4, particularly in direct comparison with the edge set of the artificial Image 10.5, is apparent.

Image segmentation is an important part of image analysis. There the main task is to identify the different objects present in a given digital image or equivalently, the issue is to find the most significant edges of the image. A main contribution to this issue was given by D. Mumford[10] and J. Shah in their celebrated paper [8]. To fix the basic ideas, think of functions u, which are piecewise smooth on a Lipschitz partition of the image domain, let S denote the union of

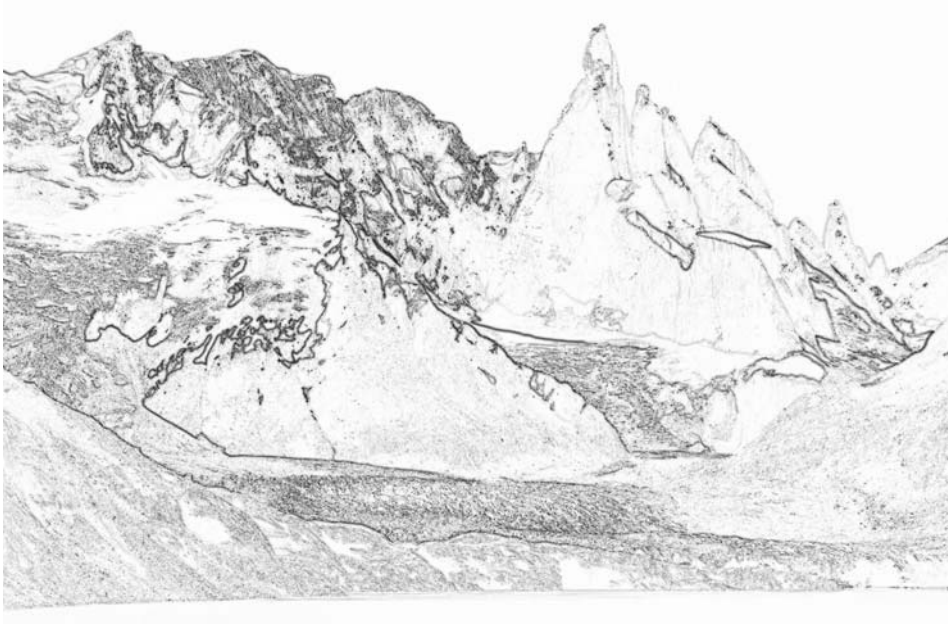

Fig. 10.6. Edge set of natural Image 10.4

[10] *http://www.dam.brown.edu/people/mumford/*

the Lipschitz manifolds of their singularities (image edges), let a noisy original image u_0 be given and consider the so called Mumford–Shah functional:

$$M(u, S, u_0) := \alpha \mathcal{H}^1(S) + \beta \int_{G-S} |\text{grad}\, u|^2 dx + \gamma \int_G (u_0 - B(u))^2 dx\,. \qquad (10.23)$$

Here $B = B(u)$ again denotes the smoothing (blurring) operator, e.g. given by a convolution (10.19), and $\mathcal{H}^1(S)$ stands for the one-dimensional Hausdorf measure ('length') of the edge set S. α, β and γ are positive constants, responsible for the relative importance of the three terms in the functional, which can be identified as the edge energy, the localised image energy and the penalisation term already used in the Rudin–Osher–Fatemi de-blurring approach. The obvious candidate for the deblurred image, with associated segmentation, would be a minimizer u (over an appropriate function space) of the functional (10.23). Clearly, the big problem here is the singularity set S, which determines the geometrical nature of the problem. Directly related to this is the fact that a precise

Fig. 10.7. Edge set of artificial Image 10.5

mathematical definition of the function space, over which the Mumford–Shah functional shall be minimized, is very subtle and requires deep insights into the theory of BV-functions and thus uses high powered tools from geometrical measure theory. We refer to [2] for results on the existence of a minimizer (of an appropriately weakened version of the Mumford–Shah functional). For a more detailed discussion and an extensive list of references, also concerning the existence of a minimizer of the strong formulation, we refer to [3].

Comments on the Images 10.1–10.7 Digital photography has reached a phase of maturity. Not only in the consumer market, where analog film-based photography has basically vanished, but also in the prosumer market, where 6–10 megapixel cameras (often Digital-Single-Lens-Reflex-Cameras, so called DSLRs) have reached a significant market share and in the professional market, too, with 12–16 megapixel DSLRs based on 35 mm full format or on so called DX sensor technology and, on the very high end, with digital backs which attach to medium format cameras and nowadays feature 22–39 megapixel sensors (see the Image 10.1). Todays high end digital cameras offer a photographic quality which was unknown in the analog days, with silky smooth imagery and the possibility to do large high resolution prints, chemically based or even using inkjet technology in the 'digital darkroom' by the photographer himself. Digital images, however, require postprocessing by sophisticated software. Images have to be white-balanced, contrast corrected, digital artifacts have to be eliminated, noise reduction and sharpening have to be performed and often images have to be compressed to jpg format for emailing and storage. All these processes require sophisticated mathematics, which to a great extent is based on partial differential equations and on variational techniques. It is clear that – with megapixel counts growing steadily – the required need of sophistication of digital image processing goes up, too (just think of getting processing times down, which are still a major nuisance for users of high megapixel-count cameras). Also, most of todays commercially available image processing software is based on linear PDE tools (heat equation) while it is well known in scientific image processing circles that nonlinear methods (Perona–Malik equation, curvature equation, Cahn–Hillard inpainting etc.) give highly superior results. We expect a 'quantum leap' in the commercial image processing software soon, which will shake up the typically very conservative photographic community.

There are other important applications of digital image processing than photography, also with high demand of mathematical sophistication. Just think of security applications based on digital reconnaissance or medical imaging. For example, automated tumor recognition in medical scanning techniques is based on image segmentation (often using the Mumford–Shah functional)! Note that in medical and in security imaging not only still images but also video sequences have to be processed and analysed.

Acknowledgement The author acknowledges support for research on image processing by the Austrian research funding agency FFG.

References

[1] L. Alvarez, Y. Gousseau and J.M. Morel, *Scales in Natural Images and a Consequence On their Bounded Variation Norm*, in Scale Space '99. Ed. M. Nielsen, P. Johansen, O. Olsen and J. Weickert, pp. 247–258 Lectures Notes in Computer Science Nº 1682, Springer Verlag, 2000

[2] L. Ambrosio, *A Compactness Theorem for a new Class of Functions of Bounded Variation*, Boll. Un. Mat. Ital. B (7), Vol. 3, pp. 857–881, 1989

[3] T.F. Chan and J. Shen, *Image Processing and Analysis*, SIAM, 2005

[4] M.G. Crandall, H. Ishii and P.L. Lions, *User's guide to viscosity solutions of second order Partial differential equations*, Bull. Amer. Soc. 27, pp. 1–67, 1992

[5] E. Fatemi, L.I. Rudin, and S. Osher, *Nonlinear total variation based noise removal algorithms*, Physica D 60, No. 1–4, 259–268. [ISSN 0167-2789], 1992

[6] F. Guichard and J.-M. Morel, *Image Analysis and P.D.E.s*[11]

[7] J. Malik and P. Perona, *Scale Space and Edge Detection using Anisotropic Diffusion*, IEEE Trans. Patt. Anal. Mach. Intell., Vol. 12, pp. 629–639, 1990

[8] D. Mumford and J. Shah, *Optimal Approximations by Piecewise Smooth Functions and associated Variational Problems*, Comm. Pure Appl. Math., Vol. 42, pp. 577–685, 1989

[9] S. Osher and L.I. Rudin, *Total Variation based Image Restoration with free local Constraints*, in Proc. 1st IEEE ICIP, Vol. 1, pp. 31–35, 1994

[11] downloadable from *http://citeseer.ist.psu.edu/guichard01image.html*

11. Socio-Economic Modeling

Peter A. Markowich and Giuseppe Toscani[1]

A comparative empirical and statistical analysis of social and economic phenomena describing the collective behavior of human beings in different countries and markets leads to a strikingly large number of similarities. This motivates the basic idea that the collective behavior of a society composed of sufficiently many individuals (agents) can be modeled using the approach of statistical mechanics, which was originally developed for the description of physical systems consisting of many interacting particles. The details of the interactions between agents then characterize the emerging statistical phenomena.

In particular the evolution of wealth in a simple market economy has been studied extensively. A very interesting point of view in the representation of markets is the kinetic one, which leads to Boltzmann type equations for the evolution of the distribution of wealth [3–6, 12]. In these models, the market is represented by a gas of physical particles, where each particle is identified with an agent, and each trading event between two agents is considered to be a binary particle collision event, with collisional rules determined by the properties of the underlying market. The knowledge of the large-wealth behavior of the steady state density is of primary importance, since it characterizes the number of rich individuals in the society and can easily be used to determine *a posteriori* if the model fits known data of real economies.

More than a hundred years ago, the Italian economist Vilfredo Pareto [11] first quantified the large-wealth behavior of the income distribution in a society and concluded that it obeys a power-law. More precisely if $f = f(w)$ is the probability density function of agents with wealth w, and w is sufficiently large, then the fraction of individuals in the society with wealth larger than w is:

$$F(w) = \int_w^\infty f(w_*)\, dw_* \sim w^{-\mu} .$$

Pareto mistakenly believed the distribution function on the whole range of wealth (positive real axis) to be a power law with a universal exponent μ approximatively equal to 1.5.

Various statistical investigations with real data during the last ten years revealed that the tails of the income distributions indeed follow the above mentioned power law behavior. The numerical value of the so called Pareto index μ generally varies between 1 and 2.5 depending on the considered market (USA

[1] *http://www-dimat.unipv.it/toscani/*

~ 1.6, Japan ~ 1.8–2.2, [6]). It is also known from statistical studies that typically less than 20% of the population of any country own about 80% of the total wealth of that country. The top income group obeys the above Pareto law while the remaining low income population, in fact the majority (80% or more), follow a different distribution, which is typically Gibbs [6] or log-normal.

Kinetic models of the time evolution of wealth distributions can be described in terms of a Boltzmann-like equation which reads

$$\frac{\partial f}{\partial t} = Q(f,f)\,, \tag{11.1}$$

where $f = f(v,t)$ is the probability density of agents of wealth $v \in \mathbb{R}_+$ at time $t \geq 0$, and Q is a bilinear operator which describes the change of f due to binary trading events among agents. We shall refer to this equation in the sequel as kinetic Pareto–Boltzmann equation.

The involved binary tradings are described by the rules

$$v^* = p_1 v + q_1 w\,; \quad w^* = p_2 v + q_2 w\,, \tag{11.2}$$

where (v,w) denote the (positive) moneys of two arbitrary individuals before the trading and (v^*,w^*) the moneys after the trading. The transaction coefficients p_i, q_i, $i = 1,2$ are either given constants or random variables, with the obvious constraint of non-negativity. Also, they have to be such that the transformation from the money states before trading and after trading is non-singular. Among all possible kinetic models of type (11.1), (11.2) the *conservative* models are characterized by the property

$$\langle p_1 + p_2 \rangle = 1\,, \quad \langle q_1 + q_2 \rangle = 1\,,$$

where $\langle\cdot\rangle$ denotes the probabilistic expectation. This guarantees conservation of the total expected wealth of the market (which is the first order moment of the distribution function, multiplied by the total number of individuals).

In weak form the *collision* operator $Q(f,f)$ is defined by

$$\int_{\mathbb{R}_+} Q(f,f)(v)\phi(v)\,dv$$
$$= \frac{1}{2}\left\langle \int_{\mathbb{R}_+}\int_{\mathbb{R}_+} \big(\phi(v^*) + \phi(w^*) - \phi(v) - \phi(w)\big) f(v) f(w) dv\,dw \right\rangle\,. \tag{11.3}$$

Here ϕ is a smooth test function with compact support in the non-negative reals.

Note that the *collision* operator is assumed to be of so-called Maxwellian type, i.e. the scattering kernel does not depend on the relative wealth of collisions and can therefore be accounted for in the computation of the statistical expectation by choosing the probability space appropriately.

In their pioneering paper A. Chakraborty and B.K. Chakrabarthi [3] started out by stating that the agents taking part in trading exchange their money according to the rule

$$v^* = v + \Delta(v, w) \; ; \quad w^* = w - \Delta(v, w) \; . \tag{11.4}$$

Here $\Delta(v, w)$ represents the amount of money to be exchanged, which has to be such that the agents always keep some money in their hands after trading. The ratio of saving to all of the money held is usually denoted by s and called the saving rate. Taking $0 < s < 1$ constant, the amount of money to be exchanged can be modeled as

$$\Delta(v, w) = (1 - s)\left[(\varepsilon - 1)v + \varepsilon w\right] , \tag{11.5}$$

where $0 \leq \varepsilon \leq 1$ is a random fraction. This model was further developed in B.K. Chakrabarthi's research group by assuming that agents feature a random saving rate [4]. Clearly, choosing a random value for s does not change the type of collision events.

A somewhat different trading law was considered by S. Cordier, L. Pareschi and G. Toscani in [5]. Their trading model reads

$$v^* = sv + (1 - s)w + \eta v \; ; \quad w^* = (1 - s)v + sw + \tilde{\eta} w \; , \tag{11.6}$$

where $0 < s < \frac{1}{2}$. Here η and $\tilde{\eta}$ are independent equally distributed random variables with variance σ^2 and mean zero. Provided both η and $\tilde{\eta}$ take values in the interval $[-s, s]$, the trade (11.6) is such that the random coefficients p_i, q_i, $i = 1, 2$ are nonnegative. Note that this trade is conservative only in the mean, since $p_1 + p_2 = 1 + \eta \neq 1$, whereas $\langle p_1 + p_2 \rangle = 1$. The last terms in the trading laws describe the spontaneous growth or decrease of wealth due to random investments in the stock market and other macro-economic factors. This mechanism corresponds to the effects of an open market economy where typically the rich get richer and the poor get poorer.

Non-conservative models have been recently considered by F. Slanina [12], who introduced a model with increasing total wealth based on the collision coefficients:

$$p_1 = s \; , \quad q_1 = 1 - s + \varepsilon \; ; \quad p_2 = 1 - s + \varepsilon \; , \quad q_2 = s \; . \tag{11.7}$$

In (11.7) ε is a fixed positive constant, so that the total money put into the trade increases, since

$$v^* + w^* = (1 + \varepsilon)(v + w) \; .$$

This type of trade intends to introduce the feature of a strong economy, which is such that the total mean wealth is increasing in time. We remark that the

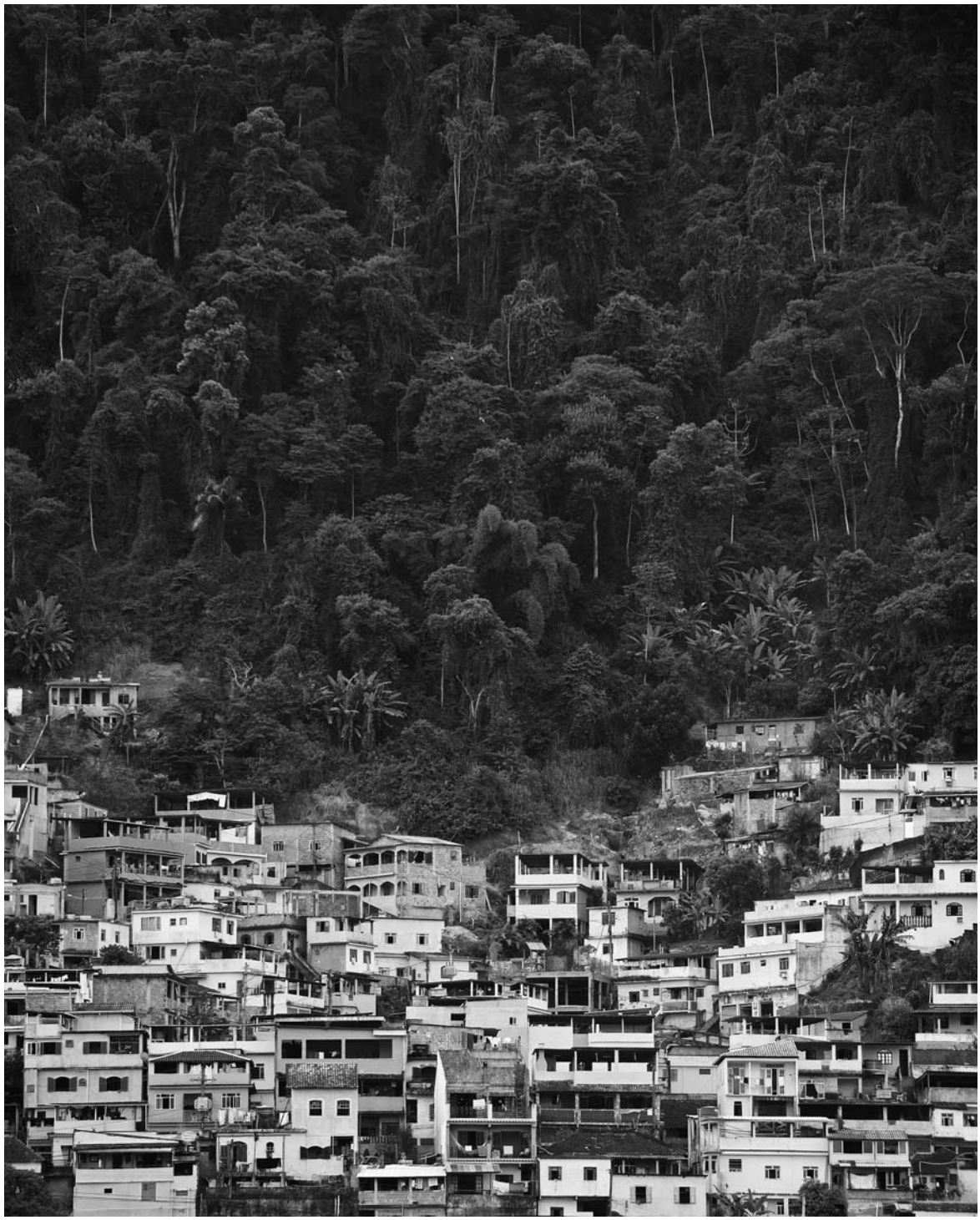

Fig. 11.1. Angra dos Reis, Brazil: on the $w = o(1)$-part of the Pareto distribution

Fig. 11.2. Salvador de Bahia, Brazil: on the $w = o(1)$-part of the Pareto distribution

same effect can also be obtained by simply allowing the random variables in the trading laws (11.6) to assume values on the whole real axis, and at the same time discarding those trades for which one of the post-trade wealths is non-positive.

A critical analysis of the discussed *collision=trading* rules reveals a deep analogy between the economic models described above and the granular material flows modeling framework of Chapter 3. They share the property that the steady (or, more generally, the self-similar asymptotic) states are different from the classical Maxwell distribution of the Boltzmann equation of gas dynamics presented in Chap. 1. Another analogy becomes evident when looking at the non-conservative properties of the *economic* and *granular* Boltzmann equations, resulting from inelastic binary collision models.

Conservative exchange dynamics between individuals redistribute the wealth among people. Without conservation, the best way to extract information on the large-time behavior of the solution relies on scaling the solution itself to keep the average wealth constant after scaling. Nevertheless, the explicit form of the limit distribution of the kinetic equation remains extremely difficult to recover, and often requires the use of suitable numerical methods.

A complementary method to extract information on the steady state distribution was linked in [5] to the possibility of obtaining particular asymptotics, which mimic the characteristics of the solution of the original problem for large times. The main result in this direction was to show that the kinetic model converges (under appropriate assumptions) in a suitable scaling limit to a par-

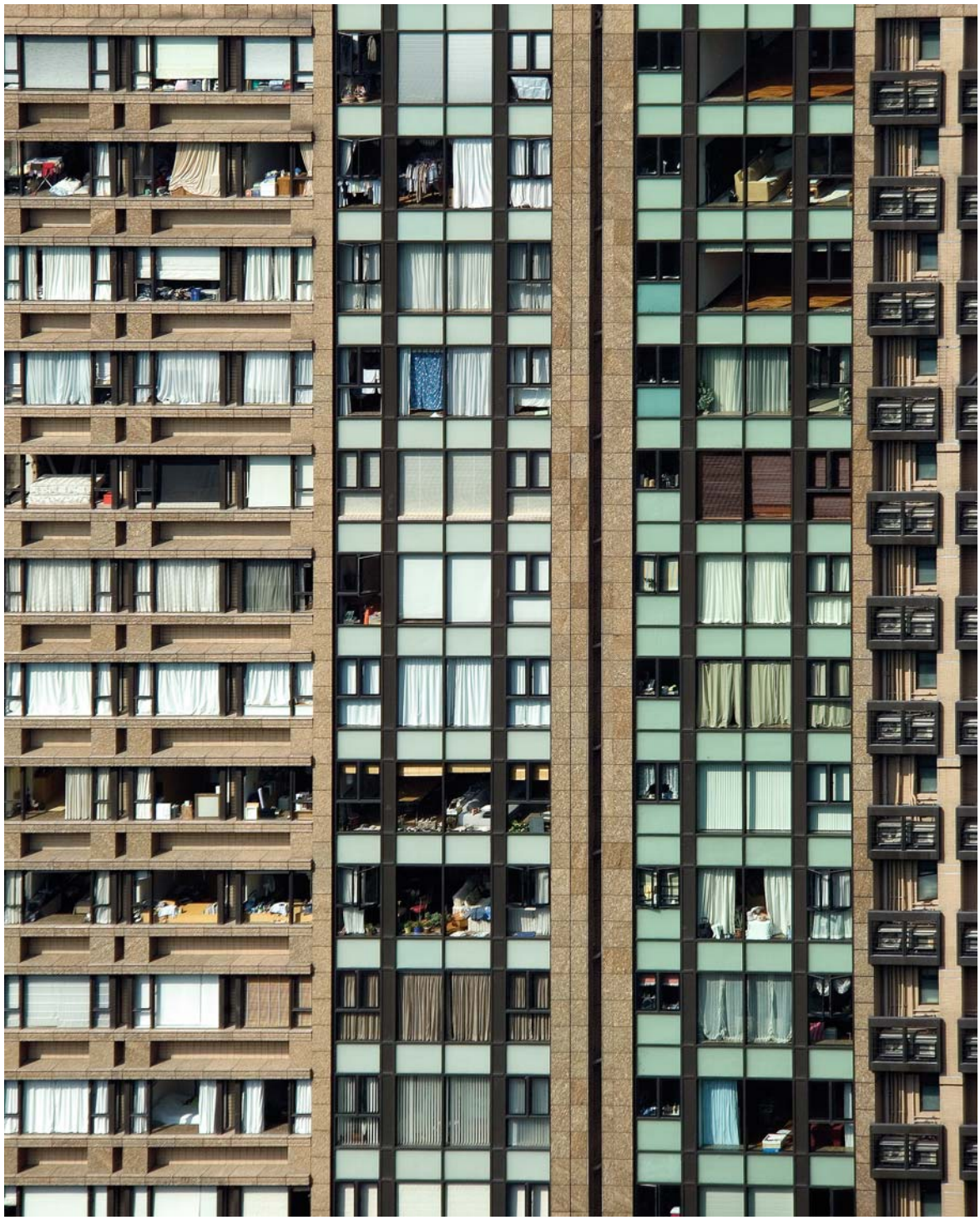

Fig. 11.3. Hongkong: in the thin $w = O(1)$-part of the Pareto distribution

tial differential equation of Fokker–Planck type for the distribution of money among individuals. This diffusion-convection equation reads:

$$\frac{\partial f}{\partial t} = \frac{\lambda}{2}\frac{\partial^2}{\partial v^2}\left(v^2 f\right) + \frac{\partial}{\partial v}\left((v-m)f\right) \ . \tag{11.8}$$

In (11.8) m is the mean wealth,

$$m = \int\limits_{\mathbb{R}_+} v f(v,t)\, dv \ ,$$

which is time-conserved assuming that f has been scaled to be a probability density. The same Fokker–Planck equation was obtained in [2] as the mean field limit of a stochastic equation, as well as in [9, 14] in the context of generalized Lotka–Volterra dynamics.

The equilibrium state of the Fokker–Planck equation can be computed explicitly and is of Pareto type, namely it is characterized by a power-law tail for the richest individuals. By assuming for simplicity $m = 1$ we find:

$$f_\infty(v) = \frac{(\mu-1)^\mu}{\Gamma(\mu)} \frac{\exp\left(-\frac{\mu-1}{v}\right)}{v^{1+\mu}} \tag{11.9}$$

where

$$\mu = 1 + \frac{2}{\lambda} > 1 \ .$$

We remark that the tails of the Pareto steady state of the Fokker–Planck equation are related to the coefficients s and σ^2 which appear in the collision rule (11.6), with $\sigma^2/s = \lambda$!

Another important field in which microscopic kinetic models describing the collective behavior and self-organization in a society [16] can be fruitfully employed is the modeling of opinion formation (cfr. [1,13,15] and the references therein).

In these studies, formation of opinion is described by mean field model equations. They are in general systems of ordinary differential equations or partial differential equations of diffusive type. In [1], attention is focused on two aspects of opinion formation, which in principle could be responsible for the formation of coherent structures. The first one is the remarkably simple compromise process, in which pairs of agents reach a fair compromise after exchanging opinions. The second one is a diffusion process, which allows individual agents to change their opinions in a random diffusive fashion. While the compromise process has its basis in the human tendency to settle conflicts, diffusion accounts for the possibility that people may change opinion through access to information. At present

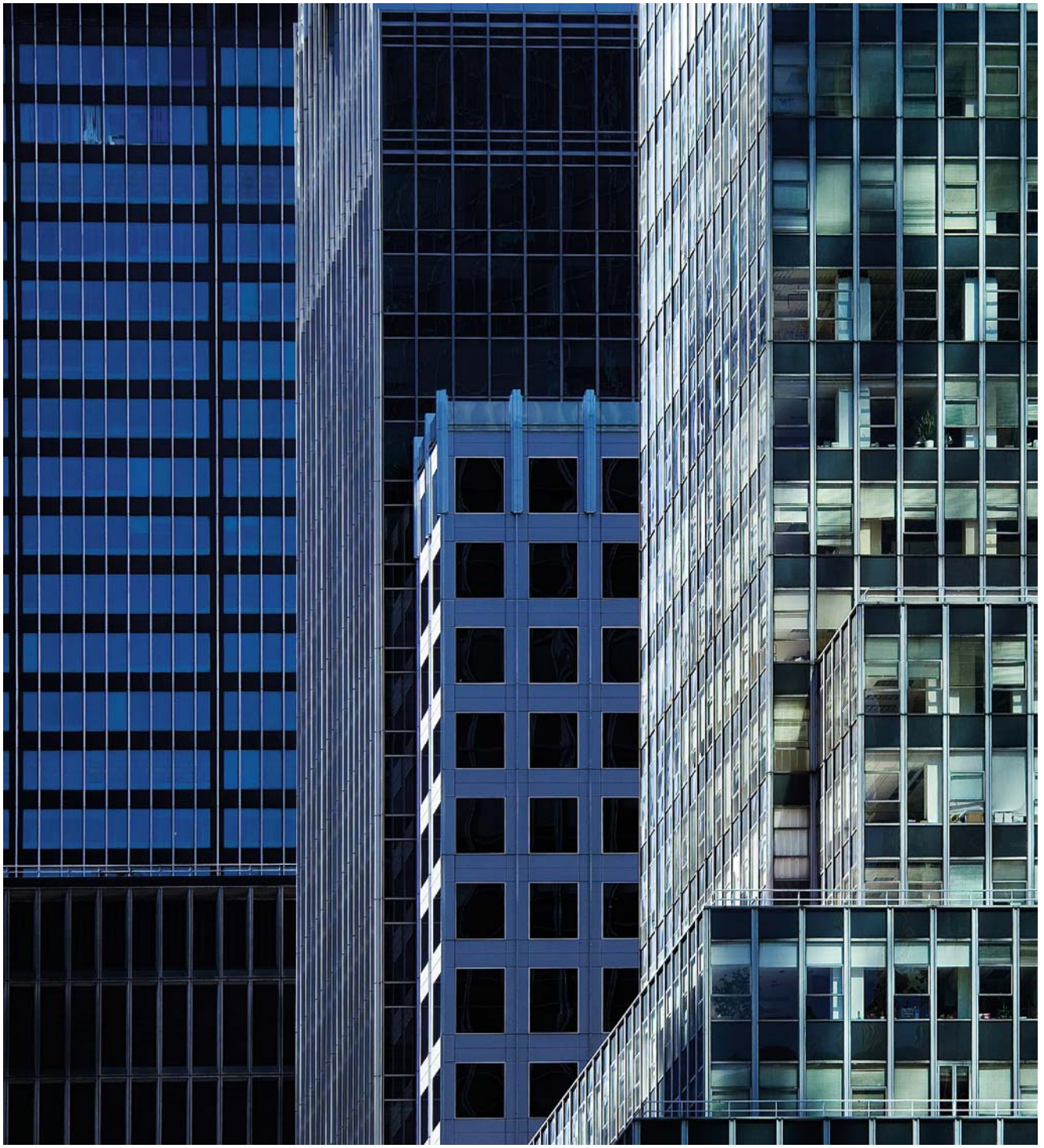

Fig. 11.4. Manhattan, New York: in the fat Pareto tail


HSBC
THE RITZ-CARLTON

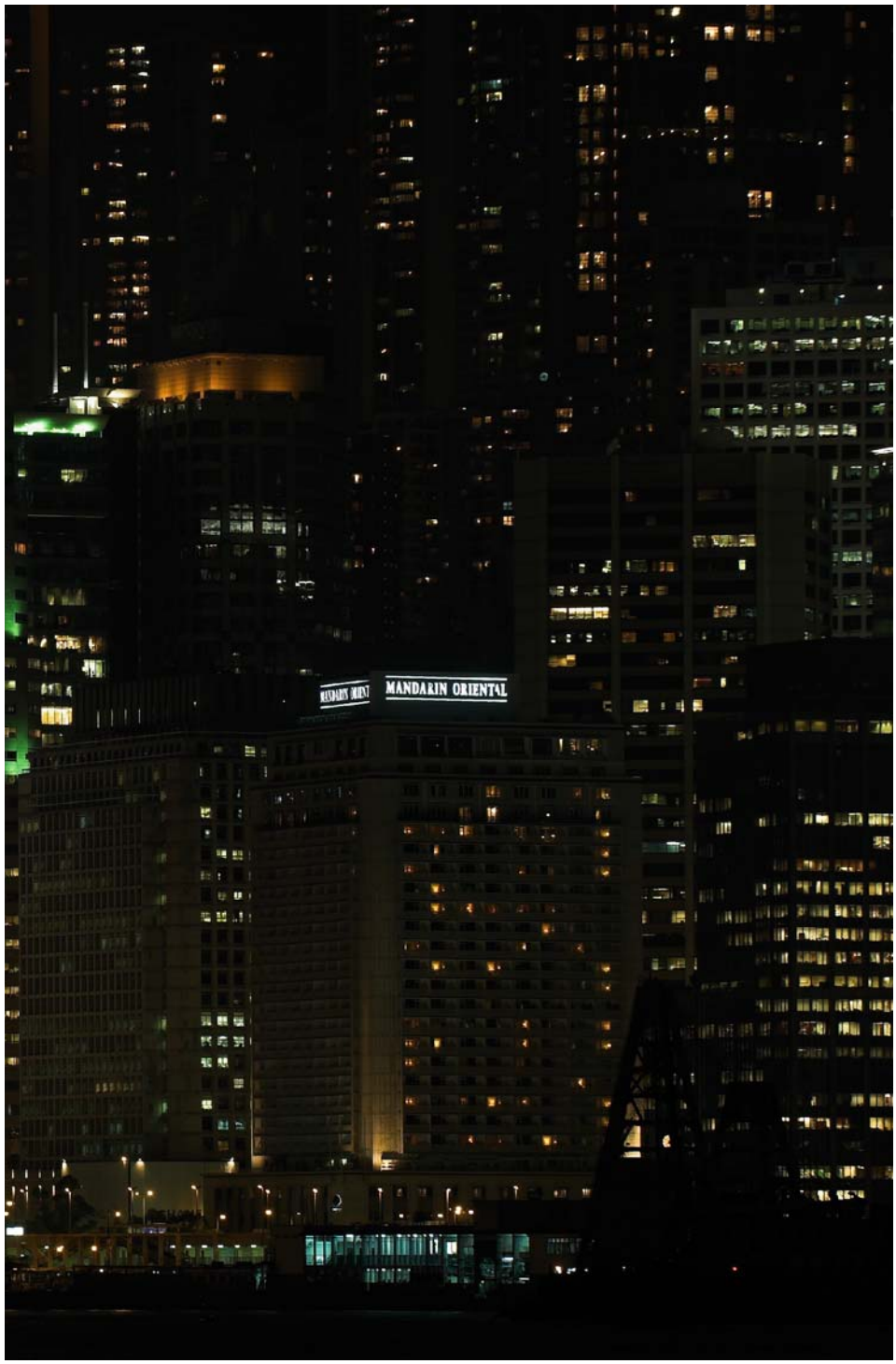

Fig. 11.5. Hongkong, China: where the fat Pareto tail is made

Fig. 11.6. Shanghai, China: some are left behind on the $w = o(1)$-part of the Pareto distribution (courtesy of Andrea Baczynski)

this aspect is gaining importance due to emerging new ways of global access to and exchange of information (among them electronic mail and web navigation).

This line of thought is at the basis of kinetic models of opinion formation [15], based on two-body interactions involving both compromise and diffusion properties in exchanges between individuals.

The goal of kinetic models of opinion formation is to describe the evolution of the distribution of opinions in a society by means of *microscopic* interactions between agents which exchange information. To fix ideas, we associate opinion with a variable which varies continuously from -1 to 1, where -1 and 1 denote the two (extreme) opposite opinions. We assume binary interactions which are such that the bounds of the admissible opinion-interval are maintained. This crucial rule emphasizes the difference between *social* interactions, where not all interaction outcomes are permitted, and collisions of molecules in the kinetic theory of rarefied gases.

Let $\mathbb{I} = [-1, +1]$ denote the interval of admissible opinions. From a microscopic view point, a binary interaction is described by

$$\begin{aligned} v^* &= v - sP(|v|)(v - w) + \eta D(|v|) \, ; \\ w^* &= w - sP(|w|)(w - v) + \tilde{\eta} D(|w|) \, , \end{aligned} \tag{11.10}$$

where the pair (v, w), denotes the opinions of two arbitrary individuals before the interaction and (v^*, w^*) their opinions after exchanging information between them and with the exterior world. Opinions are not allowed to cross boundaries, and thus the interaction takes place only if both $v^*, w^* \in \mathbb{I}$. In (11.10) the coefficient $s \in (0, 1/2)$ is a given constant (the analogue of the saving rate in (11.5), while η and $\tilde{\eta}$ are equally distributed random variables with variance σ^2 and zero mean. The constant s and the variance σ^2 measure the compromise propensity and, respectively, the modification of opinion due to diffusion. Finally, the functions $P(\cdot)$ and $D(\cdot)$ describe the local relevance of the compromise and diffusion for a given opinion.

In analogy to kinetic modeling of market economies, the binary interactions (11.10) are used to construct a Boltzmann-like equation similar to (11.1), where now

$$\int_{\mathbf{I}} Q(f,f)(v)\phi(v)\, dv = \frac{1}{2}\left\langle \int_{\mathbf{I}} \int_{\mathbf{I}} (\phi(v^*) + \phi(w^*) - \phi(v) - \phi(w)) f(v) f(w) dv\, dw \right\rangle . \tag{11.11}$$

A suitable asymptotic analysis allows to obtain a Fokker–Planck equation with variable coefficients from this Boltzmann equation [15]:

$$\frac{\partial f}{\partial t} = \frac{\lambda}{2} \frac{\partial^2}{\partial v^2} \left(D(|v|)^2 f \right) + \frac{\partial}{\partial v} \left(P(|v|)(v - m(t)) f \right) . \tag{11.12}$$

In (11.12) $m(t)$ is the mean opinion at time t,

$$m(t) = \int_{-1}^{+1} v f(v,t)\, dv\ .$$

The long-time behavior of the Fokker–Planck equation is very rich, and depends on the interaction dynamics of the Boltzmann equation. As for economic interactions, the constant λ in the Fokker–Planck equation (11.12) is related to the coefficients s and σ^2 which appear in the collision rule (11.10), with $\sigma^2/s = \lambda$. The structure of the steady state represents the formation of opinion contingent to the choice of the interaction dynamics. To show results in some simple case, we fix $P(|v|) = 1$, which implies conservation of the average opinion, again assuming that f has been scaled to be a probability density and that f and D vanish at the extreme opinions $v = +1, -1$. If in addition

$$D(|v|) = 1 - v^2\ ,$$

then the steady state distribution of opinion solves the equation

$$\frac{\lambda}{2}\frac{\partial}{\partial v}\left((1-v^2)^2 f\right) + (v-m)f = 0 \tag{11.13}$$

where m is a given constant (the average initial opinion). The solution of (11.13) is easily found:

$$f_\infty(w) = c_{m,\lambda}(1+v)^{-2+m/(2\lambda)}(1-v)^{-2-m/(2\lambda)} \exp\left\{-\frac{1-mv}{\lambda(1-v^2)}\right\}\ . \tag{11.14}$$

Here the constant $c_{m,\lambda}$ has to be fixed such that the mass of f_∞ is equal to the mass of the initial state, which is 1 by assumption, implying $-1 < m < +1$. Note that the presence of the exponential assures that $f_\infty(\pm 1) = 0$. The solution is regular, but not symmetric unless $m = 0$. Hence, the initial opinion distribution impacts on the steady state through its mean (opinion) value. In any case, the stationary distribution has two peaks (on the right and on the left of zero) with intensities depending on λ.

Comments on the Images 11.1 to 11.6 The Italian political economist Vilfredo Pareto (1848–1923)[2] is the originator of the so called empirical Pareto law[3] which in a simplified form states that – in any given country – less than 20% of the population own 80% of the total wealth. Although this was not considered a moral issue by Pareto himself, it is very hard not to think of morality when traveling through third world countries and being in direct contact with the huge number

[2] *http://cepa.newschool.edu/het/profiles/pareto.htm*
[3] *http://www.it-cortex.com/Pareto_law.htm*

Fig. 11.7. Opinion forming in Shanghai, China (courtesy of Andrea Baczynski)

of people, who are not part of the large-income Pareto tail. Mathematically speaking, a more general form of the Pareto law is represented by the fact that the large w(ealth)-tails, which correspond to the density of the rich individuals, of the large-time asymptotic states of the kinetic Pareto–Boltzmann equation (at least after an appropriate scaling limit) decay only algebraically as the wealth variable w tends to infinity, leading to so-called *heavy* or *fat* tails. The precise decay rate depends on properties of the market under consideration. Statistical data confirm the 80–20 wealth distribution rule as a surprisingly universal outcome, consistent with the algebraic decay law.

Also we remark that Pareto's work on efficiency and optimality of economic systems[4] has deep implications on mathematical game theory[5], which was turned into a precise mathematical theory in the first half of the 20th century, mainly by John von Neumann[6] and John Nash[7]. We refer to the book [17] for an excellent introduction to mathematical game theory, mainly in the context of biological systems.

Comments on the Images 11.7–11.10 Mathematical opinion formation models are based on quantifying the outcome of social interactions in the society under

[4] *http://en.wikipedia.org/wiki/Pareto_efficiency*
[5] *http://en.wikipedia.org/wiki/Game_theory*
[6] *http://en.wikipedia.org/wiki/John_von_Neumann*
[7] *http://nobelprize.org/economics/laureates/1994/nash-autobio.html*

consideration. Clearly, they have to take into account the various factors making up the social tissue of the society, which stem from the historical, religious, socio-economic, political etc. background. A lot of research in this direction has been carried out in the last years, and the interested reader can find information on the subject in the webpage of the Condensed Matter ArXiv[8].

[8] *http://xxx.lanl.gov/find/cond-mat*

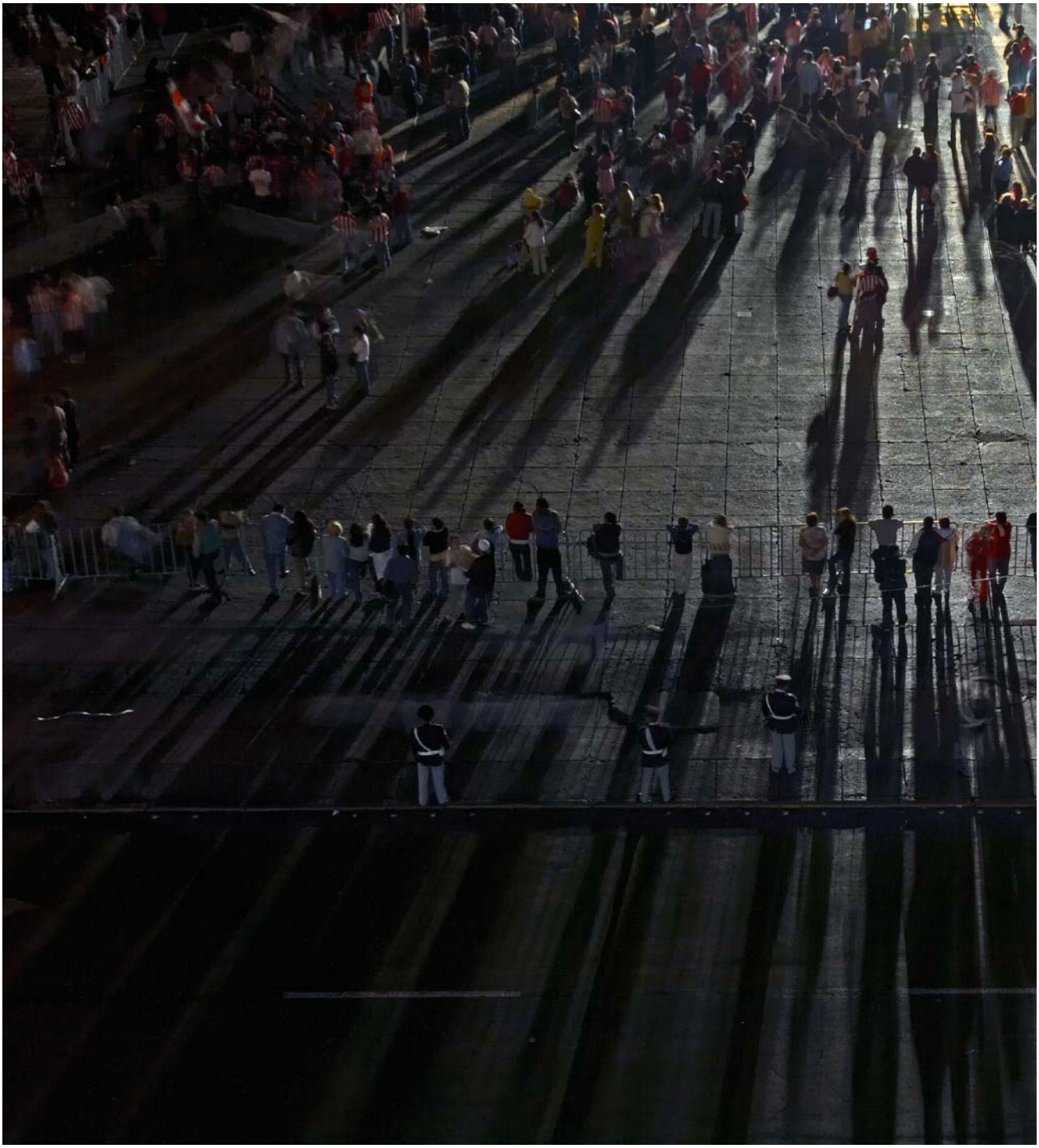

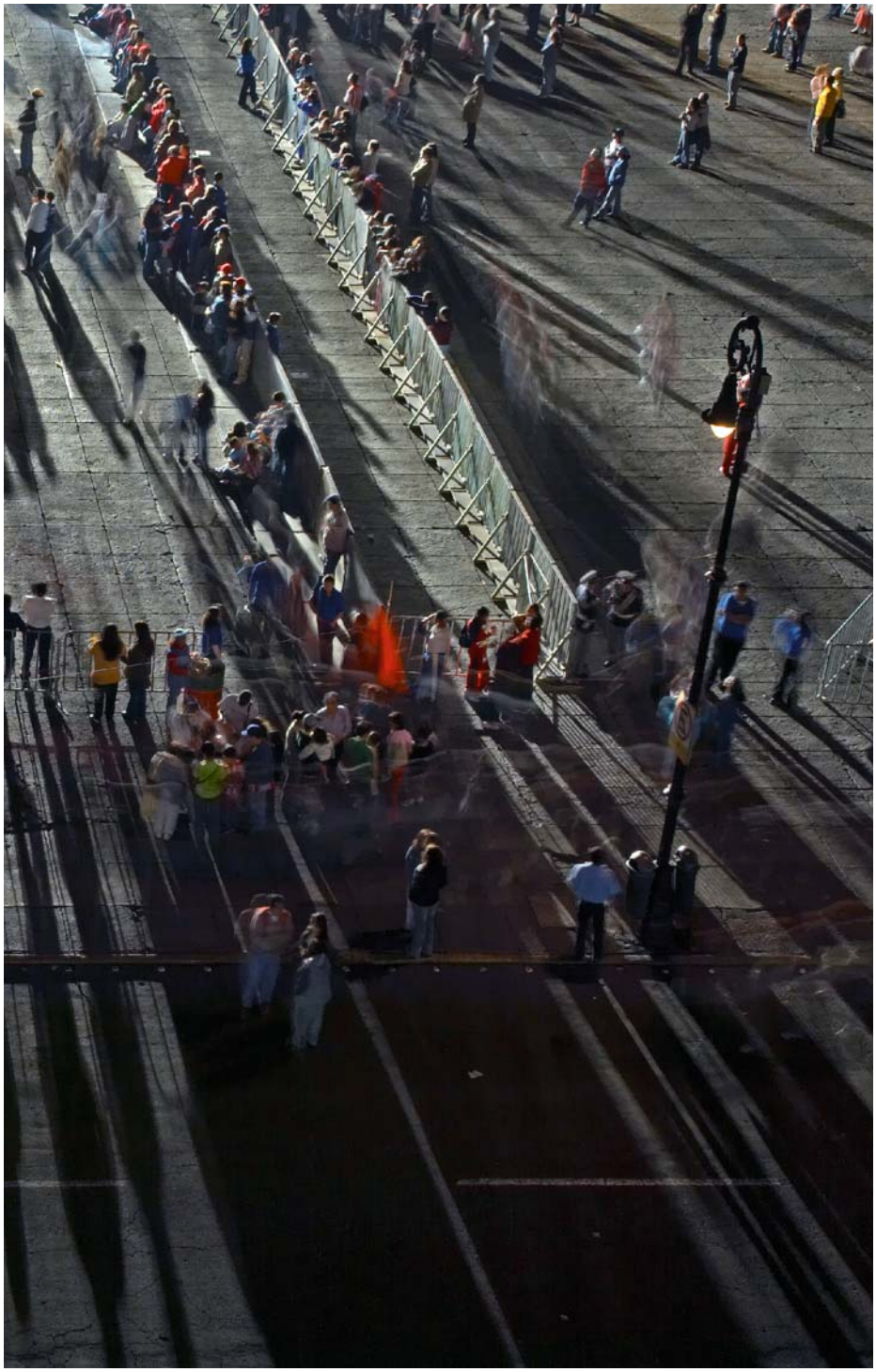

Fig. 11.8. Opinion forming on the Zocalo, Mexico City

Fig. 11.9. Opinion forming in Isfahan, Iran

Fig. 11.10. Beach in Salvador de Bahia, Brazil: what is the mean free path?

References

[1] E. Ben-Naim, *Opinion dynamics: rise and fall of political parties,* Europhys. Lett. **69**, 671–677 (2005)
[2] J.P. Bouchaud, M. Mézard, *Wealth condensation in a simple model of economy*, Physica A, **282**, 536–545 (2000)
[3] A. Chakraborti, B.K. Chakrabarti, *Statistical mechanics of money: how saving propensity affects its distributions*, Eur. Phys. J. B., **17**, 167–170 (2000)
[4] A. Chatterjee, B.K. Chakrabarti, S.S. Manna, *Pareto law in a kinetic model of market with random saving propensity*. Physica A, **335**, 155–163 (2004)
[5] S. Cordier, L. Pareschi, G. Toscani, *On a kinetic model for a simple market economy*. J. Stat. Phys., **120**, 253–277 (2005)
[6] A. Drăgulescu, V.M. Yakovenko, *Statistical mechanics of money*, Eur. Phys. J. B, **17**, 723–729 (2000)
[7] B. Hayes, *Follow the money*, American Scientist, **90**, (5), 400–405 (2002)
[8] S. Ispolatov, P.L. Krapivsky, S. Redner, *Wealth distributions in asset exchange models*, Eur. Phys. J. B, **2**, 267–276 (1998)
[9] O. Malcai, O. Biham, S. Solomon, P. Richmond, *Theoretical analysis and simulations of the generalized Lotka–Volterra model*, Phys. Rev. E, **66**, 031102 (2002)
[10] L. Pareschi, G. Toscani, *Self-similarity and power-like tails in nonconservative kinetic models*, J. Statist. Phys. (in press) (2006)
[11] V. Pareto, *Cours d'Economie Politique*, Lausanne and Paris (1897)
[12] F. Slanina, *Inelastically scattering particles and wealth distribution in an open economy*, Phys. Rev. E, **69**, 046102 (2004)
[13] F. Slanina, H. Lavička, *Analytical results for the Sznajd model of opinion formation*, Eur. Phys. J. B, **35**, 279–288 (2003)
[14] S. Solomon, *Stochastic Lotka–Volterra systems of competing auto-catalytic agents lead generically to truncated Pareto power wealth distribution, truncated Levy distribution of market returns, clustered volatility, booms and crashes*, Computational Finance 97, eds. A-P.N. Refenes, A.N. Burgess, J.E. Moody, Kluwer Academic Publishers, (1998)
[15] G. Toscani, *Kinetic models of opinion formation*, Com. Math. Sci. (in press) (2006)[9]
[16] W. Weidlich *Sociodynamics: A systematic approach to mathematical modelling in the social sciences*, Harwood Academic Publishers, (2000)
[17] K. Sigmund: *Games of Life: Explorations in Ecology, Evolution and Behaviour*, Penguin Books LTD, (1995)

[9] can be downloaded from *http://www-dimat.unipv.it/toscani/*